FULL PATTERN ANALYSIS AND COMPARISON OF THE CENTER FED AND OFFSET FED CASSEGRAIN ANTENNAS WITH LARGE FOCAL LENGTH TO DIAMETER RATIOS FOR HIGH POWER MICROWAVE TRANSMISSION

THESIS

Derek W. Mantzke, B.S.E.E, First Lieutenant, USAF

AFIT-ENG-MS-22-J-013

DEPARTMENT OF THE AIR FORCE
AIR UNIVERSITY

AIR FORCE INSTITUTE OF TECHNOLOGY

Wright-Patterson Air Force Base, Ohio

AFIT-ENG-MS-22-J-013

FULL PATTERN ANALYSIS AND COMPARISON OF THE CENTER FED AND OFFSET FED CASSEGRAIN ANTENNAS WITH LARGE FOCAL LENGTH TO DIAMETER RATIOS FOR HIGH POWER MICROWAVE TRANSMISSION

THESIS

Presented to the Faculty

Department of Electrical and Computer Engineering

Graduate School of Engineering and Management

Air Force Institute of Technology

Air University

Air Education and Training Command

In Partial Fulfillment of the Requirements for the

Degree of Master of Science in Electrical Engineering

Derek W. Mantzke, B.S.E.E

First Lieutenant, USAF

June 2022

AFIT-ENG-MS-22-J-013

FULL PATTERN ANALYSIS AND COMPARISON OF THE CENTER FED AND OFFSET FED CASSEGRAIN ANTENNAS WITH LARGE FOCAL LENGTH TO DIAMETER RATIOS FOR HIGH POWER MICROWAVE TRANSMISSION

Derek W. Mantzke, B.S.E.E
First Lieutenant, USAF

Committee Membership:

Andrew Terzuoli, Ph.D
Chair

Ronald Marhefka, Ph.D
Member

Major Timothy Wolfe, Ph.D
Member

Raymond Wasky,
Member

Justin Moll,
Member

AFIT-ENG-MS-22-J-013

Abstract

High power microwaves (HPM) have been a topic of research since the Cold War era. This paper presents a comparison between two Cassegrain-type antennas: the axially, or center fed, and the offset fed. Specifically, the 10 GHz operating frequency is investigated with large focal length to diameter (F/D) ratios. Beam patterns which encompass the entire radiation pattern are included for data validation and optimization. The simulations follow a factorial model of design to ensure all possible combinations of prescribed parameters are included. This includes an analysis of variance (ANOVA) study to find parameter influence on the outputs of interest. Outputs such as maximum gain, beamwidth, and sidelobe levels and locations are of interest. Research in this area will greatly enhance the reader's understanding of the benefits and disadvantages of the two antennas mentioned.

Acknowledgments

I would like to express my sincere appreciation to my faculty advisor, Dr. Andrew Terzuoli and the entire thesis committee for their guidance and support throughout the course of this thesis effort. A special thanks to Dr. Lee, Dr. Berglund, and Mr. Pflug for the ideas and guidance you selflessly provided to me. I appreciated all insight and feedback given to me from such great minds. I would also like to thank my five children, mother-in-law, and my parents for supporting me and providing motivation and support when I needed it the most.

Derek W. Mantzke

Table of Contents

List of Figures

Page

List of Tables

Page

FULL PATTERN ANALYSIS AND COMPARISON OF THE CENTER FED AND OFFSET FED CASSEGRAIN ANTENNAS WITH LARGE FOCAL LENGTH TO DIAMETER RATIOS FOR HIGH POWER MICROWAVE TRANSMISSION

I. Introduction

1.1 Problem Background

Research in the field of high-power microwave antennas is abundant. However, HPM research with respect to a direct comparison of antennas is lacking. Minimal research has been published on the performance of 8-10 GHz offset Cassegrain antennas with large focal length to diameter (F/D) ratios. This work will compare two Cassegrain-type antennas in the X-band frequency range with large F/D ratios. Development in this area will accelerate and progress technology in the HPM arena for the warfighter. The classical, center fed Cassegrain antenna will be discussed first, followed by the offset Cassegrain.

1.1.1 The Center Fed Cassegrain Antenna

The axially fed Cassegrain antenna design originates from the Cassegrain telescope [1]. For traditional axially fed Cassegrain antennas, the feed is normally placed at or behind the center of a parabolic main reflector (MR) and directed toward a smaller subreflector (SR) held in place by supporting struts. The struts are mounted on the MR and provide support and positioning for the SR. Common examples can be found in many sources [1, 3, 4]. The incident rays originating from the feed are directed from the SR to

the MR to be radiated into space. The geometry and shape of both the MR and SR can be manipulated to achieve desired applications. For a basic visual layout of the center fed Cassegrain antenna, see Figure 1. Furthermore, see Chapter 3 for an in-depth look at the geometry of this design. Of the many variations of the Cassegrain antenna, the second design of interest is the offset version.

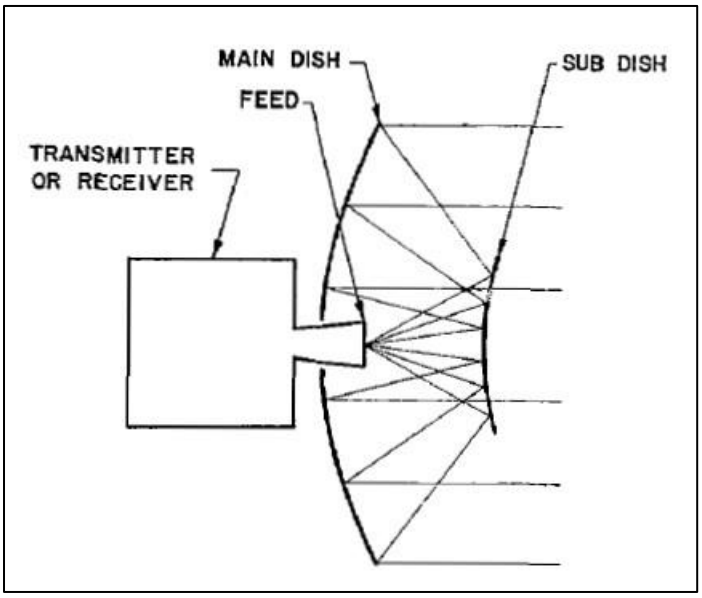

Figure 1. Basic layout of the axially fed Cassegrain antenna [1].

1.1.2 The Offset Cassegrain Antenna

For the offset Cassegrain antenna configuration, the feed and SR are situated in an offset fashion with respect to the MR. The primary benefit of the offset Cassegrain over the center-fed is the absence of aperture blockage due to the SR, supporting struts, and the SR itself [2]. The SR for both variants is hyperbolic in nature. For a basic visual layout of the offset Cassegrain antenna, see Figure 2. For the overview of the geometrical properties of the offset Cassegrain antenna, see Chapter 3.

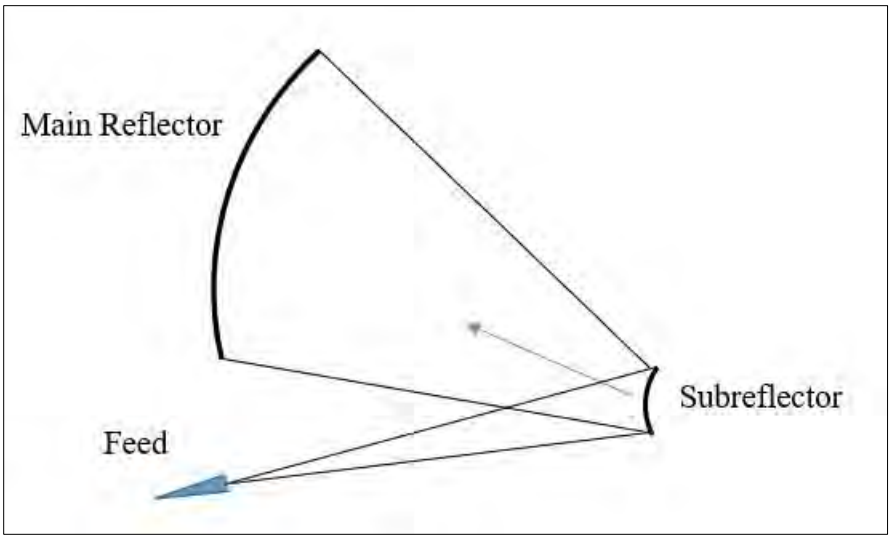

Figure 2. Basic layout of the offset Cassegrain antenna.

1.2 Research Objectives

The goal of this work is to compare performance between the Cassegrain and offset Cassegrain antenna in the 8-10 GHz range (X-band) in the far-field and near field. This work will investigate the beam pattern characteristics including maximizing gain, minimizing beamwidth, and minimizing sidelobe levels across the entire radiation pattern. To achieve the research objectives, various computational electromagnetic (CEM) software tools will be used. The simulations will follow a factorial design of experiments (DOE) approach with a thorough analysis of variance (ANOVA) study. Once the data has been collected, charts and tables will be presented in an organized manner, relating the outputs of interest to the focal length to diameter (F/D) ratios.

1. 3 Methodology

The correlation between the two different antennas will be performed by way of a factorial design of experiments (DOE) approach with analysis of variance (ANOVA) support using simulations. Each antenna will have a set of parameters that will be varied. Initial parameters will be derived from many sources [1,2,3,4,6,12,17]. The parameters will be adjusted and simulated with all possible combinations considered. The computational electromagnetic (CEM) software used for data collection is GRASP Student Edition (SE) and SATCOM for validation purposes. Any further use of the term GRASP or GRASP SE can be assumed to represent GRASP SE. MATLAB and Microsoft EXCEL will be used for data processing, presentation, and ANOVA tests. GRASP uses physical optics (PO) and physical theory of diffraction (PTD) to calculate scattered fields, while SATCOM uses PO and the uniform theory of diffraction (UTD). An overview of PO and PTD will be presented in Chapter 2. Furthermore, an overview of DOE and ANOVA can be found in Chapter 2.

1. 4 Assumptions and Limitations

Due to the nature of the CEM software, all surfaces for both designs will be considered perfect electrical conductors (PECs). This assumption will eliminate losses due to manufacturer imperfections and the quality of material that is available. In doing this, the results presented in this paper will be assumed the “best case” for their respective

designs. For both the center fed and offset Cassegrain antennas, the chosen MR diameter will be 6 meters. The MR size was chosen based on previous work and other practical design considerations [6]. The frequency range of interest is the X-band; the specific operating frequency for this work is 10 GHz. The electromagnetic polarization was selected to be linear to standardize results between the computational electromagnetic software (CEM). Although the practical design considerations have limited the scope of certain parameters, Chapter 2 covers motivation behind choosing the key parameters for this work.

There are limitations to the GRASP SE software due to the readily available, free student version. Utilizing GRASP SE will limit the ability to use supporting struts. Additionally, GRASP SE does not allow for a realistic feed model. There is only one choice of feed (Gaussian beam). This type of feed does a fair job of representing typical horn patterns. It is important to note that the full edition of GRASP accounts for the limitations listed here.

II. Background and Literature Review

2.1 Previous Efforts

Analysis of the offset Cassegrain design with a 6-meter MR diameter in the X-band frequency range are limited with respect to parameter sizes and design considerations. However, work has been performed by Harris on the characterization of a 6-meter, center fed Cassegrain antenna in the X-band [6]. Within this work is a comprehensive sensitivity analysis of a 6-meter center fed Cassegrain antenna in the 9-11 GHz range. GRASP SE and SATCOM were both used in tandem to compare a previous work's 10-meter Cassegrain design. It is important to note, however, that this work did not investigate large focal length to diameter (F/D) ratios but performed simulations with common F/D ratios, whereas this work will. The primary objective of the previous work was to optimize the beam pattern across the entire radiation pattern. The work begins by validating a previous 10-meter Cassegrain antenna then moves to the 6-meter version. The methodology followed an approach where a set of baseline parameters were chosen. The baseline parameters can be seen in Table 1. Notice in Table 1 there is a column including struts. GRASP SE is unable to include struts in simulations, however, SATCOM was used in the previous work to simulate the inclusion of struts.

Parameter	Struts	No Struts
Frequency	10 GHz	10 GHz
Polarization	Right Hand Circular	Right Hand Circular
Feed Location	Main Reflector Base	Main Reflector Base
Edge Taper	-10 dB	-10 dB
Dm	6 m	6 m
$\frac{F}{Dm}$	0.3125	0.3125
$\frac{Ds}{Dm}$	0.1	0.1
SR Vertex	1.6749m	1.6749m
Eccentricity	1.2712	1.2712
Strut Angle	39.26°	None

Table 1. Initial 6-meter Cassegrain parameters.

One parameter was varied at a time while the remaining parameters were held to the baseline values in Table 2.1. The four parameters of interest were focal length to MR diameter ratio F/D, SR diameter to MR diameter ratio Ds/Dm, eccentricity of the SR, and edge taper (feed taper). The feed taper is the value in decibels of the attenuation of the feed toward the edge of the SR. The term edge taper and feed taper will be used interchangeably throughout this work. Section 2.7 will discuss the significance of feed taper. For a list of the parameters, sweep range, step size, and typical values, see Table 2. For the typical value for Ds/Dm in Table 2, it is supposed to read 0.1.

	Typical	Sweep Range	Step Size
$\frac{F}{Dm}$	0.1 to 0.8	0.1 to 0.6	0.01
$\frac{Ds}{Dm}$	¡= 0.1	0.01 to 0.3	0.01
Eccentricity	Derived	1.05 to 3.0	0.05
Edge Taper	-15 to -10 dB	-30 to 0 dB	1 dB

Table 2. Typical parameters used in previous 6-meter Cassegrain analysis [6].

Using the parameter sweeps in Table 2 and the initial values in Table 1, Harris was able to perform numerous simulations to find optimized values for each. The outputs of interest were main lobe maximum level, main lobe beamwidth, side lobe level and

locations, and the back lobe for fratricide analysis. Points were made for each parameter sweep and plotted against each of the outputs of interest. An attempt was made to use the optimized values found from the parameter sweeps; however, it was noted that this did not yield an optimized outcome. The antenna could not be optimized with the optimal values found for each individual parameter sweep because of the parameter relationships. Changing one parameter will affect other parameters, thus changing the output.

It is the goal of this work to use a similar, but different approach to parameter sweeps and simulations. By using a DOE factorial approach with an analysis of variance (ANOVA), more optimal values can be found. The DOE factorial approach will be much more intensive than the aforementioned work but will exhaust all of the possible combinations of parameters within the given ranges and step sizes. Furthermore, statistical support in the form of ANOVA will be presented to support observations.

2.2 Physical Optics

To gain a foundation in electromagnetic (EM) scattering, it is imperative to provide an overview of physical optics (PO). Also known as wave optics, PO is a high frequency approximation of how radiation waves react when illuminating objects. Furthermore, the object in question must be much larger than the wavelength of the frequency under test. This holds true for any shape in question. PO uses geometrical optics (GO) to apply boundary conditions. GO in its most basic form models waves as rays. Using the law of reflection, GO can approximate the direction of the reflected wave

as seen in Figure 3 where the incident ray angle is equal to the scattered ray angle [8]. Equation (2.1) shows the mathematical relationship to the angles of the incident ray θ_i and the scattered ray θ_s.

$$\theta_i = \theta_s \tag{2.1}$$

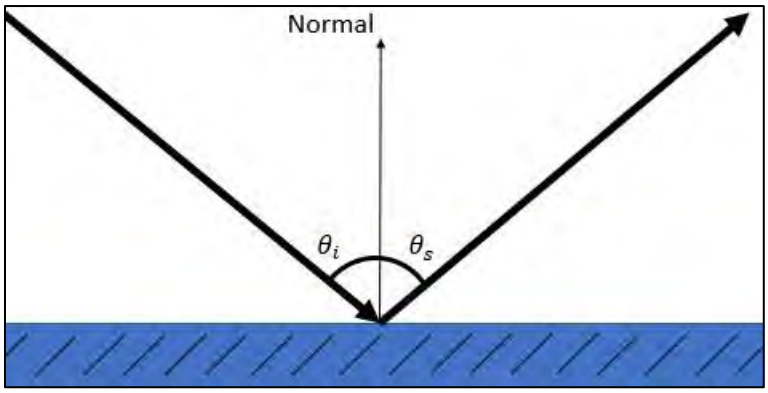

Figure 3. Visual representation of the Law of Reflection.

In the far-field, a transmitted wave can be approximated to a plane wave. As the incident wave illuminates the antenna aperture, current is induced on the surface. Since the material of the object in question is considered a PEC, the relationship between the incident and scattered electrical field can be related by Equation (2.2).

$$E_{total} = E_{inc} + E_{sc} \tag{2.2}$$

Now consider the surface of an object to have many different points illuminated by the wave. The PO solution integrates the currents along the surface of the antenna to produce the scattered field strength approximation. For a visual representation of the points on a surface see Figure 4. The tangential components of the currents J are defined as $J = \hat{n} \times H_{inc}$, where $\hat{n}$ is the unit-normal vector and H_{inc} is the incident magnetic

field. One the PO currents are defined, they exist in free space. With the help of GO, the direction of propagation can be determined, and a complete model of the scattered waves can be produced. It is important to note that an in-depth explanation of PO is outside the scope of this work.

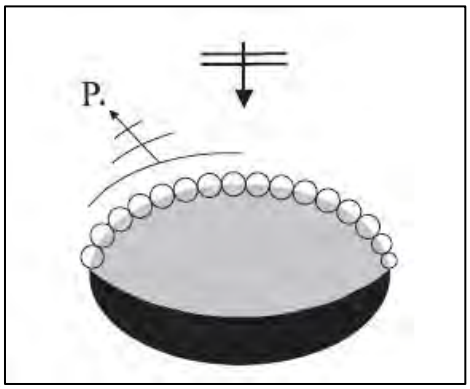

Figure 4. PO visualization with incident plane wave, points of incident, observation point P, and shadow region (black) [8].

The major drawback of PO is that the shadow regions, edges, and caustic areas are neglected. Using PO alone will not yield a realistic model of the entire RF environment. A more realistic approach in which the edges, shadow regions, and caustic areas are modeled is known as the physical theory of diffraction (PTD).

2.3 Physical Theory of Diffraction

PTD is an extension of PO and provides a solution to field strength from scattered RF due to edges. The development of PTD occurred in the 1950's by Ufimtsev [9]. The edges of the surface under observation are considered the non-uniform surface, while the

rest of the surface is considered uniform. The surface currents in the uniform area can be determined by the PO method, while the non-uniform area is determined by PTD.

Now consider an incident field illuminating a parabolic reflector. PTD accounts for both the uniform and non-uniform surface currents induced by the incident rays in the form of Equation (2.3).

$$j_{total} = j_o + j_i \tag{2.3}$$

In Equation (2.3), j_o is the surface current from PO analysis, and j_i are the corrections provided by PTD for edge diffraction. The edge of the reflector is modeled as an infinite wedge using two equations, f and g.

$$\begin{aligned} f &= X - Y + \frac{1}{2}\{\tan\left(\frac{(\psi_i - \psi_s)}{2}\right) - \tan\left(\frac{(\psi_i + \psi_s)}{2}\right)\} \\ g &= X + Y + \frac{1}{2}\{\tan\left(\frac{(\psi_i - \psi_s)}{2}\right) + \tan\left(\frac{(\psi_i + \psi_s)}{2}\right)\} \end{aligned} \tag{2.4}$$

In Equation (2.4), X and Y are known as the diffraction coefficients, while ψ_i and ψ_s are the angle of incidents and scattering respectively, which are measured perpendicular to the edge. X and Y are modeled in the form of Equation (2.5).

$$\begin{aligned} X &= \frac{\left(\frac{1}{n}\right)\sin\left(\frac{\pi}{n}\right)}{\cos\left(\frac{\pi}{n}\right) - \cos\left[\frac{\psi_i - \psi_s}{n}\right]} \\ Y &= \frac{\left(\frac{1}{n}\right)\sin\left(\frac{\pi}{n}\right)}{\cos\left(\frac{\pi}{n}\right) - \cos\left[\frac{\psi_i + \psi_s}{n}\right]} \end{aligned} \tag{2.5}$$

In Equation (2.5), n represents the exterior wedge angle. Once the surface currents are determined by PO and PTD, Equation (2.2) can be modified to represent the total electrical field.

$$E_{total} = E_{po} + E_{ptd} \tag{2.6}$$

For a visual representation of a single ray diffracted by the edge of a disk, see Figure 5.

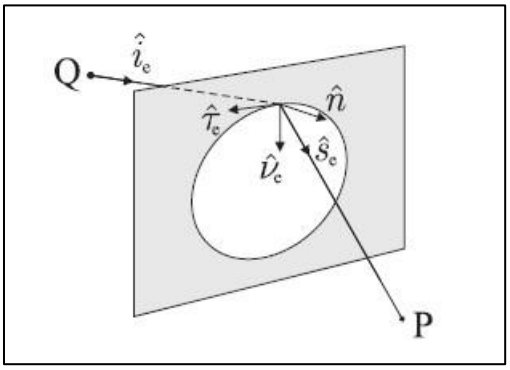

Figure 5. Single diffracted ray from point Q in the direction of $\hat{\imath}_c$ onto the edge of a disk [8].

Notice the direction of diffraction $\hat{S}_c$ to point P in Figure 5. PTD provides the solution to edges and shadow regions that PO does not account for. Another process in which shadow regions and diffracted rays can be modeled is known as the geometrical theory of diffraction (GTD).

2.4 Geometrical Theory of Diffraction

Originally introduced by Joseph Keller in 1962, GTD provides a solution to diffracted rays that enter the shadow region bounded by GO [10]. The famous *Keller's*

Cone describes the cone-shaped diffraction that occurs when an oblique incident ray interacts with an impenetrable surface [10]. For a visual representation of Keller's explanation of diffracted rays see Figure 6. Like PTD, the basic mathematical form of representing the electric field by GTD is described in Equation (2.7).

$$E_{GTD} = E_{go} + E_d \tag{2.7}$$

With the difference from PO, the fields only exist in the un-shadowed regions, that is, metallic objects block the propagation of the GTD rays. In Equation (2.7), E_{go} is the calculated electric field from GO (like the integration method in PO), and E_d is the contribution from the edges, i.e., diffraction coefficients. The diffracted rays are the product of the incident rays and the diffraction coefficient. Let A_i be an arbitrary incident wave, $\psi_d(r, \theta_s)$ be the diffracted cylindrical wave, $D(\theta_s, \theta_i)$ be the diffraction coefficient, $\frac{e^{-jkr}}{\sqrt{r}}$ represent the cylindrical wave, k is the wave number, and r is the distance from the origin, then Equation (2.8) represents the diffracted ray.

$$\psi_d(r, \theta_s) = A_i D(\theta_s, \theta_i) \frac{e^{-jkr}}{\sqrt{r}} \tag{2.8}$$

However, the diffraction coefficient is proportional to $\lambda^{1/2}$ for edges, λ for vertices, and decrease exponentially λ^{-1} for surfaces [11]. The primary difference between GTD and PTD are that GTD strictly uses rays to model RF whereas PTD considers RF as waves.

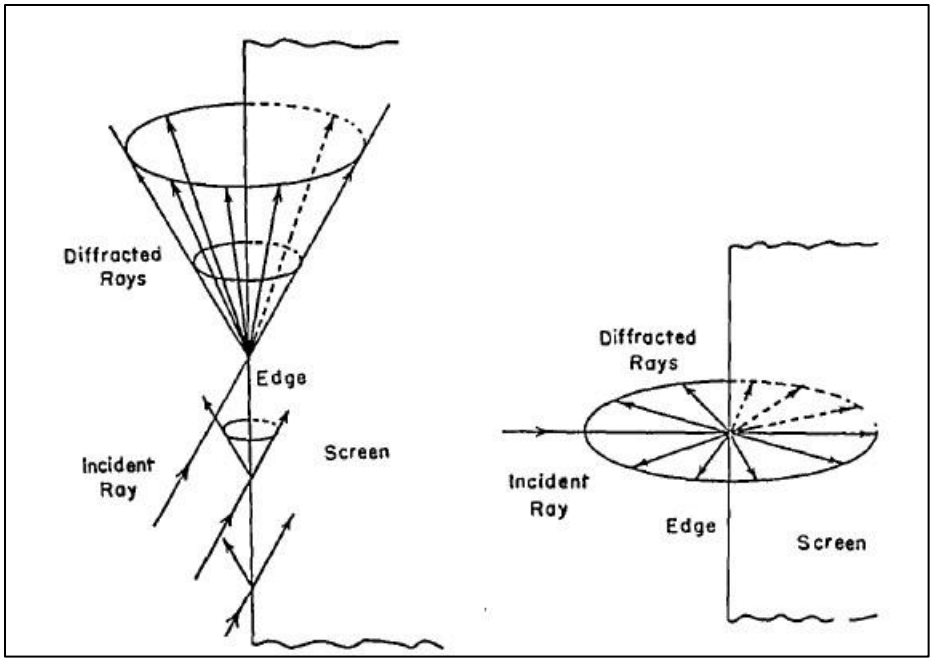

Figure 6. Keller's cone from a diffracted oblique incident ray (left) and a diffracted ray normal to a thin screen (right).

2.5 Geometry of the Offset Cassegrain Antenna

The first component to consider for any Cassegrain antenna is the main reflector (MR). The MR is a paraboloid that depends on the diameter Dm and the focal length F. The focal length is a significant parameter that changes the way the columnated beam is focused. If the diameter and depth d is known, focal length can be determined by Equation (2.9).

$$F = \frac{D_m^2}{d} \tag{2.9}$$

When looking at the side profile of the offset Cassegrain in Figure 7 where the antenna is projected onto the x-z plane, Equation 2.10 represents the shape of the MR with respect to the MR coordinate system (x_{mr}, y_{mr}, z_{mr}).

$$z_{mr}(x_{mr}, y_{mr}) = \frac{x_{mr}^2 + y_{mr}^2}{4F} - F \tag{2.10}$$

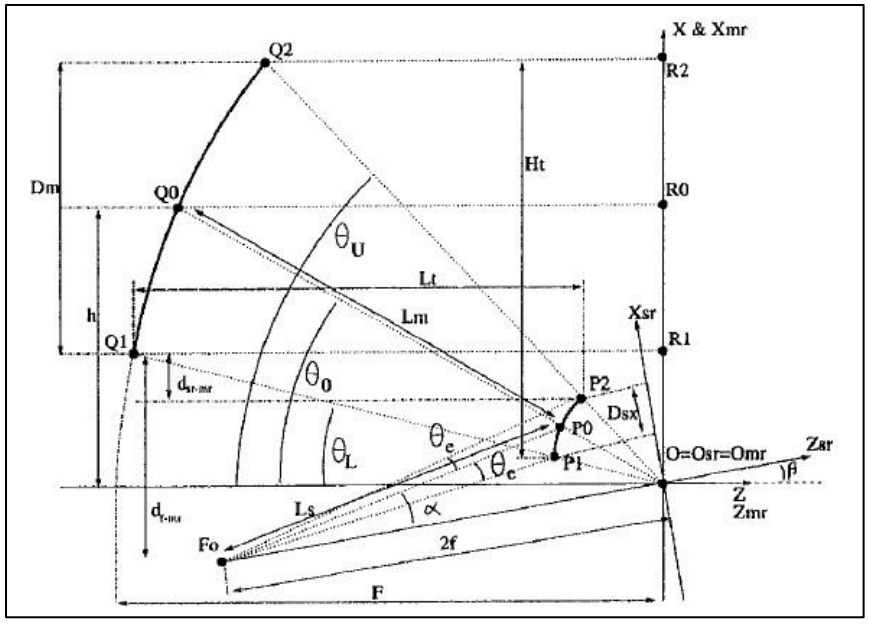

Figure 7. Offset Cassegrain geometry [12].

When the MR is projected onto the x-y plane, the aperture is circular with a height above the x-axis determined by h in Figure 7. Equation (2.10) represents the circular aperture projected onto the x-y plane, where h is the distance between vertex Q_0 and the z_{mr} axis in Figure 7.

$$\frac{4(x-y)^2}{D_m^2} + \frac{4y^2}{D_m^2} = 1 \tag{2.11}$$

The next component to discuss is the SR. Using the same coordinate system in Figure 7, the SR is a convex hyperboloid and can be expressed using Equation (2.12) – Equation (2.14) with the surface parameter a and c (midpoint of the focal length), the focal length f, and the eccentricity e. See Figure 8 for an example of the convex hyperboloid nature of the subreflector.

$$a = \frac{c}{e} \tag{2.12}$$

$$f = 2c \tag{2.13}$$

$$z_{sr}(x_{sr}, y_{sr}) = a\sqrt{1 + \frac{x_{sr}^2 + y_{sr}^2}{f^2 - a^2}} - f \tag{2.14}$$

Note that e must be greater than 1 for a hyperbolic curve. For a visual representation of the SR projected onto the x-z plane, see Figure 7. Also notice that in Figure 7, the SR coordinate system is tilted at an angle β but still shares the same origin as the MR coordinate system. Finally, the distance between the MR and SR vertexes Lm can be determined by Equation (2.15), where θ_0 is the angle tended by the MR z-axis and the MR vertex in Figure 7. In this work, Lm will also be used to define the distance from the main reflector vertex and the feed in the center fed Cassegrain designs.

$$L_m = -\alpha\frac{e^2 - 1}{e\cos(\beta - \theta_0) + 1} - \frac{h}{\sin(\theta_0)} \tag{2.15}$$

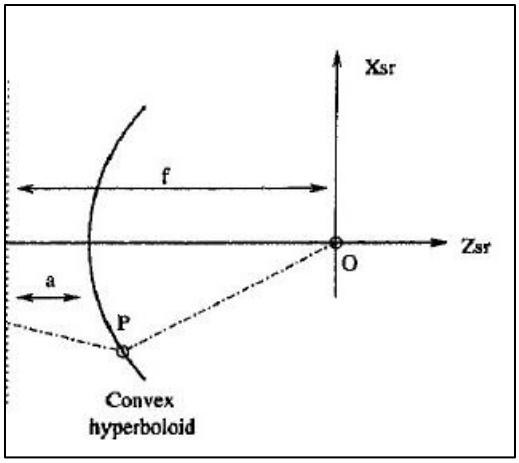

Figure 8. Convex hyperboloid SR surface parameter a and focal length f.

The feed placement is the third and final geometric component of the offset Cassegrain system. In reference to Figure 7, the feed can be described geometrically with the tilt angle β of the SR coordinate system, the distance between the feed and the vertex of the SR L_s, the half-angle subtended by the vertex and the edge of the SR θ_e, the eccentricity of the SR e, and the tilt angle of the feed with respect to the SR z-axis α. To satisfy the zero cross-polarization condition or, the *Mizugutchi condition*, α is determined by Equation (2.16) [2].

$$\alpha = \arctan\left[\frac{e+1}{e-1} tan\left(\frac{\beta}{2}\right)\right] \tag{2.16}$$

Equations (2.17) and (2.18) are the remaining equations that determine the geometry and placement of the feed.

$$L_s = \alpha\left[2 + \frac{e^2-1}{e\cos(\beta-\theta_0)+1}\right] \tag{2.17}$$

$$\theta_e = -\sigma\left\{2\arctan\left[\frac{1-e}{1+e}\tan\left(\frac{\theta_U-\beta}{2}\right)\right] - \alpha\right\} \tag{2.18}$$

In Equation (16) θ_U is the angle from the MR z-axis to the upper edge of the MR.

2.6 Computational Electromagnetic Software

The two primary computational electromagnetics (CEM's) used in this work for simulations will be GRASP and SATCOM. As mentioned in Chapter 1, GRASP uses PO plus PTD to determine the radiation pattern. The student edition of the software allows for many different types of single and dual-reflector designs. However, the student edition only allows for a gaussian beam feed model. GRASP only requires a few parameters to design a basic antenna model. For a screen shot of the initial requirements for a dual reflector antenna, see Figure 9. Once the initial parameters are entered, a 3D model of the antenna is rendered. From there, many options are available to manipulate the parameters. For an example of the 3D model layout with additional options, see Figure 10. When a simulation is performed, the result is the radiation pattern with the preset θ and ϕ values set by the user. From there, the data can be exported to MATLAB for further processing and plotting.

SATCOM is an Ohio State University (OSU) program that simulates many different reflector antenna designs. Like GRASP, SATCOM has a wizard that asks for certain parameters to build the antenna. However, SATCOM does allow the user to set up the entire antenna space with the wizard instead of rendering after selecting initial parameters like GRASP. For a screen shot of the initial set up and list of the types of

reflector antennas that SATCOM can design, see Figure 11. Once the wizard is complete, SATCOM builds a wireframe 3D model of the antenna. To change any of the parameters from the initial setup, the user can code in new parameters. The wizard and associated coding window can be seen in Figure 12. SATCOM is not restricted to the gaussian beam feed model that GRASP uses. The program allows the user to define their own feed model by importing a feed profile.

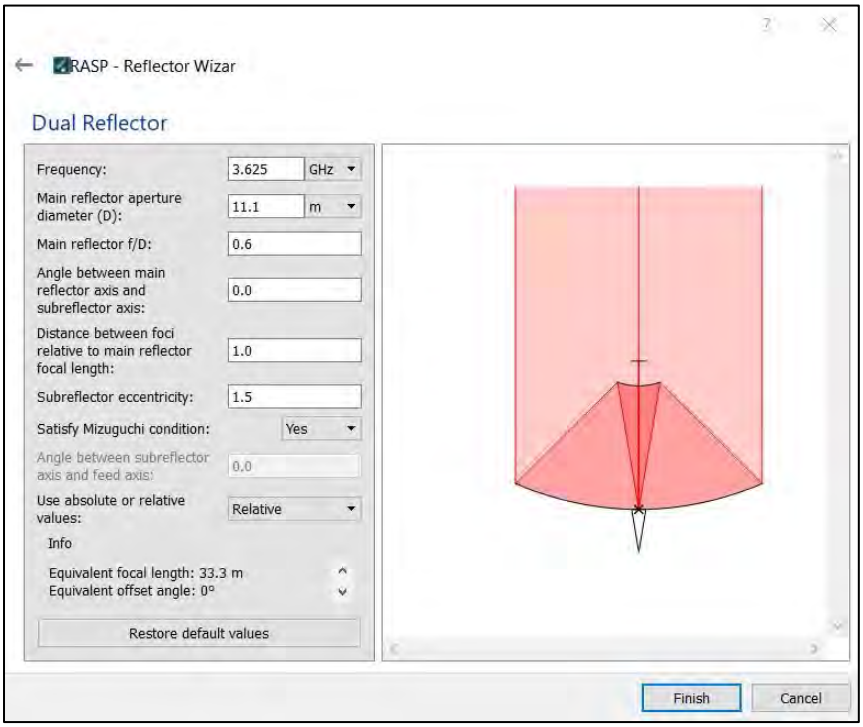

Figure 9. GRASP initial requirements for the dual-reflector wizard.

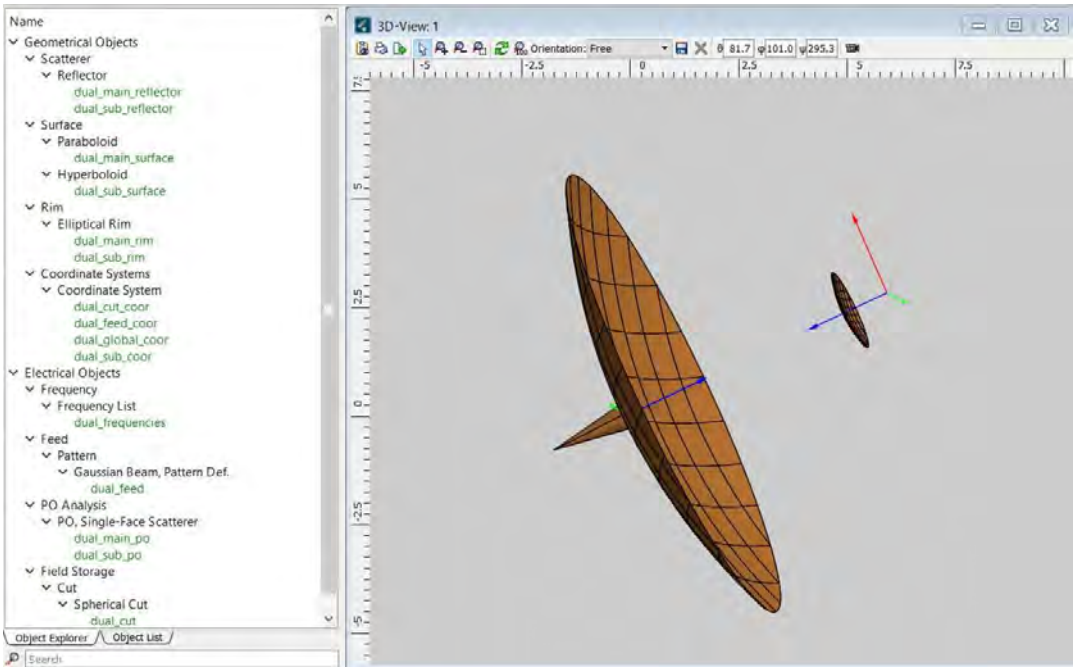

Figure 10. GRASP 3d model (right) with additional parameter options (left).

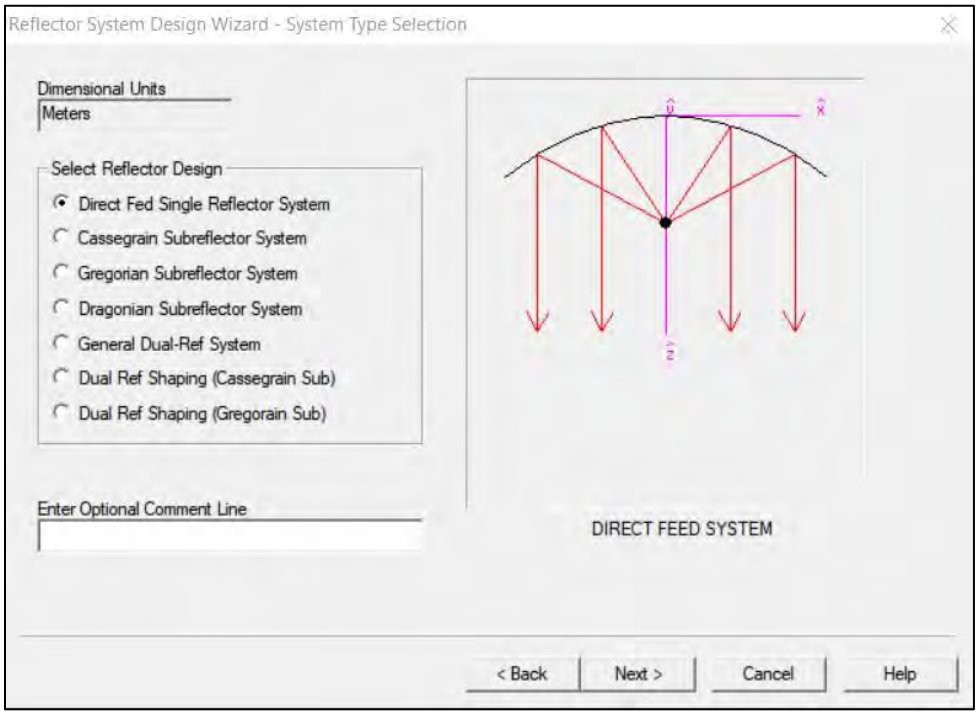

Figure 11. SATCOM antenna wizard example.

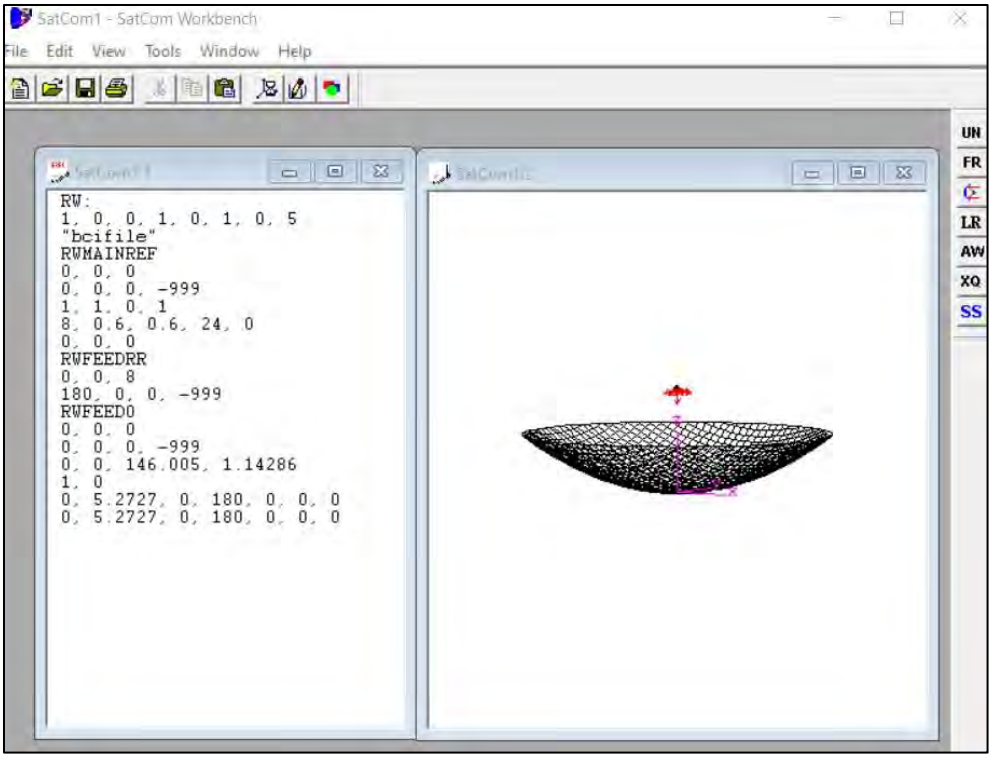

Figure 12. SATCOM wireframe 3d model (right) and coding window with prescribed parameters (left).

2.7 Parameter Decisions

This section will provide a background of the parameters for the two type reflector antennas of interest (Ds/Dm, feed taper, F/D, eccentricity,), and reasoning behind choosing certain values. The axially fed Cassegrain antenna will be referenced; however, note that the same principals apply to the offset Cassegrain. Understanding the general desired radiation pattern is important to selecting the correct antenna parameters. For example, a large main reflector (MR) diameter will yield a higher gain. This relationship can be described generally for as illuminated aperture by Equation (2.19)

where A is the physical area of the projected aperture in Equation (2.19) assuming a uniform distribution.

$$G = 4\pi \frac{A}{\lambda^2} \tag{2.19}$$

Using Equation (2.19), the general frequency and area of the aperture can be determined to produce a best-case scenario for maximum gain. For systems such as satellites that need higher gain to communicate at great distances, a larger antenna may be used to compensate for atmospheric losses. In the specific case of the center fed Cassegrain antenna, the gain equation is modified in Equation (2.20) where η is the aperture efficiency and the variables Dm and Ds are the MR and sub reflector (SR) diameters respectively.

$$G_{cassy} = \eta \frac{\pi^2 (D_m^2 - D_s^2)}{\lambda^2} \tag{2.20}$$

The aperture efficiency η is defined by the ratio of the effective aperture to the physical aperture and includes losses such as ohmic, spillover, and illumination, which will be covered later in this section. In Equation (20), both MR and SR diameters play a role in maximizing gain in the axially fed Cassegrain system. As the SR diameter gets larger in Equation (2.20), the gain will decrease due to RF blockage. This blockage also decreases directivity and increases the side-lobe level [14]. Recall that directivity is an antenna's ability to focus emitted energy in a certain direction. The relationship between Ds/Dm, directivity, and side lobe level can be seen in Figure 13.

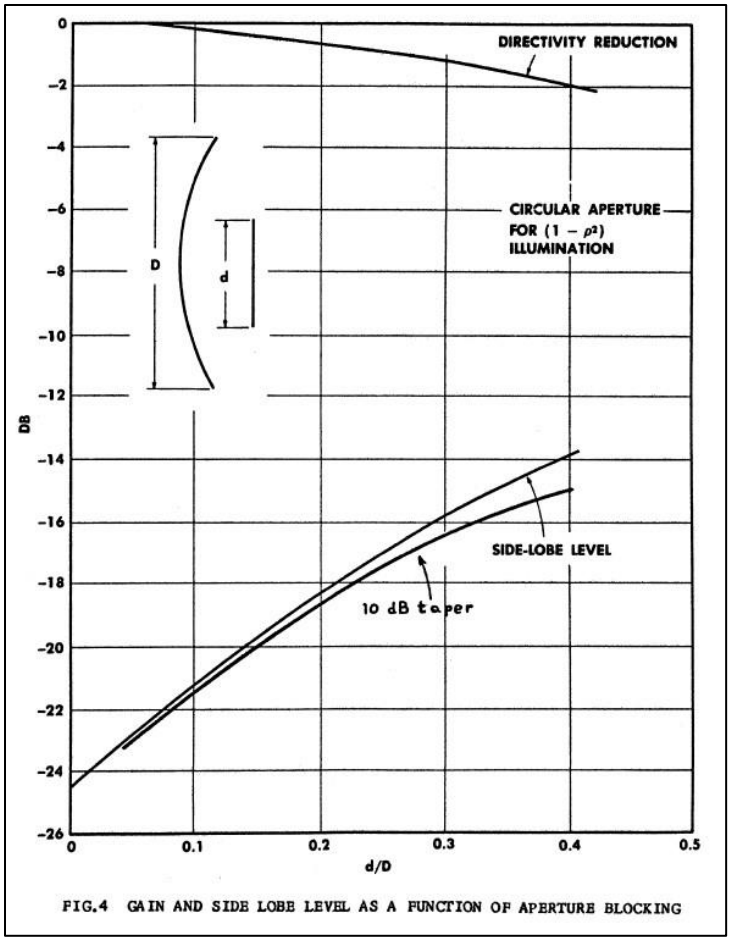

Figure 13. Relationship between the D_s/D_m ratio, the antenna directivity, and the side lobe level given two feed tapers.

The chart in Figure 14 provides the relationship between the Ds/Dm ratio and the blockage efficiency. Choosing a $Ds/Dm \leq 0.1$ will ensure $\gg 99\%$ blockage efficiency [3]. When considering the Ds/Dm for the offset Cassegrain, other equations are used to determine the size of Ds, however, for the sake of this work, similar Ds/Dm ratios will be used for both antenna variants to make proper output comparisons. Note that Figure 13 also shows two different feed taper values.

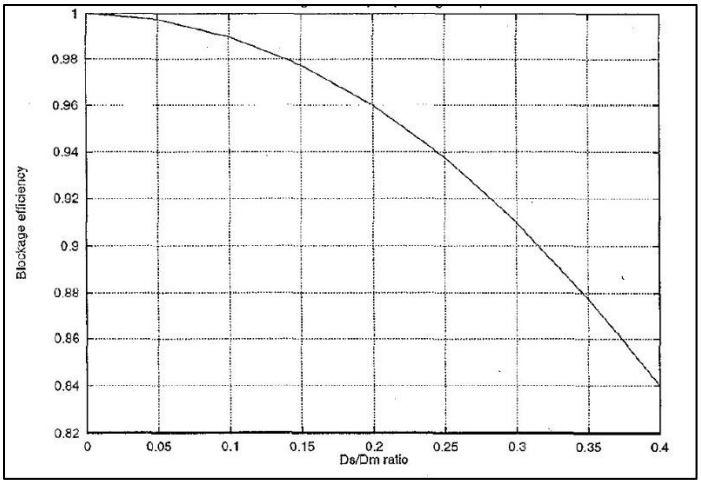

Figure 14. Relationship between Ds/Dm and the blockage efficiency for the axially fed Cassegrain antenna [3].

Feed taper is the amount of attenuation, in decibels, towards the edge of an illuminated aperture at a given feed taper angle. Studies have determined the accepted values of feed taper range from -10 dB and -12 dB [15, 16]. Using values that lie in this range will ensure an acceptable balance between illumination loss and spillover loss. See Figure 15 for a physical interpretation of illumination loss and spillover loss. As feed taper decreases, more spillover occurs, thus spillover loss increases. Conversely when feed taper increases, illumination loss increases. See Figure 16 for a chart that shows the relationship between spillover and illumination efficiency as a function of feed taper. In Figure 16, the term "efficiency" refers to how well the feed taper makes use of the aperture area. Hence, a feed taper of 0 decibels will illuminate the entire aperture evenly but have a very large spillover. Depending on the feed pattern, the F/D ratio can also aid in spillover and illumination loss.

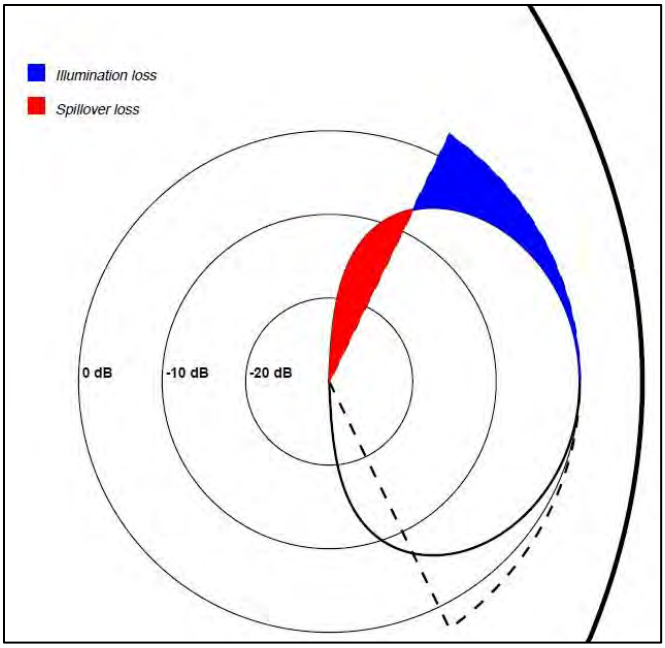

Figure 15. Example of illumination and spillover loss from a typical feed (solid line) and a desired feed (dotted line) pattern [16].

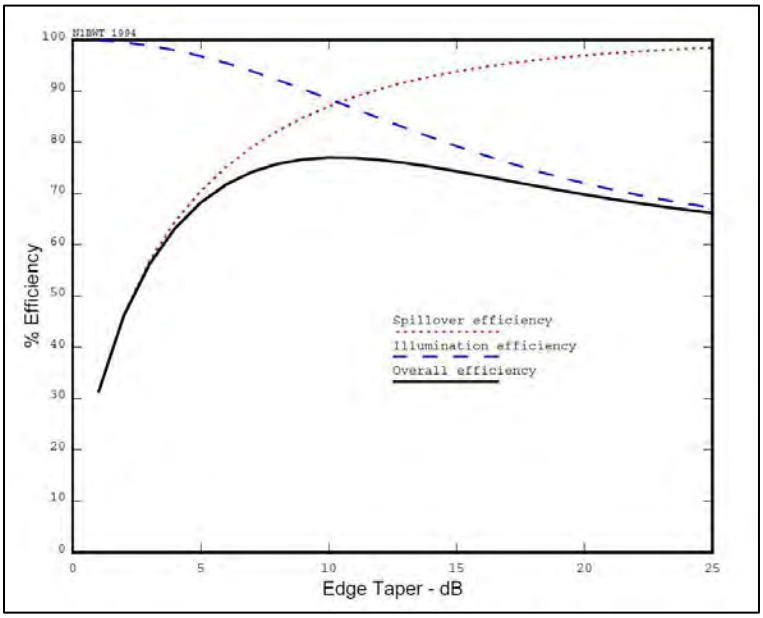

Figure 16. Illumination and spillover efficiency as a function of edge taper (feed taper) [16].

The F/D ratio determines the flatness of the parabolic reflector. Matching the feed type and geometry to the curvature of the reflector can aid in spillover and

illumination loss. For the sake of this work, a Gaussian beam feed pattern will be used, however, it is important to note that feed geometry can be manipulated to create a more customized pattern. Typical values of F/D range between 0.25 and 0.85 [3, 4, 6, 16, 17]. Large F/D ratios are very efficient in terms of illumination loss; however, the opposite is true for spillover. As the F/D ratio increases, the parabolic reflector becomes increasingly flat, therefore a larger taper angle is needed to illuminate the dish at the edges. As the taper angle increases, spillover also increases as in Figure 16. As for the radiation pattern, the primary difference between small and large F/D ratios are the effect on the side lobes and back lobes. To highlight the effects on the back and side lobes due to varying F/D ratios, a series of simulations were performed in GRASP. The baseline parameters used were 6-meter main dish diameter, 10 GHz operating frequency, and a subreflector eccentricity of 1.3. All other parameters were automatically chosen by the GRASP software. See Figure 17 and 18 for the co-polar and cross-polar radiation pattern results with varying F/D ratios.

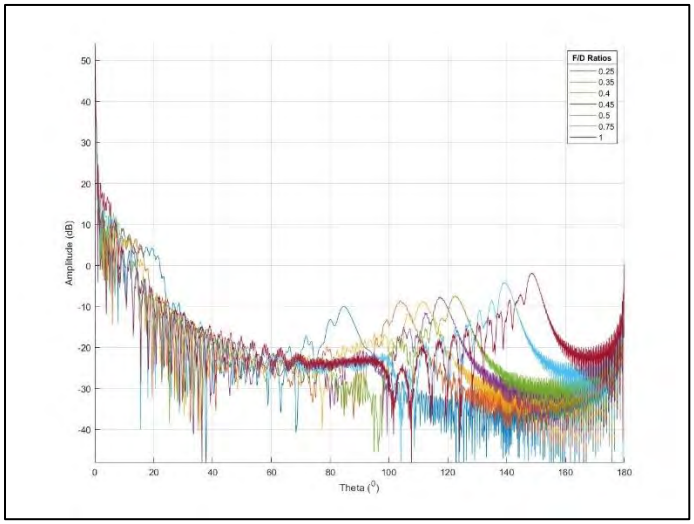

Figure 17. Co-polar radiation pattern of 6m Cassegrain antenna with varying MR F/D ratios from 0 to 180^0 θ.

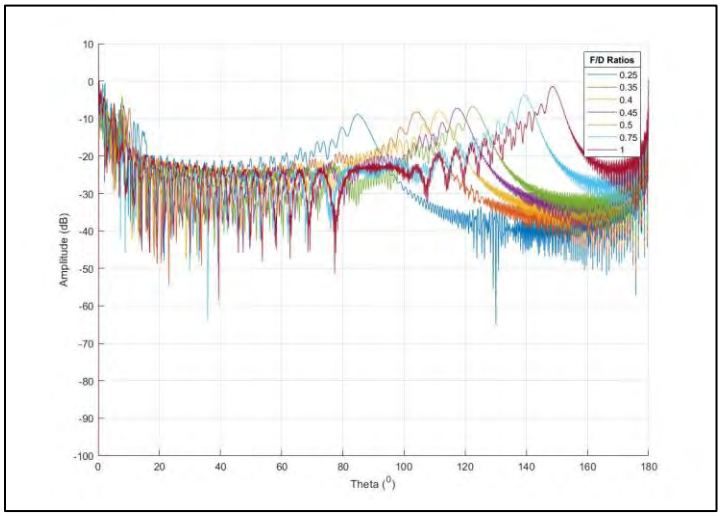

Figure 18. Cross-polarization radiation pattern of 6m Cassegrain antenna with varying MR F/D ratios from 0 to 180^0 θ.

It is clear in Figure 17 and 18 that the 60^0 to 80^0 θ range is most affected by changing the F/D ratio of the main reflector. The peaks of the back lobes seem to increase on a parabolic trend as they increase in amplitude and move further toward the edge of the pattern at $180^0\theta$. This trend could be important to an antenna designer concerned with fratricide due to the large back lobes. Again, it is important to note that no other parameters were changed besides the F/D ratio. This small case study was provided to highlight the possible effect of increasing or decreasing the F/D ratio alone.

The SR alone can be described by the diameter and the eccentricity, or curvature of the dish, where a value of 0 would be a circle, a value of ∞ would be a straight line, and a value of 1 would be a parabola. The eccentricity of a SR for a Cassegrain system will always be greater than 1 to satisfy the hyperbolic nature of the SR. The general equation for eccentricity can be seen in Equation (2.21) where f is half the distance

between foci and a is half the distance between the major axis. See Figure 19 for a visual representation of the f and a parameters.

$$e = \frac{f}{a} \tag{2.21}$$

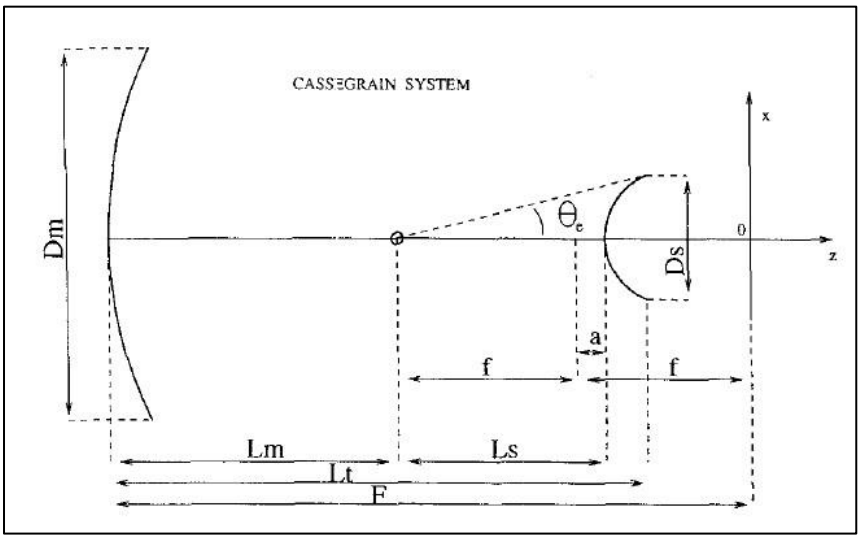

Figure 19. Diagram of SR geometry showing f and a for the center-fed Cassegrain system [3].

From Figure 19, it is clear to see that the parameter a can be found by taking the difference of Ls, the distance from the feed to the SR, and f, the focal length of the SR as in Equation (2.22).

$$a = Ls - f \tag{2.22}$$

Based on Equation (2.20) and (2.21), GRASP will automatically choose the positioning of the SR to ensure the focal length of the MR and SR are aligned. As the eccentricity is increased, the SR will move closer to the feed to allow proper illumination of the MR. It is also important to note that the value of Lm will be held to 0 for the center

fed Cassegrain, that is, the feed is placed at the surface of the MR. Also note that Lm will be used interchangeably between the center fed and offset, however, the value for the offset is considered a function of Ls in Figure 7. The values of SR eccentricity chosen for this work will be 1.1 to 1.5 to satisfy the hyperbolic nature of the SR.

2.8 Design of Experiments

Originally conceptualized for agricultural purposes, DOE was developed by Ronald A. Fisher in the 1920s [13]. DOE aims to find relationships and correlation in multivariable experiments. This is a perfect approach to have if variables may influence other variables simultaneously. Due to the nature of antenna systems, a DOE approach is suited to gain the most understanding of how the variables will change the outcome. One of the most common DOE approaches, the *full factorial* is a method where all possible combinations of an experiment are performed. The full factorial approach can be easily understood in Equation (2.23) where n is the number of experiments, x is the number of replications, L is the number of levels, and f is the number of factors.

$$n = xL^f \tag{2.23}$$

For example, in Equation (2.23), x could represent the number of different antennas under investigation; two in the case of this work. The number of levels L would be considered the number of parameters/variables changing in each experiment. The factors f would essentially be the step size within each parameter. For two antennas with

three parameters and ten factors for each parameter, the number of experiments required to perform a full factorial DOE would be $n = 2(3)^{10} = 118{,}098$ simulations. It is important to note that in this example, each parameter has equal step-sizes (10 in this case). The full factorial approach can quickly become inefficient. This is where the *fractional factorial* approach comes into play.

As the name suggests, the fractional approach only takes a fraction of the factors to determine the experiment size. An adjustment on the example above for a fractional approach would be to select the factors within each parameter that represent a *low, medium,* or *high* value within the range selected. This would cut down the total factors to three per level. The total number of experiments would then be reduced to $n = 2(3)^3 = 54$. Further reducing the number of factors would greatly reduce the number of experiments, however, there is a price in the form of lost information. To alleviate this downside, proper factors must be chosen carefully. Furthermore, step-sizes can be altered within each parameter to decrease or increase the overall simulation count.

For instance, initially choosing only high or low values for each level may lead to optimizing a certain output. Once that output is optimized, choosing a new high/low value from the newly optimized parameters may confirm the decision to optimize the output. If the newly chosen factors yield an even more optimized result, the process can continue until a fully optimized output is achieved. It is the goal of this work to optimize and compare outputs from the center fed and offset Cassegrain antennas using a fractional factorial approach. Furthermore, the step size within each parameter will differ in size. Because the step sizes between each parameter will be different, the possible combinations will reduce to simply the product of each step size. For example, six values

of F/D, five values of Ds/Dm, three values of subreflector eccentricity e, and two values of feed taper will simply be $n = 6 * 5 * 3 * 2 = 180$ simulations. Chapter 3 will discuss more of the methodology of this approach.

A subsequent test known as analysis of variance (ANOVA) is used to support the DOE factorial approach. ANOVA aims to seek out statistical relationships between groups within the data set. Going into depth on ANOVA is outside the scope of this work, however, a brief explanation of the charts that will be presented in Chapter 4 is necessary to understand the results. See Table 3 for an example of the ANOVA results that will be presented in this work. From the top of Table 3, the R^2 value is known as the *coefficient of determination*. The R^2 value gives a fair idea of how much variability being explained by the given parameters. In Table 3, the R^2 value is 0.991, meaning 99.1% of the variability of the data is being explained by the parameters (on a scale from 0 to 1). The parameters are then listed individually, then in pairs to show how the combination of parameters affected the variability of the data. The bold numbers in Table 3 are highlighting the F-statistic and p-value. A p-value of greater than 0.05 will typically mean you can accept the *null hypothesis*, which is a claim that the parameters have no effect on the variability of the data. Notice in Table 3 that the p-values are all zero, meaning we can reject the null hypothesis. Now look at the F-statistic values; the higher the value, the more variability associated with the parameter.

R^2	0.991				
Source	DF	Sum of squares	Mean squares	F	Pr > F
F/d	5.000	7.985	1.597	**23.685**	**0.000**
Ds/Dm	4.000	111.717	27.929	**414.219**	**0.000**
Ecc	2.000	3515.551	1757.775	**26069.560**	**0.000**
F/d*Ds/Dm	20.000	6.499	0.325	**4.819**	**0.000**
F/d*Ecc	10.000	17.112	1.711	**25.379**	**0.000**
Ds/Dm*Ecc	8.000	62.090	7.761	**115.107**	**0.000**

Table 3. Sample three-way factor ANOVA result.

III. Methodology

3.1 Preamble

The analysis of the center fed Cassegrain and offset Cassegrain will begin by presenting the methods used to extract maximum gain with respect to the F/D ratio. The subsequent parameters Ds/Dm, subreflector (SR) eccentricity, and feed taper will also be compared with the F/D ratio. The second set of simulations will allow GRASP to choose an appropriate Ds/Dm ratio while the distance between the main reflector (MR) vertex and the feed Lm is varied. The CEM's discussed in Chapter 2 will be used to simulate the prescribed geometry and parameters, while MATLAB will be used process and generate the data into a spreadsheet for further analysis. The data and plots generated in this work must be free from ambiguity. Therefore, a definition and physical example of theta (θ) and phi (ϕ) will be given first.

3.2 Theta and Phi Definition

The simulations performed incorporate the entire 360^0 radiation pattern where $\theta = -180^0 - 180^0$. In terms of the coordinate system used, this is rotation around the y-axis where theta sweeps from the z-axis clockwise towards the x-axis in the positive direction. On the other hand, the elevation ϕ rotates around the z-axis where phi sweeps from the x-axis counterclockwise towards the y-axis in the positive direction. See Figure 20 and 21 for a physical definition of theta (θ) and (ϕ).

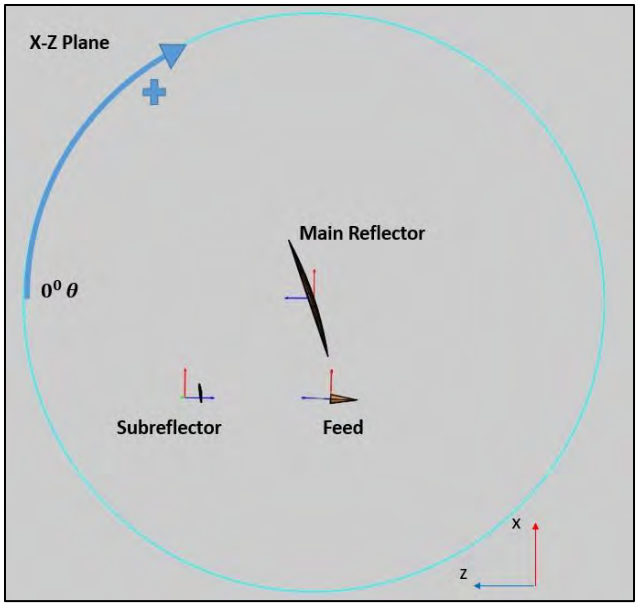

Figure 20. Physical representation of θ with positive rotation around the y-axis using a generic offset Cassegrain model.

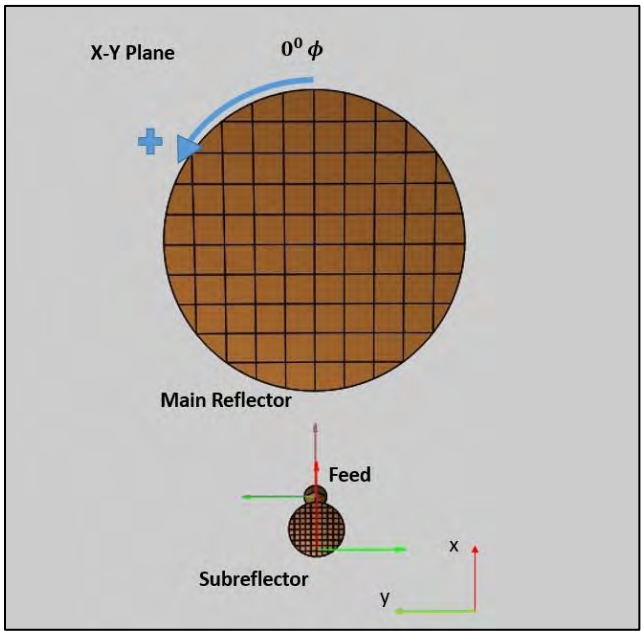

Figure 21. Physical representation of ϕ with positive rotation around the z-axis using a generic offset Cassegrain model.

3.2 Data Verification

As stated in Chapter 1, the Ohio State University proprietary software SATCOM will be compared with the GRASP SE outputs to verify the data. This will be done by choosing one design from GRASP SE and manually transferring all parameters to SATCOM. The output graphs will be overlayed, and a separate graph will show the decibel differences between the two sets of data. The data verification results will be presented in Chapter 4.

3.3 Data Collection Approach

Using the design of experiments (DOE) approach as mentioned in Chapter 2, all possible combinations of parameters will be modeled and simulated. The entire 360 degree θ range to include $0^0, 45^0$, and 90^0 ϕ elevation angles will be included. The parameters that will be varied are the focal length to diameter F/D ratio, the subreflector to main reflector diameter Ds/Dm ratio, the subreflector eccentricity e, and the feed taper. To prevent an intractably large number of simulations, logical step-sizes were chosen based off of the parameter ranges in Chapter 2. See Table 4 For a tabular breakdown of the parameters of interest, step-sizes, ranges, and totals (per antenna variant).

Parameter	Range	Step-size	Total Changes
F/D	$1\ to\ 1.25$	0.01	6
Ds/Dm	$0.12\ to\ 0.16$	0.01	5
$eccentricity$	$1.1\ to\ 1.3$	0.1	3
$feed\ taper$	$-12\ to\ -10\ dB$	2	2
		Total simulations needed	**180**

Table 4. Parameters of interest, range values, step-sizes, total changes, and total simulations needed per antenna variant.

A second set of parameters were chosen due to the abnormalities in the back lobe analysis. These abnormalities will be covered in Chapter 4; however, a new table was derived, and a new parameter was chosen to be varied: the distance between the main reflector vertex and the feed, Lm. See Figure 19 for a physical representation of Lm. Furthermore, instead of varying the Ds/Dm ratio, GRASP SE was allowed to automatically choose the subreflector diameter and Lm was varied. See Table 5 for the second set of parameters chosen. In both sets of parameters, the total number of simulations (i.e., all possible combinations) were derived from the product of the total changes of each parameter.

Parameter	Range	Step-size	Total Changes
F/D	$1\ to\ 1.25$	0.01	6
Lm	$0\ to\ 1$	0.5	3
$eccentricity$	$1.2\ to\ 1.5$	0.05	7
$feed\ taper$	$-12\ dB$	1	1
		Total simulations needed	**126**

Table 5. Second set of parameters of interest, range values, step-sizes, total changes, and total simulations needed per antenna variant.

A numbered list of the pertinent parameters were developed to ensure all possible combinations were accounted for. The simulations, numbered 1 to n were listed by F/D ratio, Ds/Dm ratio (or Lm for the second set of simulations), eccentricity e, and feed taper. See Table 6 for an example of the master list layout.

Simulation Number	F/D	Ds/Dm	$eccentricity$	$feed\ taper$
1	1.0	0.12	1.1	-12
2	1.0	0.12	1.1	-10
…	…	…	…	…
180	1.25	0.16	1.3	-10

Table 6. Example of the simulation master list layout for the first set of parameters.

GRASP SE was used to simulate the antenna designs in Table 4 and 5. To ensure smooth plotting in MATLAB, each run in GRASP SE required 5,313 data points per ϕ elevation value; 15,939 points each simulation. The data was exported from GRASP SE to MATLAB where the data was organized and processed to extract the outputs of interest. The data was then exported to a spreadsheet and columnized for further processing and plotting via MATLAB. Rather extensive scripting was required to properly organize and process the data from GRASP SE. The scripts can be made available upon request.

Since the F/D ratio was separated into six different values (i.e., 1, 1.05, 1.1, 1.15, 1.2, 1.25), for the first set of parameters in Table 4, each value of F/D was allotted 30 simulations each. This allowed the proper combination of the Ds/Dm, eccentricity e, and edge taper to be accounted for. For the second set of parameters in Table 5, each F/D value needed 21 simulations to properly account for the remaining parameters. Note:

when referring to a single simulation, it is implied that it also encompasses three ϕ elevation values.

3.4 Fratricide Ratio

Due to the potentially destructive nature to equipment and personnel, high power microwave (HPM) back lobe analysis must be considered [18]. Initial consideration was given to the maximum value, in dB, of the back lobes. However, this did not account for the total energy found in the back lobes, only a small portion. Furthermore, the peak back lobe value is not considering the entire 360 degree θ radiation pattern. The term *fratricide ratio* denoted F_r, attempts to relate the total energy apparent in the frontal lobes of the antenna to the back lobes. Once the fratricide ratio is known, accompanied by power output from the feed, an estimate of the effects due to back lobes can be estimated without requiring a full simulation to generate irradiance profiles [19]. This level can then be compared to the appropriate standard of application, such as personnel exposure in the telecommunication industry of 100 mW/cm^2 in the range of 0.3-3.0 GHz in occupational exposures [20]. The "frontal lobes" of the antenna are defined as the entire area encompassing -90 to 90 degrees θ. The rest of the area not included in the frontal lobe section is comprised of back lobes. This straight-forward technique can be described generally by Equation (3.1), expanded in Equation (3.2), and the MATLAB implementation in Equation (3.3). See Figure 22 for a physical representation of the front and back area of the center fed Cassegrain antenna. See Figure 23 for an example of the front and back areas of the radiation pattern.

$$Fratricide\ Ratio\ F_r = \frac{P_{back}}{P_{front}} \tag{3.1}$$

$$F_r = \frac{\int_{-180^\circ}^{-90^\circ} ||G|| + \int_{90^\circ}^{180^\circ} ||G||}{\int_{-90^\circ}^{90^\circ} ||G\,||} \tag{3.2}$$

$$F_r = \frac{\sum_{-180^\circ}^{-90^\circ} ||G|| + \sum_{90^\circ}^{180^\circ} ||G||}{\sum_{-90^\circ}^{90^\circ} ||G||} \tag{3.3}$$

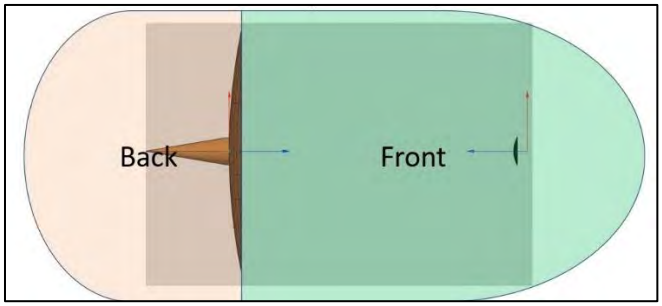

Figure 22. Physical representation of the front and back areas of the center fed Cassegrain antenna.

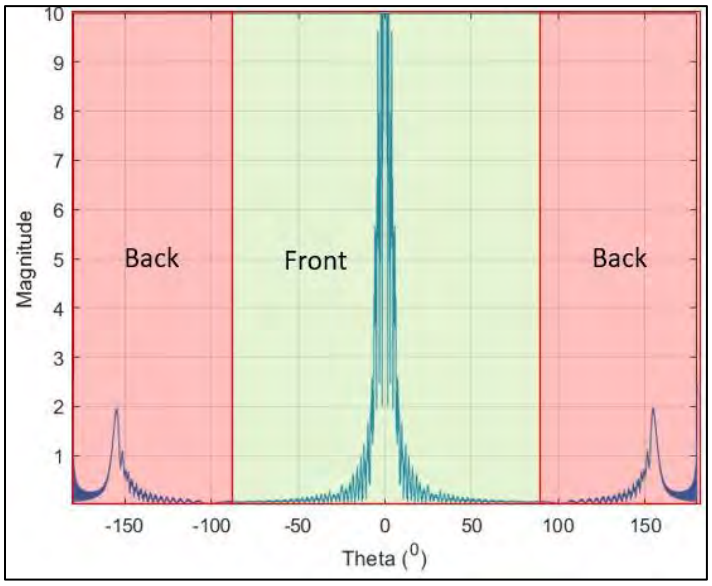

Figure 23. Example of magnitude plot with partitioned front/back portions of the 360 degree θ radiation pattern.

IV. Analysis and Results

4.1 Preamble

This Chapter will present the data collected and processed based on the methodology described in Chapter 3. The primary focus of this chapter will be presenting the results with respect to the F/D ratio. Most figures in this chapter will show all six F/D ratio values overlayed on each other versus the output of interest (max gain, half power beamwidth (HPBW), side and back lobe levels). Observations will be made based on the graphical data to attempt to find connections between the other parameters of interest (i.e., Ds/Dm, eccentricity e, edge taper, and Lm). Subsequently, two sets of parameters were used due to the abnormal back lobe energy observed in the first set of parameters. The results from the first set of parameters will be presented, followed by the results from the second. Furthermore, comparisons will be made between the center fed and offset fed Cassegrain results following each set of data.

4.2 First Parameter Set Results

Center fed Cassegrain results will be presented first, followed by the offset Cassegrain results. This section contains the results from both antenna variants for the first set of parameters in Table 4. Following the results, some comparisons will be made between the two variants, along with the corresponding F/D ratios.

4.2.1 Center Fed Cassegrain Results

The first set of parameters yielded a total of 180 simulations for the center fed Cassegrain antenna with an operating frequency of 10 GHz. Parameters were altered systematically to account for all possible scenarios as laid out in Chapter 3. See Figure 24 for the maximum gain values for each F/D ratio vs. simulation number. Only $\phi = 0^0$ is shown due to the identical nature of all three ϕ-values. The simulation number can be thought of as the search area, because each F/D value is allotted 30 simulations each.

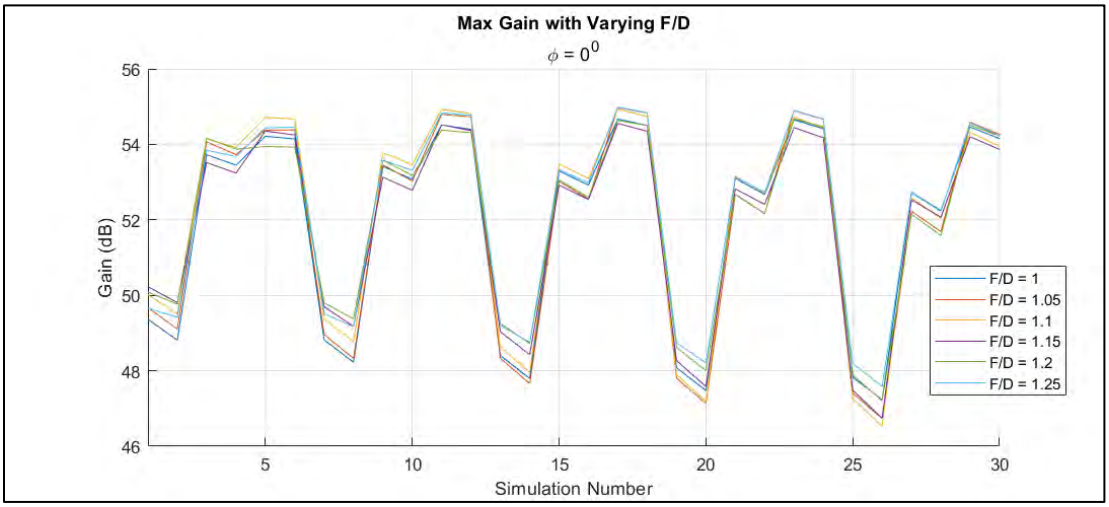

Figure 24. Peak gain values with varying F/D ratios over the search area; $\phi = 0^0$, 6m center fed Cassegrain antenna, operating frequency: 10 GHz. Note: max gain is identical to all three ϕ-values.

No correlation between F/D and maximum gain for the given parameters can be observed. The largest difference between the individual F/D ratios and maximum gain was observed to be no more than 1dB. Figure 24 presents some interesting patterns that were investigated. The eccentricity had the largest effect on the maximum gain. This observation can be seen in Figure 25 and explains the step-up/down nature of the gain

chart. Each eccentricity value was given two simulations to account for the two different feed taper values. Therefore, there are minor deviations for each eccentricity value. See Figure 26 for this observation. Finally, the Ds/Dm was observed to be inversely proportional to the max gain value. See Figure 27 for the Ds/Dm effect on the maximum gain. Notice that the chart has global minima – highlighted by the red line in Figure 27 – as the Ds/Dm increases. Since the main reflector diameter does not change, the Ds/Dm is merely increasing/decreasing the subreflector diameter. Therefore, a larger subreflector diameter will not aid in blockage efficiency.

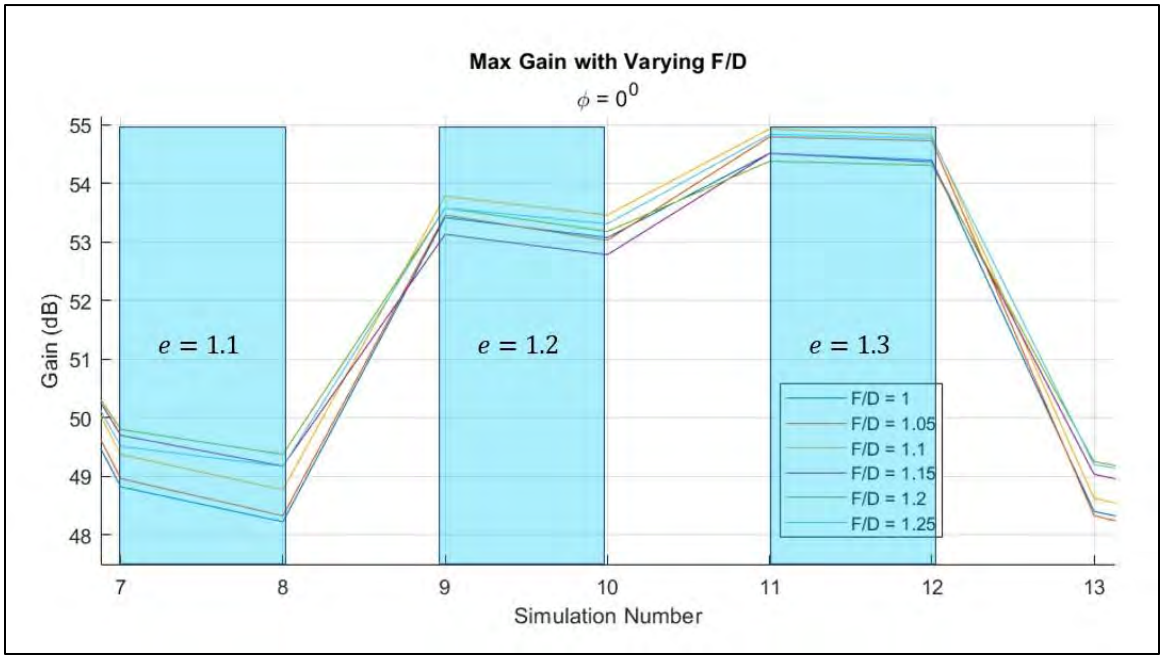

Figure 25. The repeating pattern effect of varying the subreflector eccentricity over the search area.

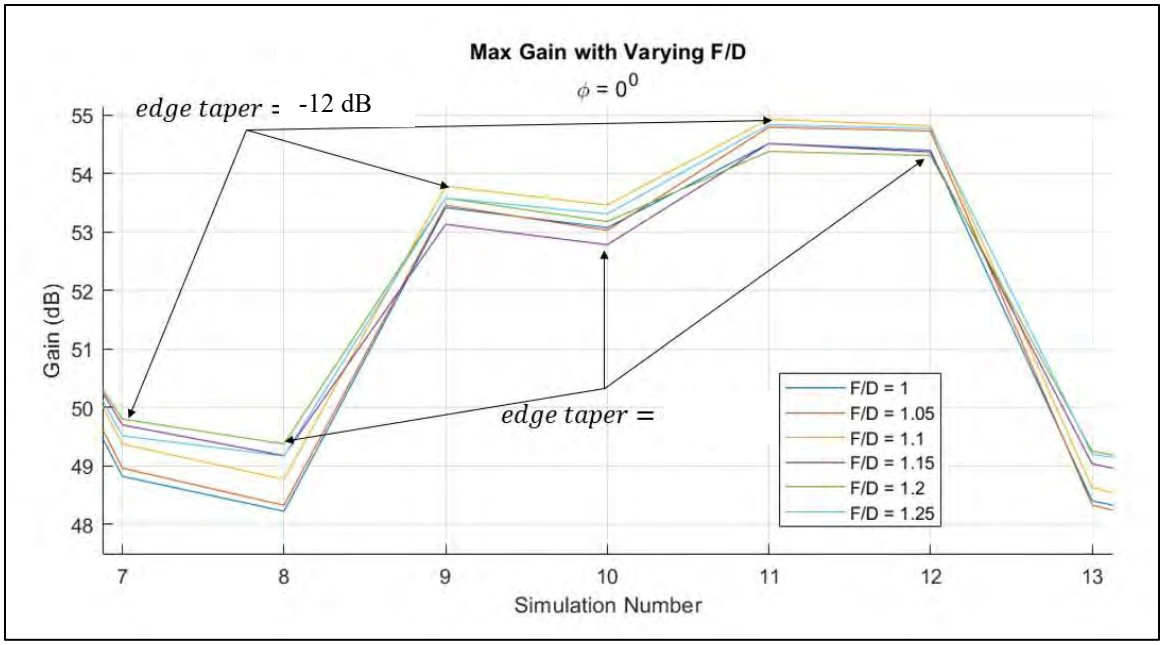

Figure 26. The repeating pattern effect of varying the feed edge taper value over the search area.

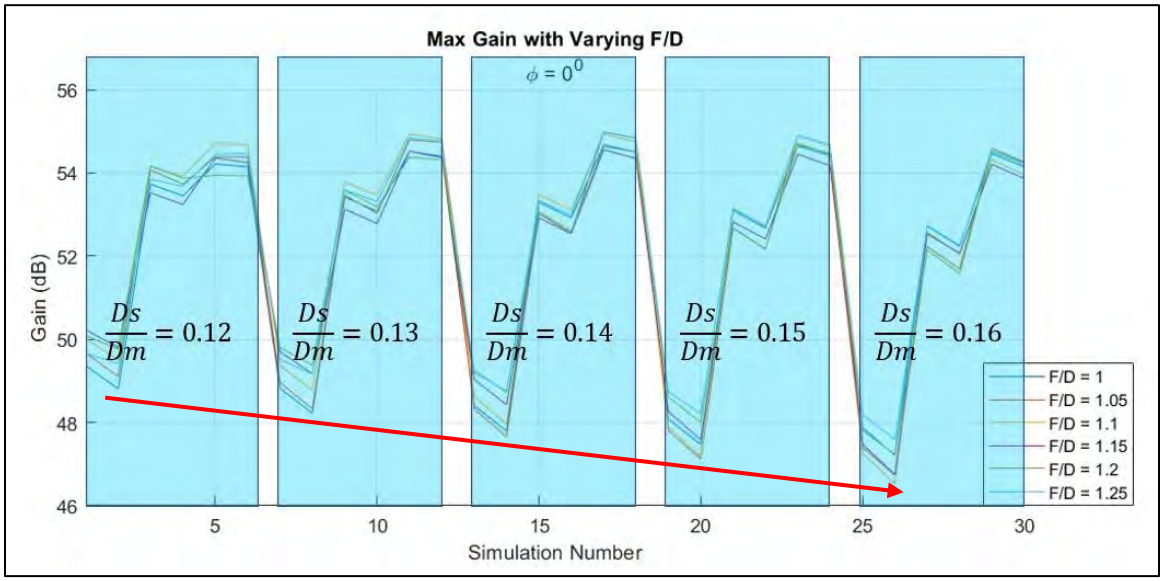

Figure 27. The repeating pattern effect of varying the Ds/Dm over the search area. General trend denoted by red line.

The next output investigated was the half power beamwidth (HPBW). See Figure 28 for the HPBW output with varying F/D values. The differences between the ϕ values and the HPBW were negligible i.e., 0.006^0 at most, therefore only $\phi = 0^0$ is shown. There was no clear correlation between the individual F/D ratios and the HPBW. However, other trends were observed with HPBW chart. For instance, the Ds/Dm was observed to decrease the HPBW for all F/D values. Notice the overall "compression" in HPBW values as the Ds/Dm increases in Figure 29. The eccentricity was also observed to play a role in the "spiking" in the HPBW data. See Figure 30 for the correlation between eccentricity values and the HPBW.

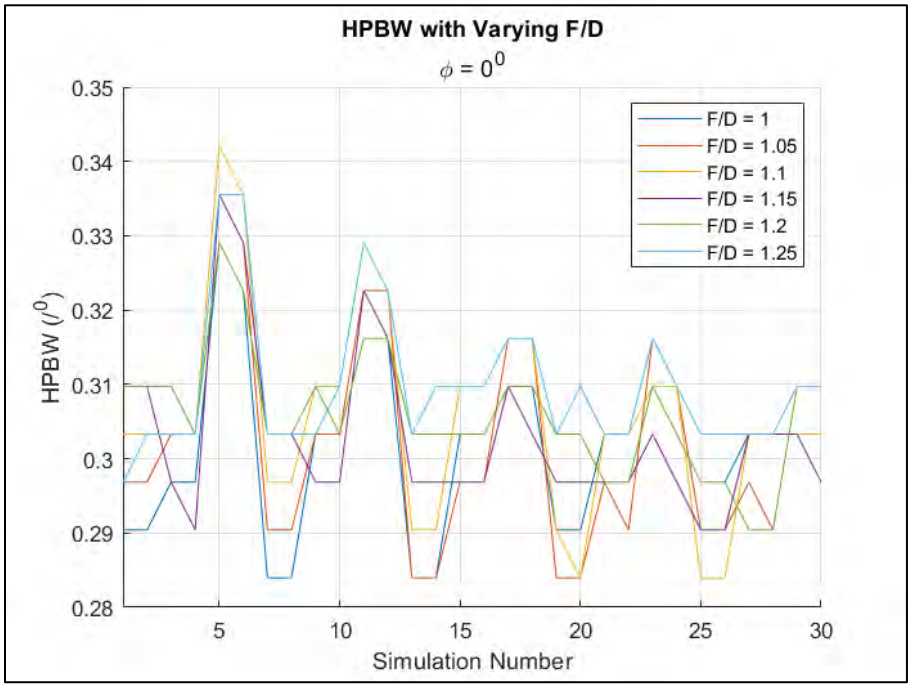

Figure 28. Half-power beamwidth (HPBW) over the search area for prescribed F/D values. Identical for all ϕ values.

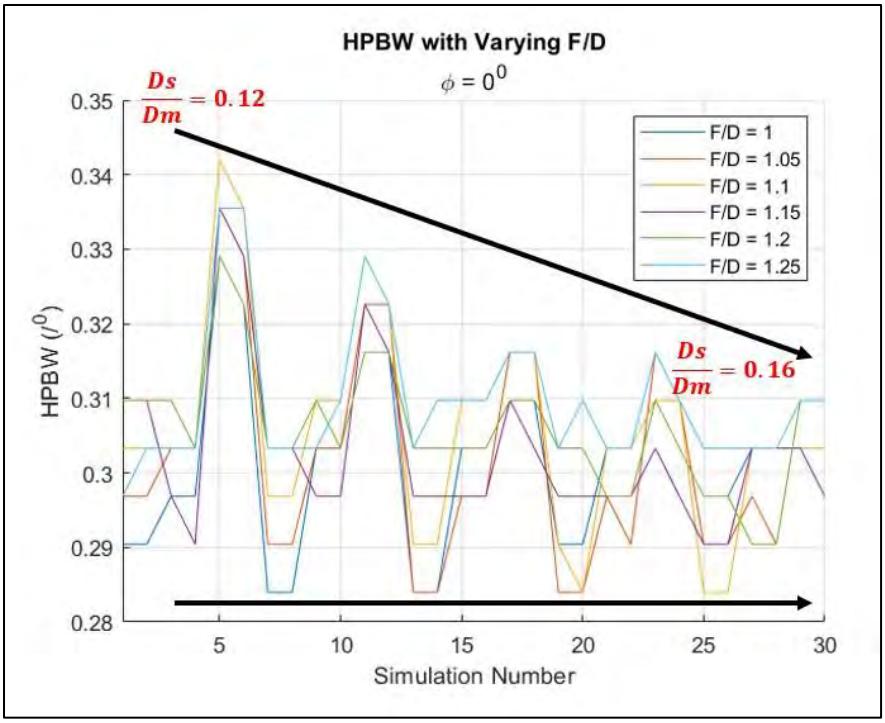

Figure 29. Effect of Ds/Dm on the HPBW denoted by the black trendlines.

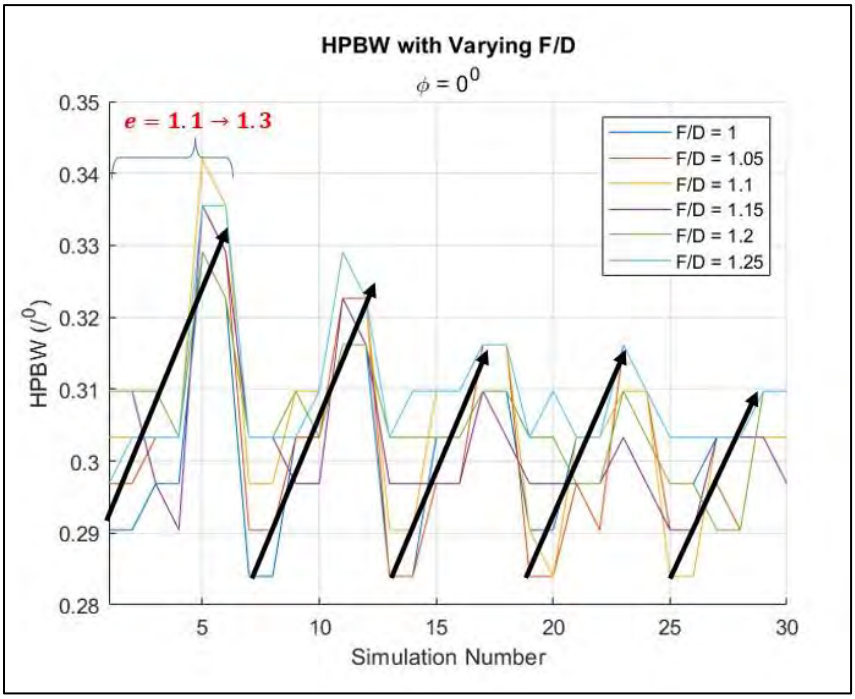

Figure 30. Effect of eccentricity on HPBW with varying F/D ratios denoted by the black trendlines.

The first sidelobe level was observed to vary greatly when the data was plotted against the search area. See Figure 31 for the first sidelobe level with varying F/D ratios. The difference between ϕ values were negligible, therefore only $\phi = 0^0$ is shown. Generally speaking, the larger F/D ratios (i.e., 1.15 to 1.25) gave the lowest gain levels, however, the fluctuations were much more rapid. The F/D value of 1.1 gave the least fluctuation and is highlighted in Figure 32. There is an overall converging trend as the Ds/Dm is increased, also denoted in Figure 32 by the red trendlines.

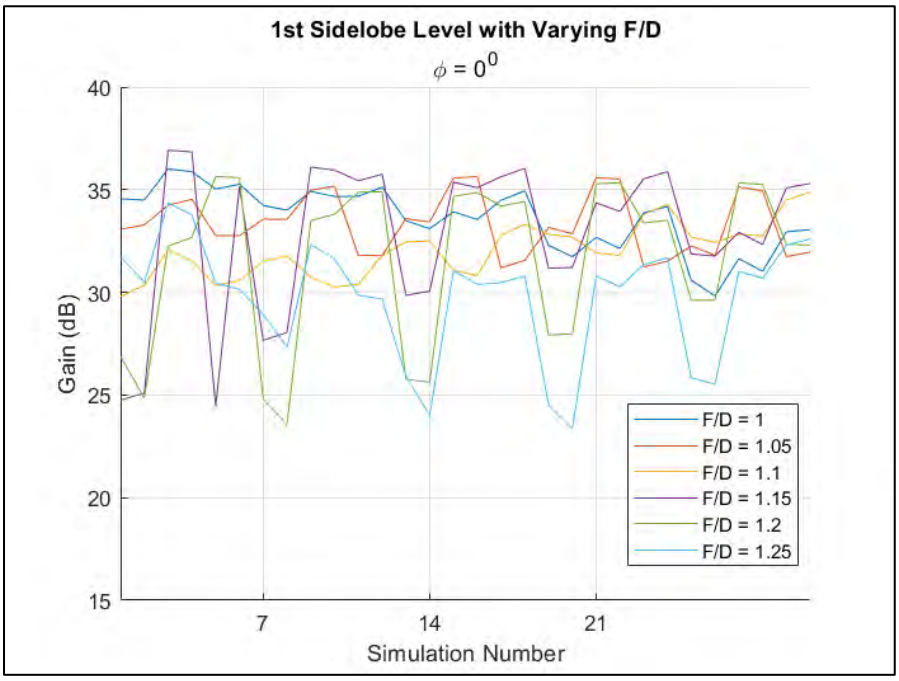

Figure 31. Gain value of the 1st sidelobe level for varying F/D ratios; negligible difference between ϕ values.

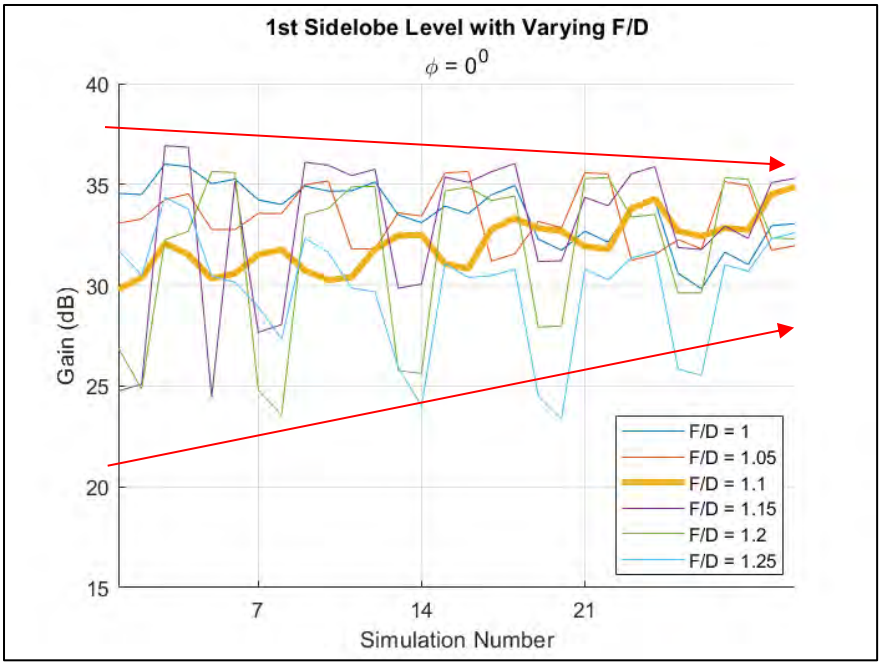

Figure 32. First sidelobe level convergence as Ds/Dm increases. Orange line depicting the most stable F/D ratio in terms of side lobe level gain.

The first sidelobe location was observed to be relatively the same across the F/D ratios. The exception to this was F/D values of 1.15 and 1.1. All other F/D values followed the same trend as the F/D value of 1.25 in Figure 33. As in previous observations, only $\phi = 0^0$ is shown due to negligible differences in data.

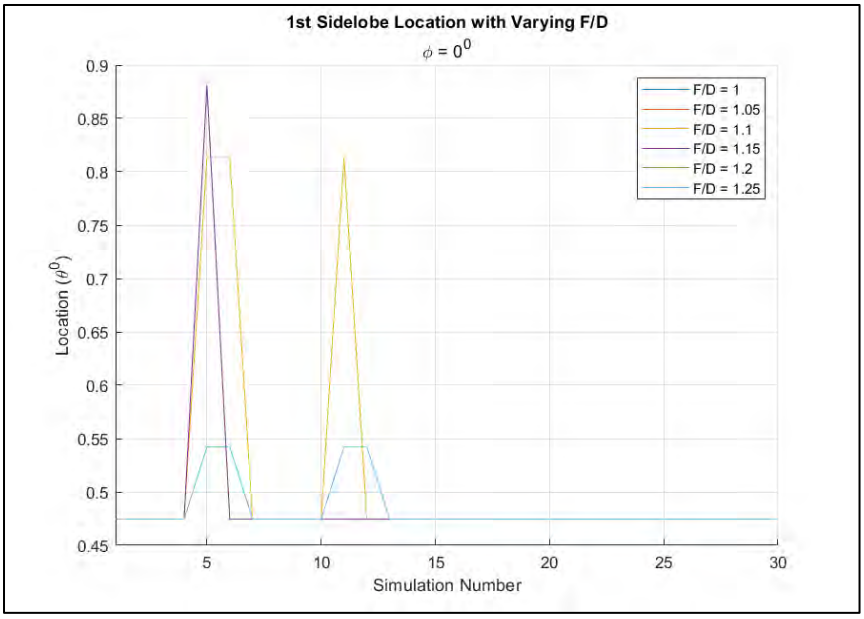

Figure 33. First sidelobe location for varying F/D ratios over the search area. Negligible difference between ϕ values.

Finally, the fratricide ratio was observed across all collected data for the center fed Cassegrain. There were very noticeable differences between the ϕ values, therefore Figures 34 through 36 show the fratricide ratio for $\phi = 0^0, 45^0, 90^0$ over the search area. For perspective, Figure 34 shows a maximum fratricide ratio of 0.77. That means that 77% of the energy apparent in the main/front lobes of the antenna are also apparent in the back lobes. This would require extreme hardening of systems as well as personnel safety measures. These fratricide ratio results were the main driving factor to use a second, more optimized, range of parameters for further analysis. The effects of the eccentricity are observed in Figure 37, where increasing the eccentricity drastically lowers the fratricide ratio. Conversely, as the Ds/Dm ratio increases, the fratricide ratio increases. See this relationship in Figure 38. Also note in Figure 35 that $\phi = 45^0$ has a much lower overall fratricide ratio as well as fluctuations.

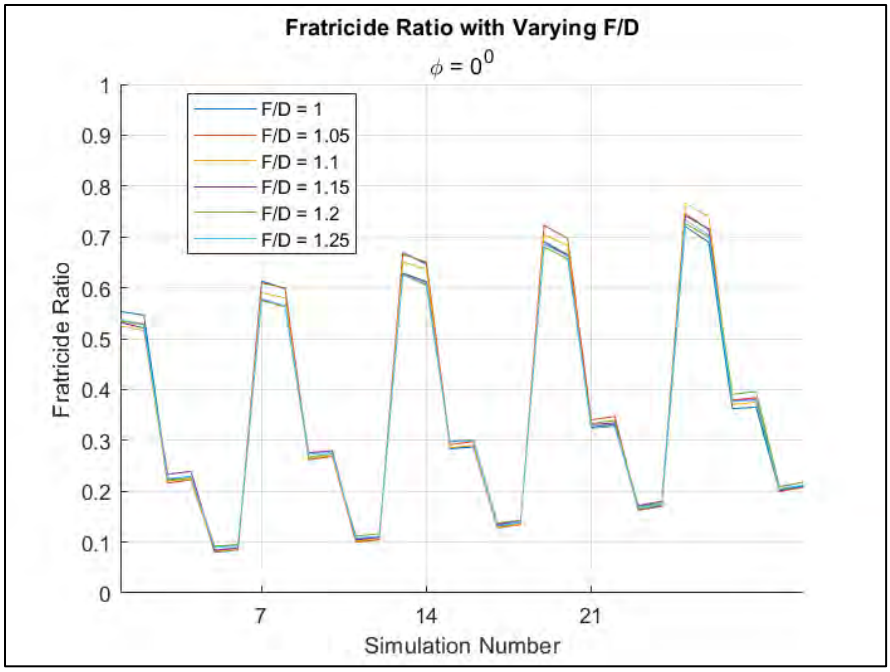

Figure 34. Fratricide ratio for varying F/D values over the search area; $\phi = 0^0$.

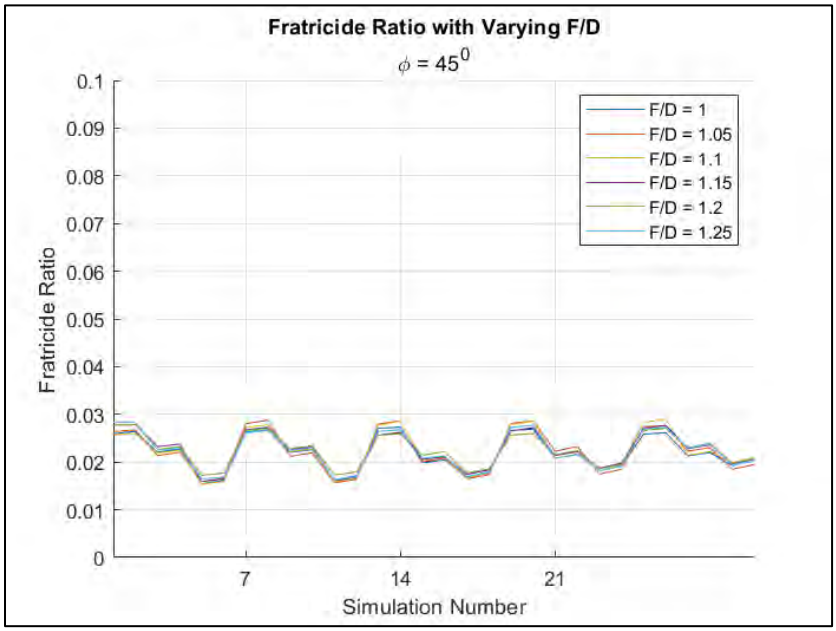

Figure 35. Fratricide ratio for varying F/D values over the search area; $\phi = 45^0$.

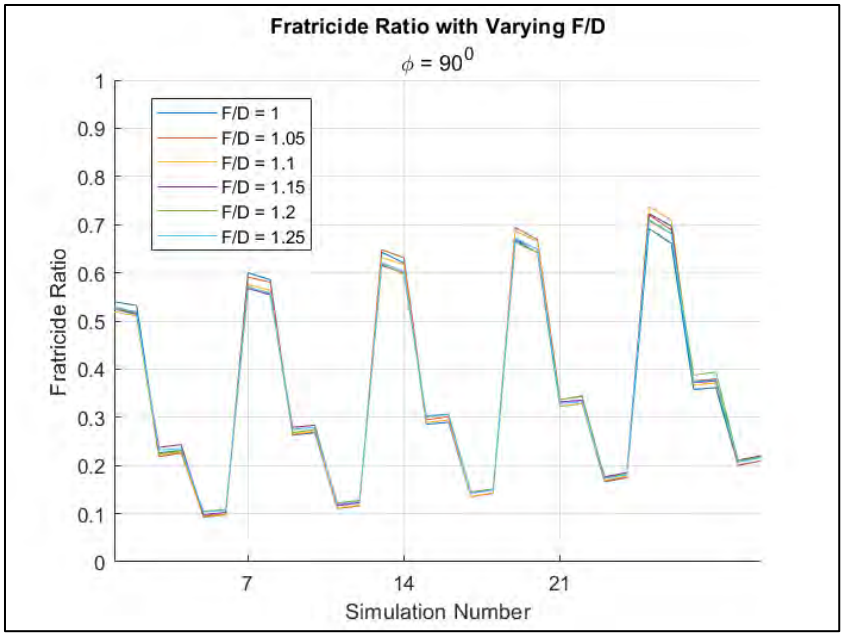

Figure 36. Fratricide ratio for varying F/D values over the search area; $\phi = 90^0$.

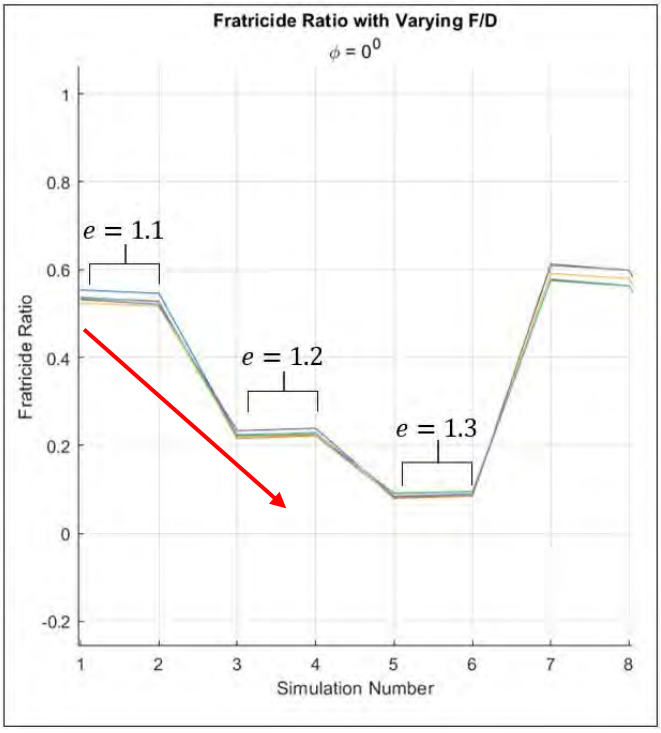

Figure 37. Effect of eccentricity on the fratricide ratio.

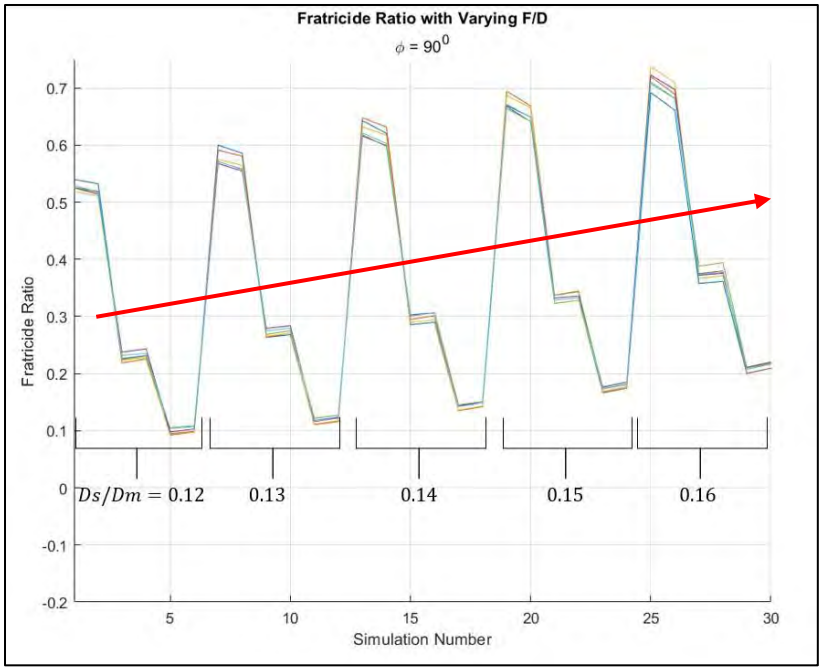

Figure 38. Effect of Ds/Dm on the fratricide ratio.

4.2.2 Offset Cassegrain Results

This section will show the results from the offset Cassegrain antenna using the first set of parameters in Table 4. The same pattern of plots will be presented as the previous section, beginning with the peak gain values over the search area. See Figure 39 for the peak gain values over the search area with varying F/D ratios. Data was uniform across all three ϕ values, therefore only $\phi = 0^0$ is shown. It was observed that lower values of F/D gave higher values of maximum gain. See Figure 40 for an expanded view of the maximum gain chart to see the difference between the F/D values at the given peaks. The F/D value of 1 had the highest average gain of 49.46 dB. Varying the eccentricity was observed to alter the gain values in an unintuitive way. Gain increased when eccentricity increased from 1.1 to 1.2, whereas gain decreased when eccentricity

was increased from 1.2 to 1.3. See Figure 41 for the relationship between eccentricity and peak gain values. The Ds/Dm ratio only affected the gain values slightly. A very subtle convergence can be seen in Figure 39, denoted by the red lines.

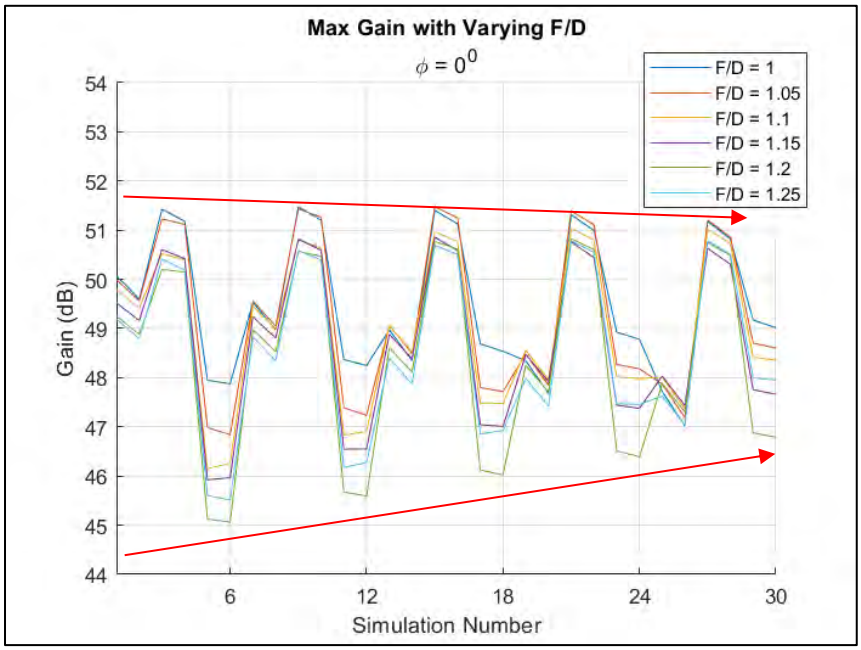

Figure 39. Peak gain value in dB for the offset fed Cassegrain antenna. Identical data between all three ϕ values. Subtle convergence denoted by red lines as Ds/Dm in increased.

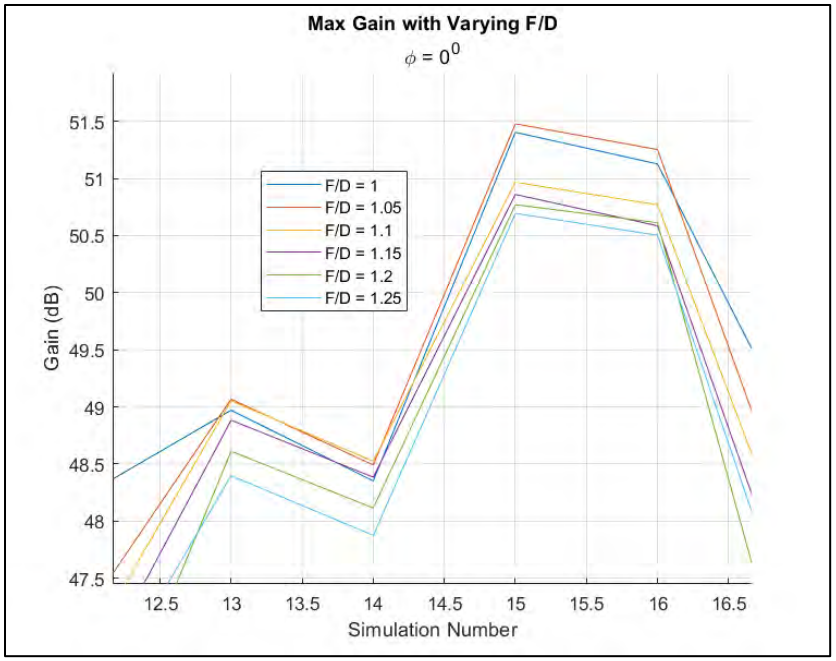

Figure 40. Expanded gain chart showing relationship between F/D and peak gain values.

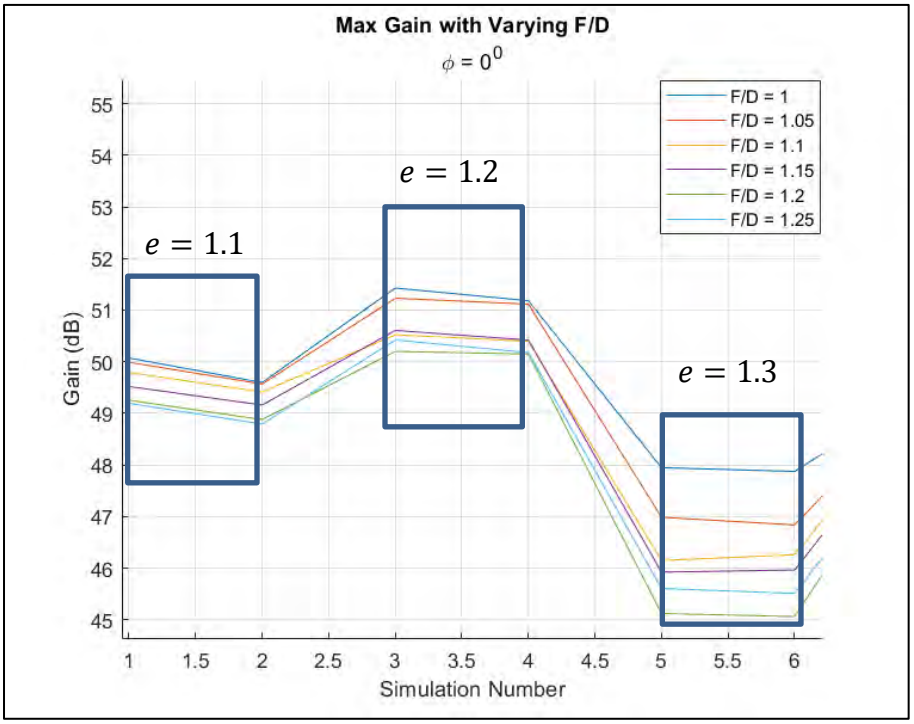

Figure 41. Effect of eccentricity on the peak gain value.

Unlike the center fed resutls, the HPBW across the ϕ values varied, therefore, all three are show in Figure 42 through 44. The HPBW increased as the eccentricity was increased. This relationship can best be seen using the less-noisy $\phi = 90^0$ chart in Figure 45. Ds/Dm was observed to narrow the beam when increased. See Figure 42 through 44 for the trend, denoted by the red arrows.

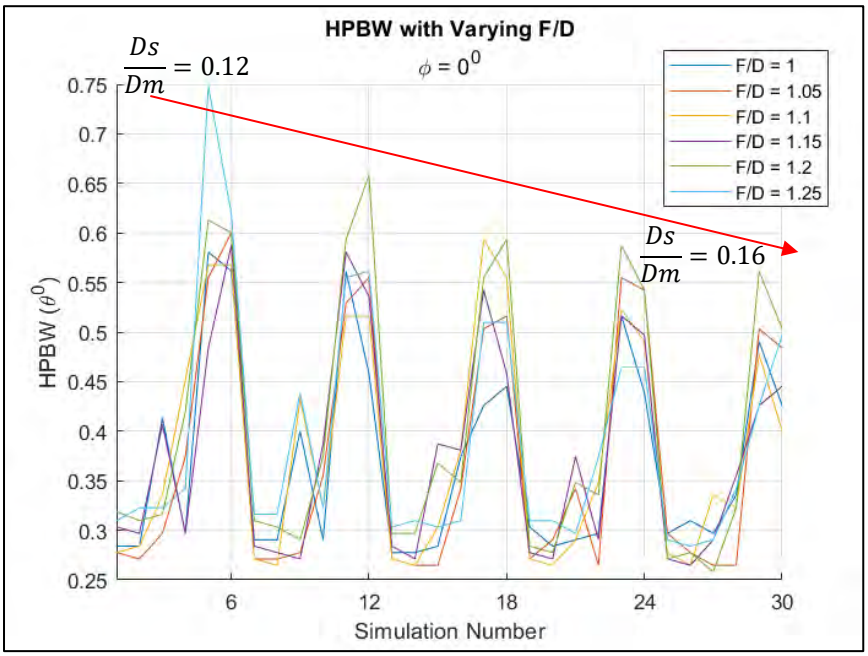

Figure 42. HPBW over the search area with varying F/D values for the offset fed Cassegrain. Red line denoting decreasing HPBW as Ds/Dm is increased.

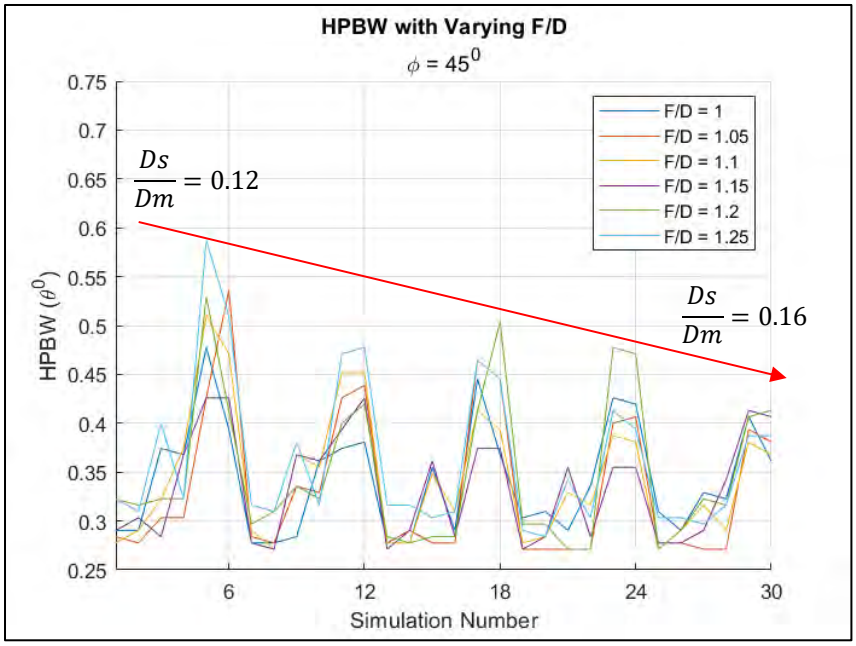

Figure 43. HPBW over the search area with varying F/D ratios over the search area for the offset fed Cassegrain. Red line denoting decreasing HPBW as Ds/Dm is increased.

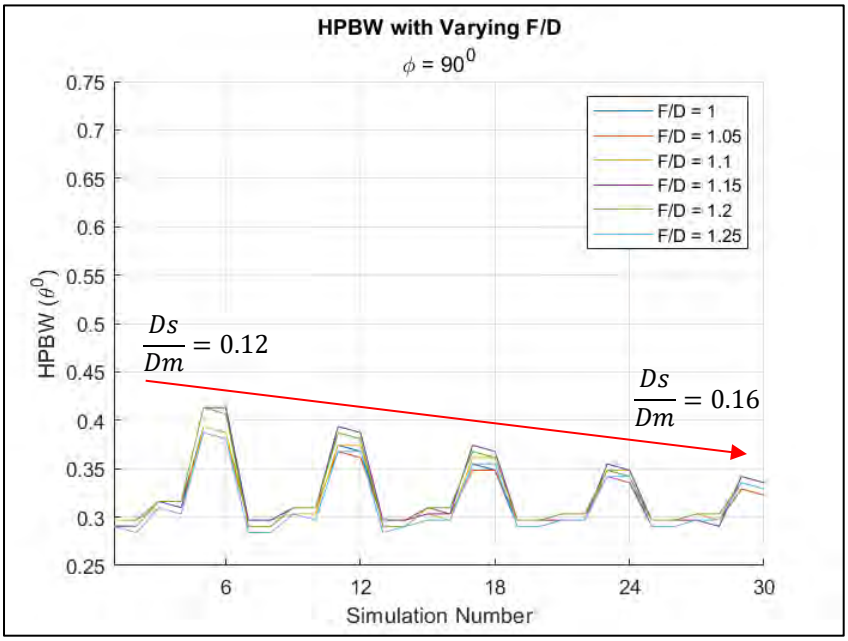

Figure 44. HPBW over the search area with varying F/D ratios over the search area for the offset fed Cassegrain. Red line denoting decreasing HPBW as Ds/Dm is increased.

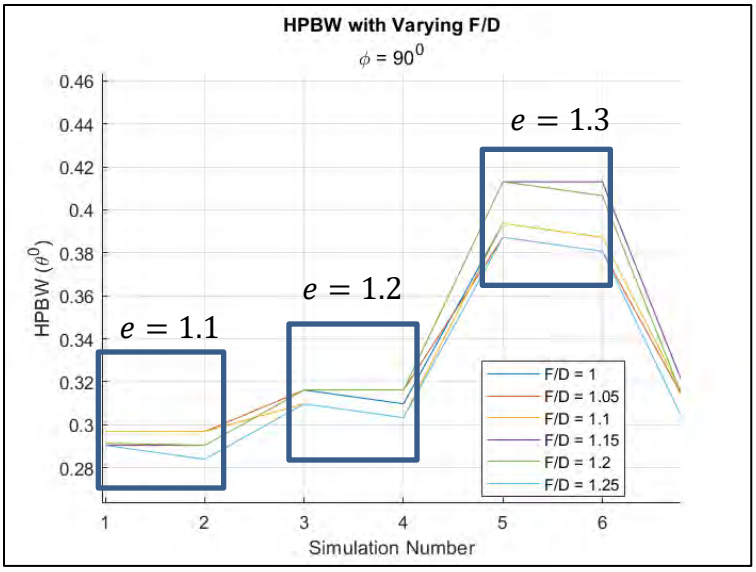

Figure 45. Effect of eccentricity on the HPBW.

For the first sidelobe level results see Figure 46 through 48. All ϕ values are shown due to the differences between the data. Gain attenuation in the first sidelobe level was observed to be the lowest with an F/D value of 1.2 apart from $\phi = 90^0$, where an F/D of 1.0 yielded the lowest sidelobe level. There is no clear correlation between the F/D value or the Ds/Dm and the first sidelobe level. However, observations can be made about varying the eccentricity. An eccentricity of 1.3 will yield a lower sidelobe level, whereas an eccentricity of 1.2 will yield the highest. See Figure 49 for an example of the effect of eccentricity on the first sidelobe level. Only one ϕ value is shown for the general repeating pattern.

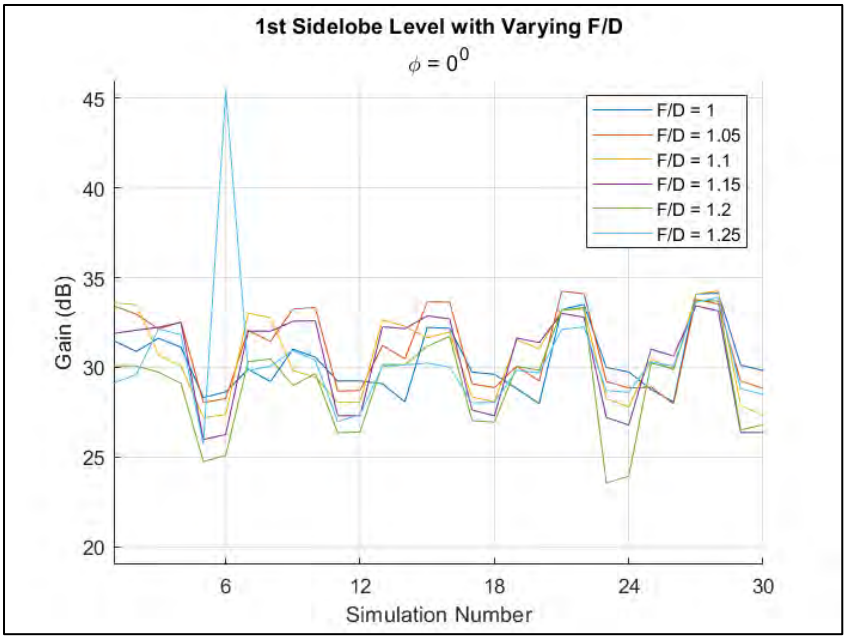

Figure 46. First sidelobe level gain with varying F/D ratios over the search area for the offset fed Cassegrain; $\phi = 0^0$.

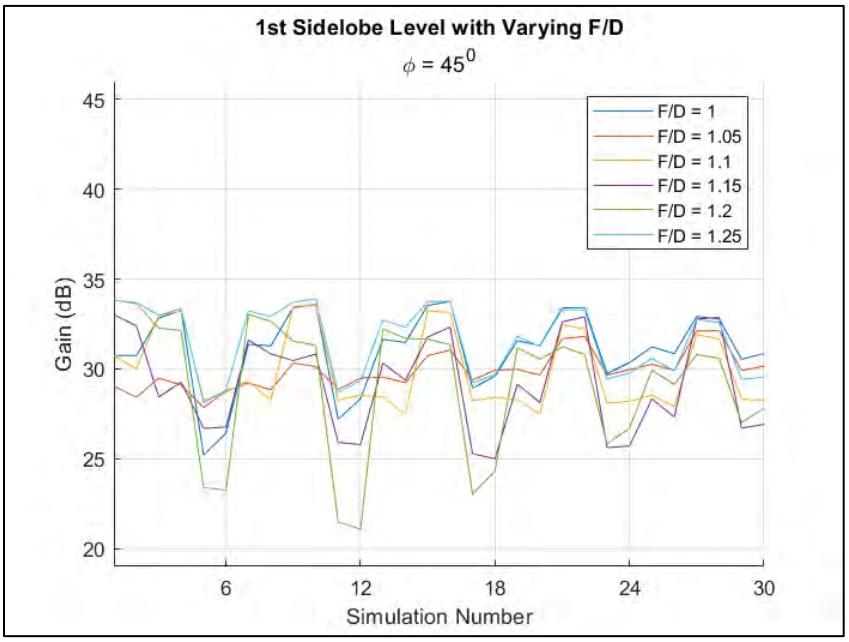

Figure 47. First sidelobe level gain with varying F/D ratios over the search area for the offset fed Cassegrain; $\phi = 45^0$.

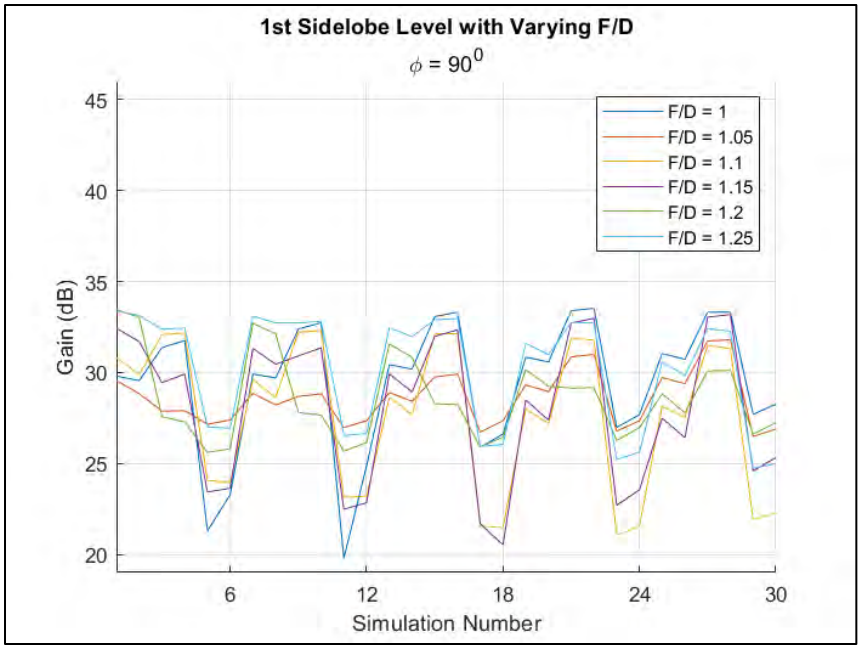

Figure 48. First sidelobe level gain with varying F/D ratios over the search area for the offset fed Cassegrain; $\phi = 90^0$.

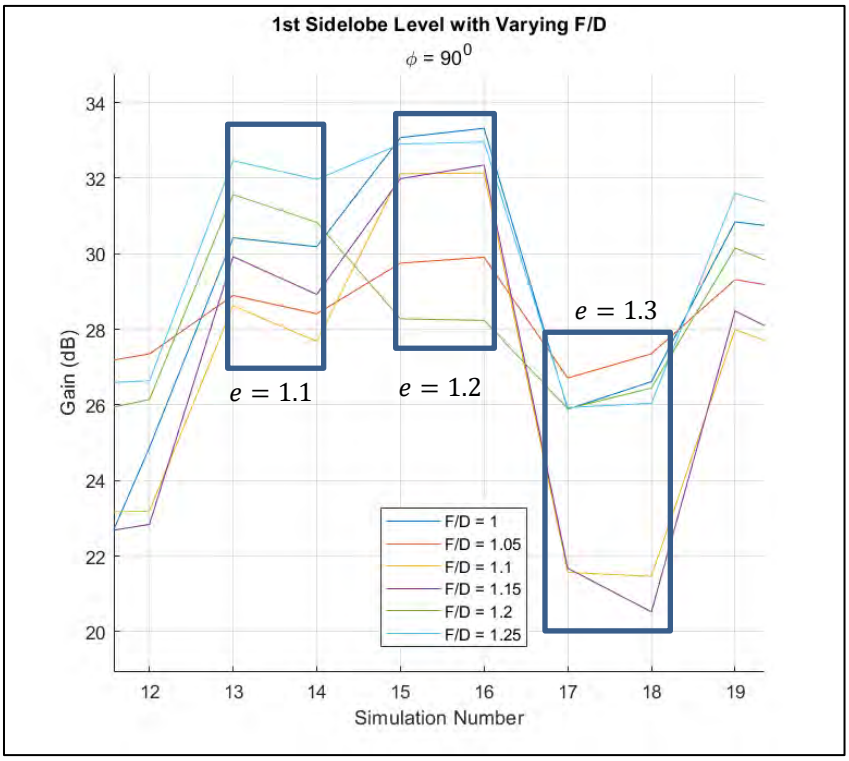

Figure 49. The increasing/decreasing effect of eccentricity on the first sidelobe level gain.

See Figure 50 through 52 for the first sidelobe location with varying F/D ratios. All three ϕ values are shown due to the differences in data sets. There is no clear correlation between the F/D ratio or the eccentricity and the first sidelobe location, however, a relationship exists between the Ds/Dm ratio and the first sidelobe location. In Figure 50 through 52, this relationship is shown using a red line. As Ds/Dm increases, the general trend is that the first sidelobe location decreases, that is, moves closer to the main lobe.

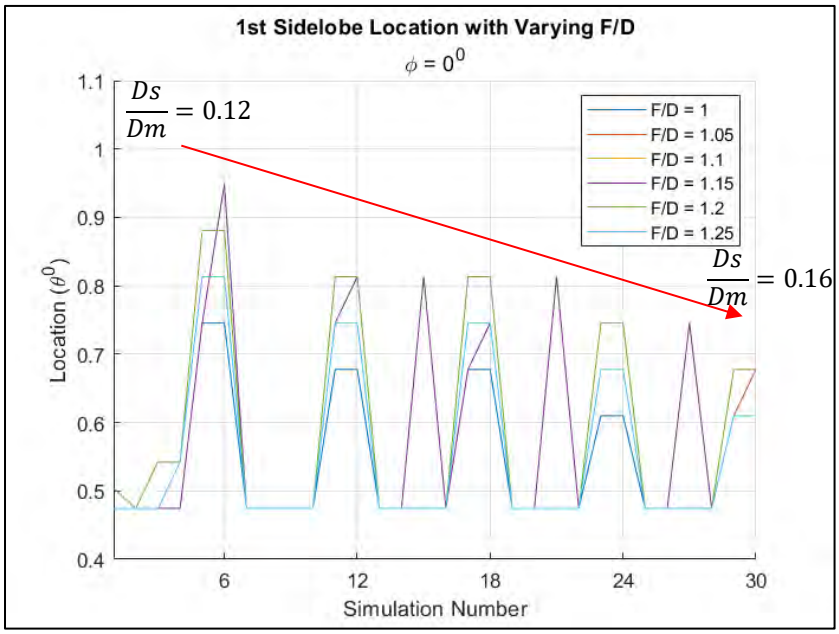

Figure 50. First sidelobe location with varying F/D ratios over the search area for the offset fed Cassegrain; $\phi = 0^0$.

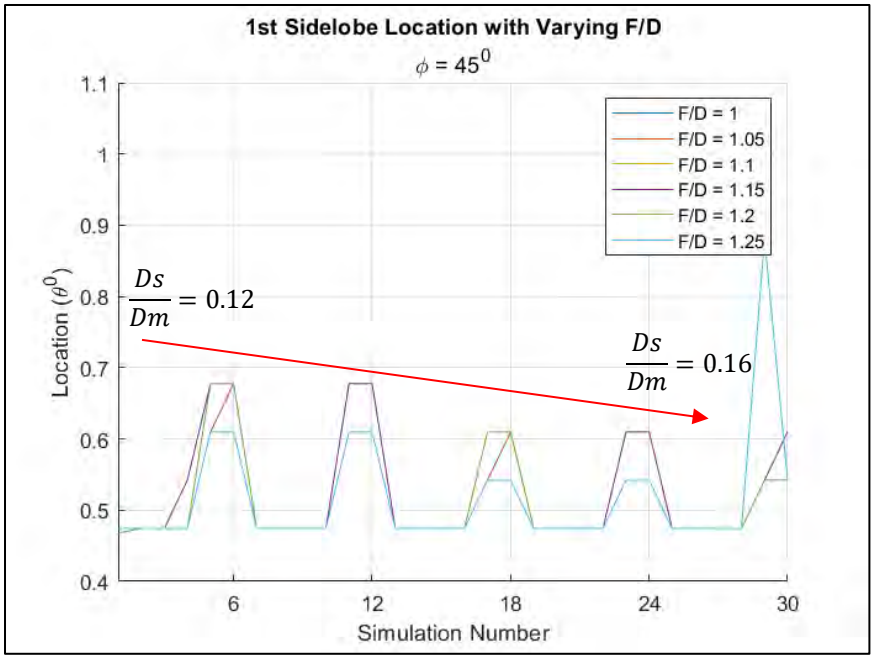

Figure 51. First sidelobe location with varying F/D ratios over the search area for the offset fed Cassegrain; $\phi = 45^0$.

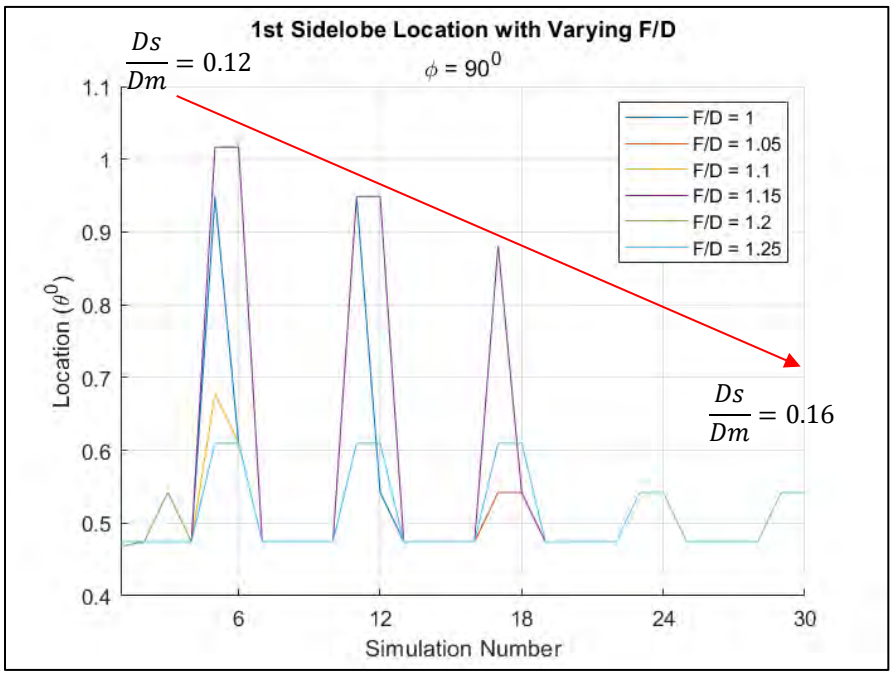

Figure 52. First sidelobe location with varying F/D ratios over the search area for the offset fed Cassegrain; $\phi = 90^0$.

Finally, see Figure 53 through 55 for the fratricide ratio results for the offset Cassegrain antenna. Aside from $\phi = 45^0$, the ratios are very large. For example, Figure where $\phi = 90^0$ has a maximum value of 0.94. Recall this is even larger than the maximum center fed fratricide ratio of 0.77. This result is confirmation that optimized values should be explored.

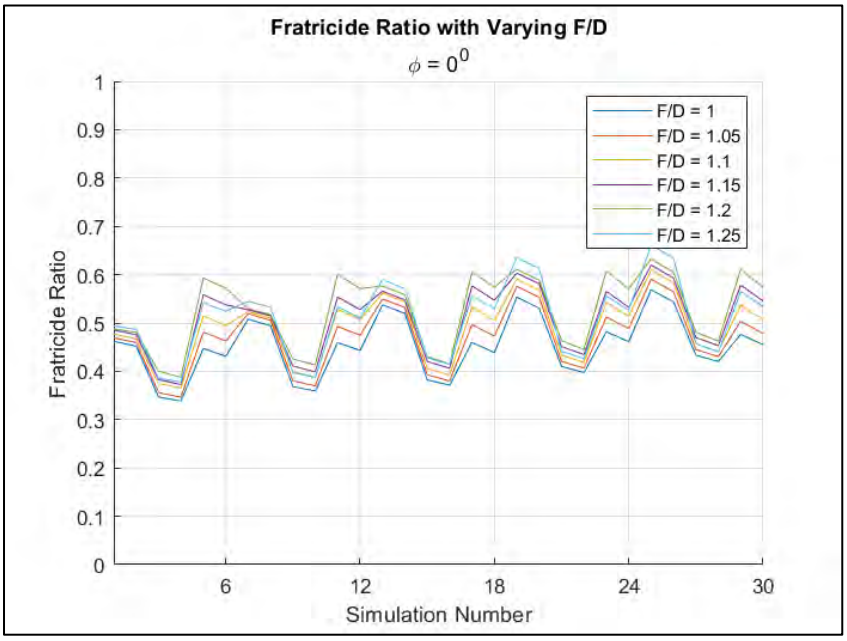

Figure 53. Offset Cassegrain fratricide ratio for varying F/D ratios over the search area for the offset fed Cassegrain.

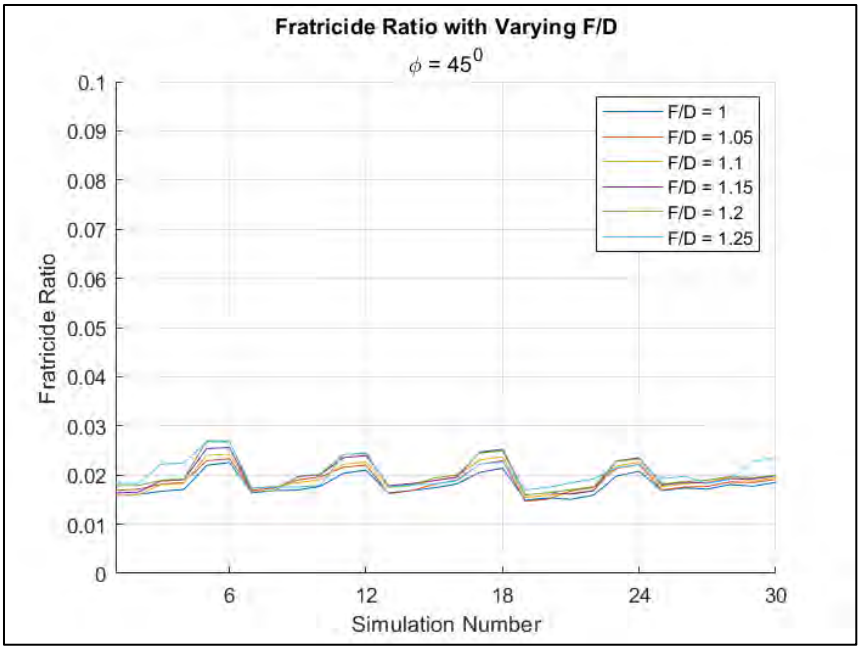

Figure 54. Offset Cassegrain fratricide ratio for varying F/D ratios over the search area for the given ϕ value. Note: the y-axis scale was changed to show variation.

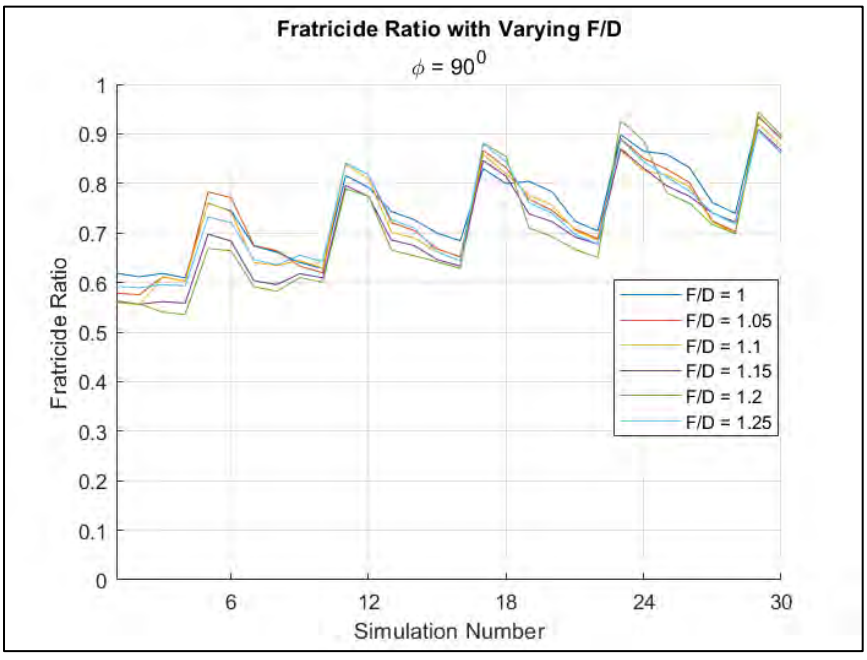

Figure 55. Offset Cassegrain fratricide ratio for varying F/D ratios over the search area for the given ϕ value.

4.2.3 Output Comparison for First Parameter Set

This section will present comparisons between the center fed and offset fed results using the first parameter set. See Table 7 for a comparison of the maximum values of outputs of both variants and the differences between the two. See Table 8 for the comparison of the minimum values of outputs for both variants. Also notice the F/D that corresponds to the maximum/minimum values in Table 7 and 8. If there were multiple F/D values with the same maximum/minimum values, the F/D values will be listed, or "All" denoted that all F/D values corresponded to the given output.

Maximum Values and Change				Corresponding F/D	
	Center Fed	Offset	Change	Center Fed	Offset
Gain (dB)	54.98	51.48	-3.5	1.25	1.05
HPBW (^{0})	0.34	0.75	0.41	1.1	1.25
First SL (dB)	36.95	45.41	8.46	1.15	1.25
First SL Loc (^{0})	0.88	1.02	0.14	1.15	1.15
Frat Ratio	0.77	0.94	0.17	1.1	1.2

Table 7. Maximum values for the center fed and offset fed Cassegrain with corresponding F/D ratios.

With respect to gain in Table 7, the offset variant maximum gain value was 3.5 dB less than that of the center fed. The half power beamwidth (HPBW) was 0.41 degrees larger in the offset, providing a wider beam than the center fed variant. The center fed Cassegrain provided 8.46 dB more attenuation than the offset when examining the first side lobe level. When comparing the location of the first side lobe levels, the difference was 0.14 degrees. The fratricide ratio maximum for the offset was 0.17 higher than the

center fed variant. There is no clear correlation between the maximum values and the F/D ratios.

Minimum Values and Change				Corresponding F/D	
	Center Fed	Offset	Change	Center Fed	Offset
Gain (dB)	46.53	44.76	-1.77	1.1	1.2
HPBW (^{0})	0.28	0.26	-0.02	1, 1.05, 1.1	1.2
First SL (dB)	23.3	19.78	-3.52	1.25	1
First SL Loc (^{0})	0.47	0.14	-0.33	All	1.25
Frat Ratio	0.01	0.01	0	1.1	1.05

Table 8. Minimum values for the center fed and offset fed Cassegrain with corresponding F/D values.

The minimum values in Table 8 yielded fewer extreme variations than the maximum values. For instance, the gain differed by 1.77 dB, the HPBW difference was a negligible 0.02 degrees, and the fratricide ratio minimum difference was zero. However, the first side lobe level was attenuated more by the offset variant than the center fed; by 3.52 dB. Furthermore, the first side lobe location differed by 0.33 degrees. It is important to note that the offset Cassegrain provided differing gain and location values for the first side lobe when comparing the ϕ values due to the blockage apparent from the feed/subreflector when using the 0^0 and 45^0 ϕ cuts. This results directly from Chapter 3 θ and ϕ definition discussion.

4.3 Second Parameter Set Results

Due to the back lobe analysis performed in the previous sections, new parameters were chosen to investigate a more stable Cassegrain design with respect to the back

lobes. This section will cover the results from using the second set of parameters in Table 3.2 for the center fed and offset fed Cassegrain antenna designs. Recall that the Ds/Dm was allowed to vary based on GRASP SE's calculations, however, the parameter Lm was manually varied, which increases or decreases the distance between the feed and the main reflector vertex. Furthermore, eccentricity e step-size was increased to seven, along with the overall maximum value of 1.5. It is also important to note that the feed taper was held constant to -12 dB. The decision to hold this value constant was due to the negligible difference between -10 dB and -12 dB feed taper values during the first set of parameter sweeps.

4.3.1 Center Fed Cassegrain Results

This section will begin with comparing the peak gain values and the F/D ratios over all simulations followed by half-power beamwidth (HPBW), first side lobe level, first side lobe level location, variation between ϕ values and first side lobe level, and finally the fratricide ratio. The variation between ϕ values was an added analysis due to the sporadic nature of the side lobe analysis. See Figure 56 for the peak gain values for the second set of parameters using the center fed Cassegrain analysis results. Only $\phi = 0^0$ is shown due to the negligible differences between $\phi = 45^0$ and 90^0.

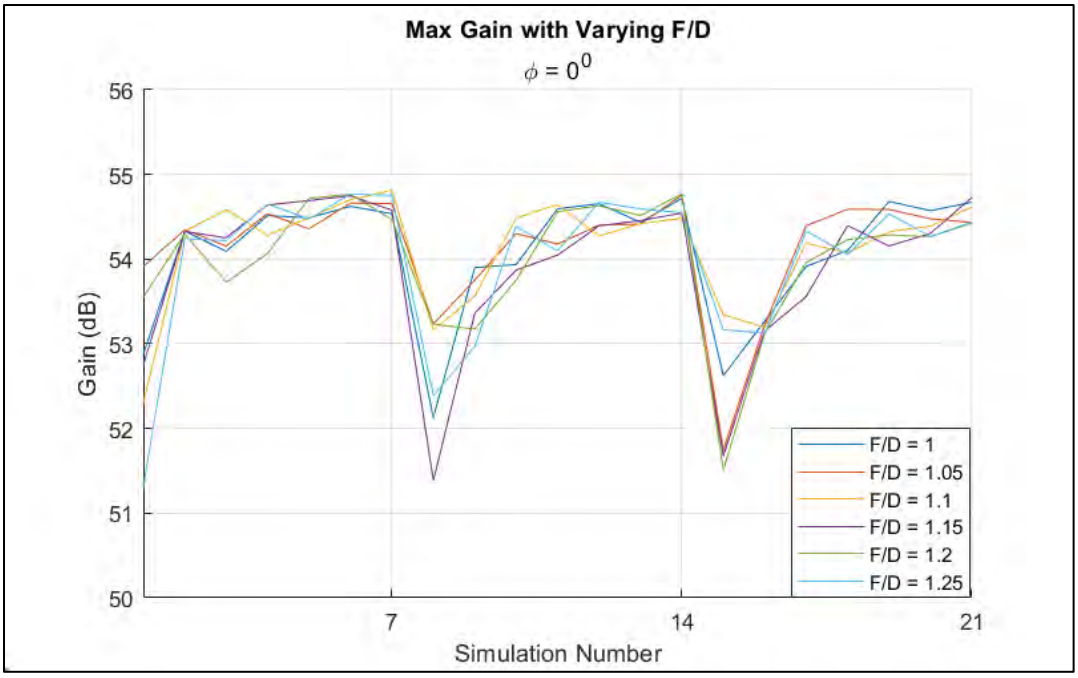

Figure 56. Peak gain values for the center fed Cassegrain over the search area for $\boldsymbol{\phi = 0^0}$.

In reference to Figure 56, notice the repeating rising/falling pattern every seven simulations. As in the previous sections, this is due to the increasing eccentricity. There are three instances in Figure 56 of rising peaks. This pattern is due to the Lm values changing three times. Due to the fluctuations between each of the F/D values, there was no clear correlation between the F/D value and peak gain, however, increasing the eccentricity e allows for maximum gain using the prescribed parameters.

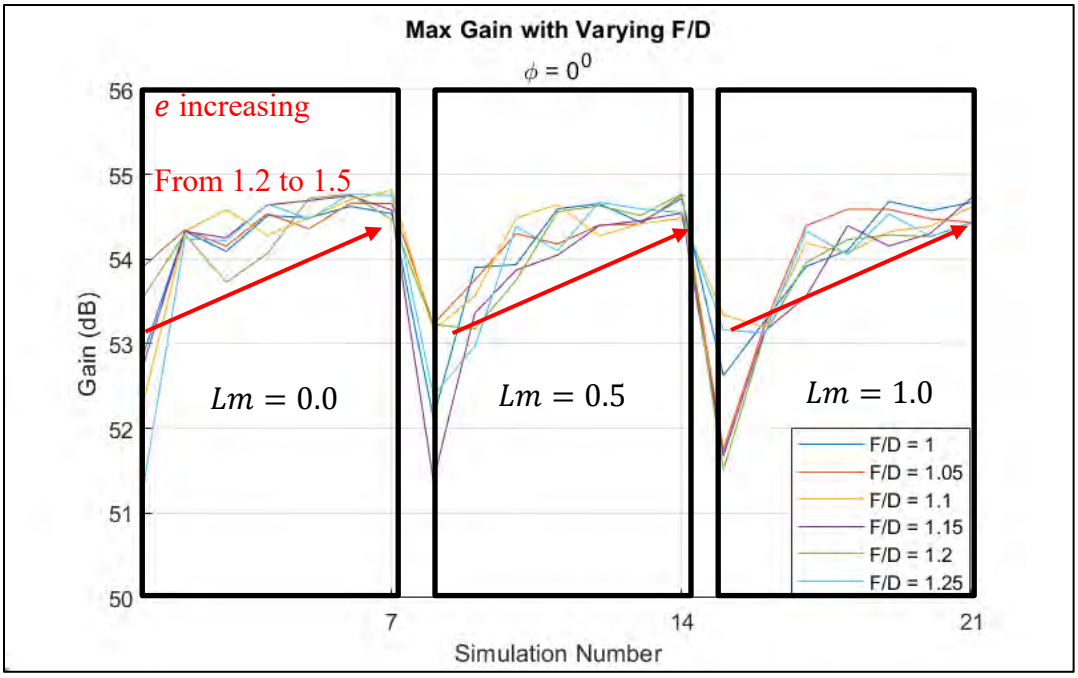

Figure 57. Effect on gain due to subreflector eccentricity and *Lm*.

Next, the HPBW was analyzed across the F/D values for all 126 simulations. See Figure 58 for the HPBW analysis results. Notice the HPBW stays roughly within 0.3 and 0.36 degrees. There is no clear correlation between the F/D values or other parameters of interest and the HPBW. Only $\phi = 0^0$ was shown due to the negligible differences between $\phi = 45^0$ and 90^0.

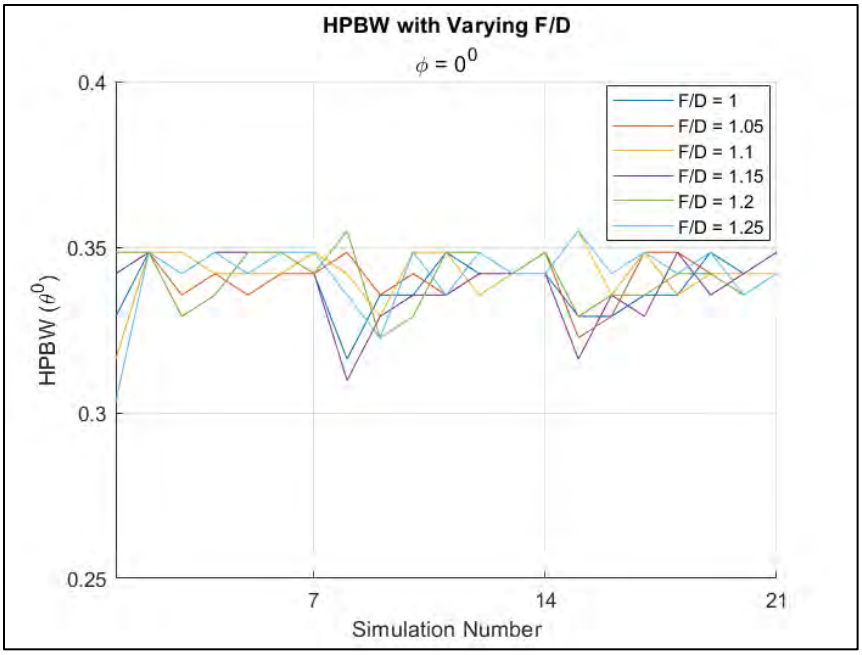

Figure 58. Half-power beamwidth for the center fed Cassegrain over the search area.

The first sidelobe level analysis yielded differences between all three ϕ values. The data for $\phi = 0^0$ and $\phi = 45^0$ and 90^0 are primarily seen in Figures 59 through 61 are shown again in Figures 62 and 63 to better illustrate the fine differences. When comparing $\phi = 0^0$ to 45^0 in Figure 62, when F/D is 1.0, there is an attenuation of -8 dB, which is a significant difference. This observation is also apparent when comparing $\phi = 0^0$ and 90^0 in Figure 63.

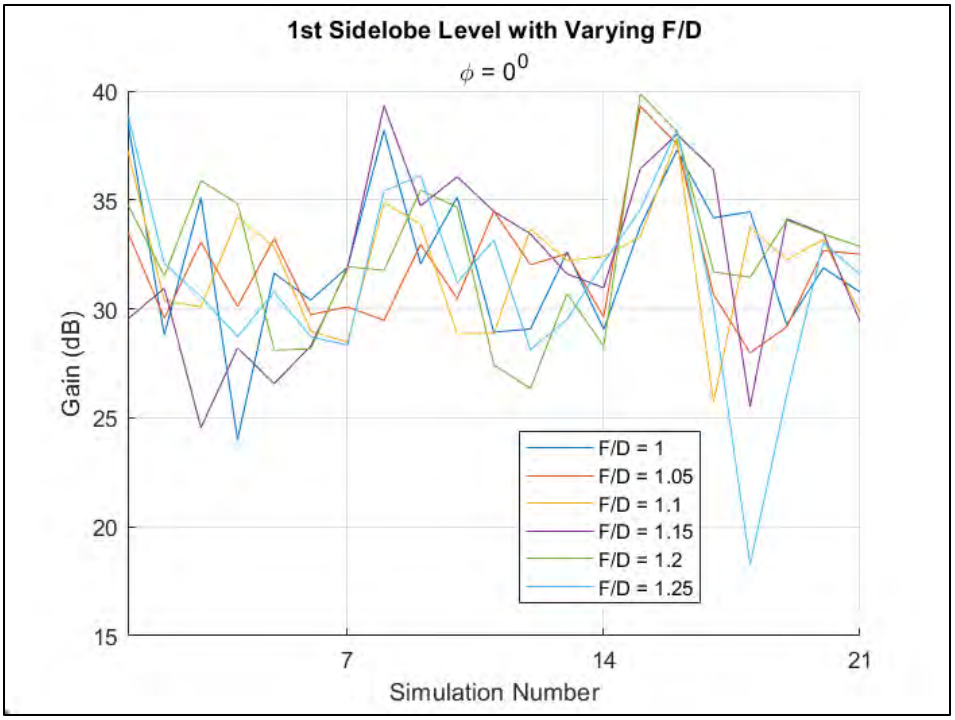

Figure 59. First sidelobe peak gain value for the center fed Cassegrain over the search area for $\phi = 0^0$.

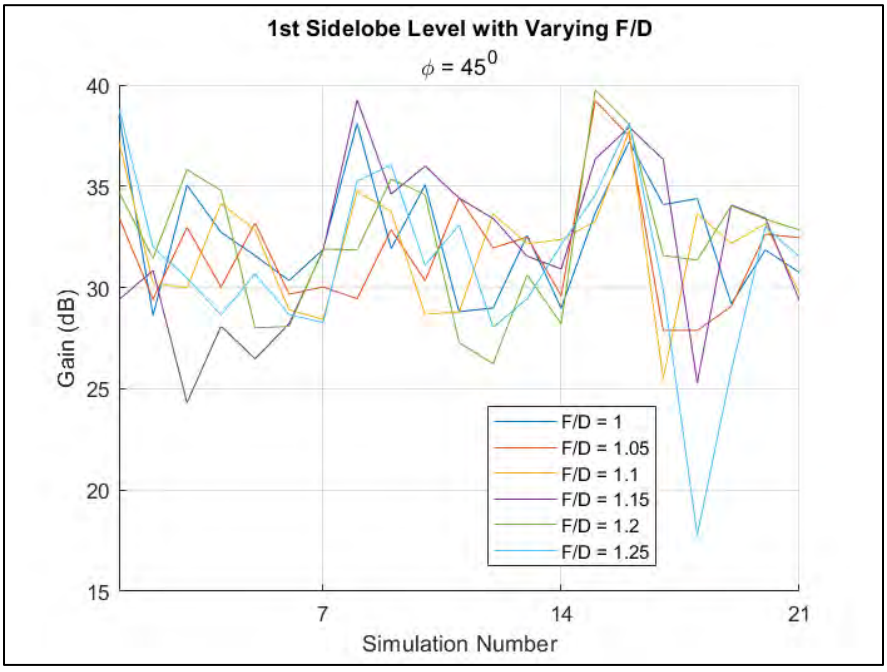

Figure 60. First sidelobe peak gain value for the center fed Cassegrain over the search area for $\phi = 45^0$.

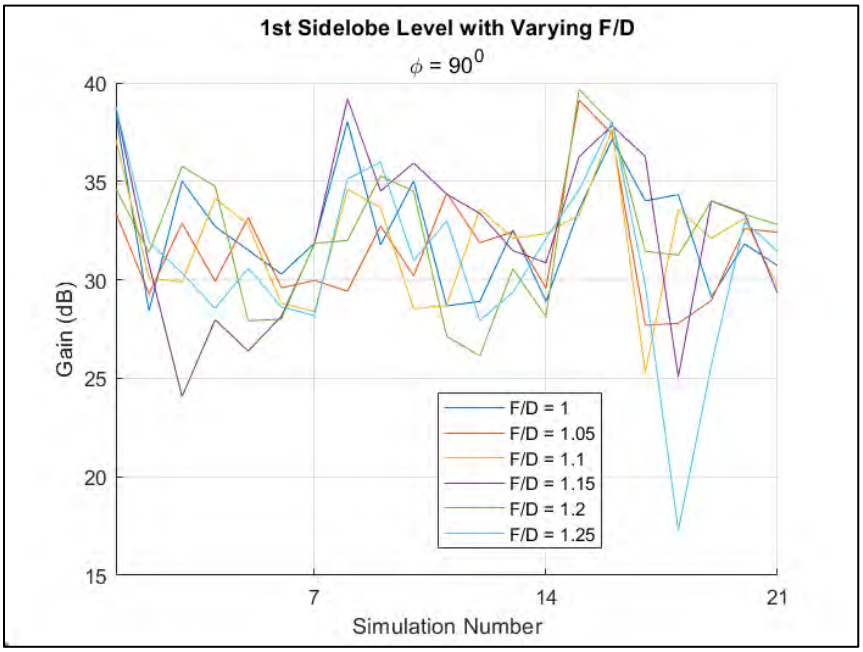

Figure 61 First sidelobe peak gain value for the center fed Cassegrain over the search area for $\boldsymbol{\phi = 90^0}$.

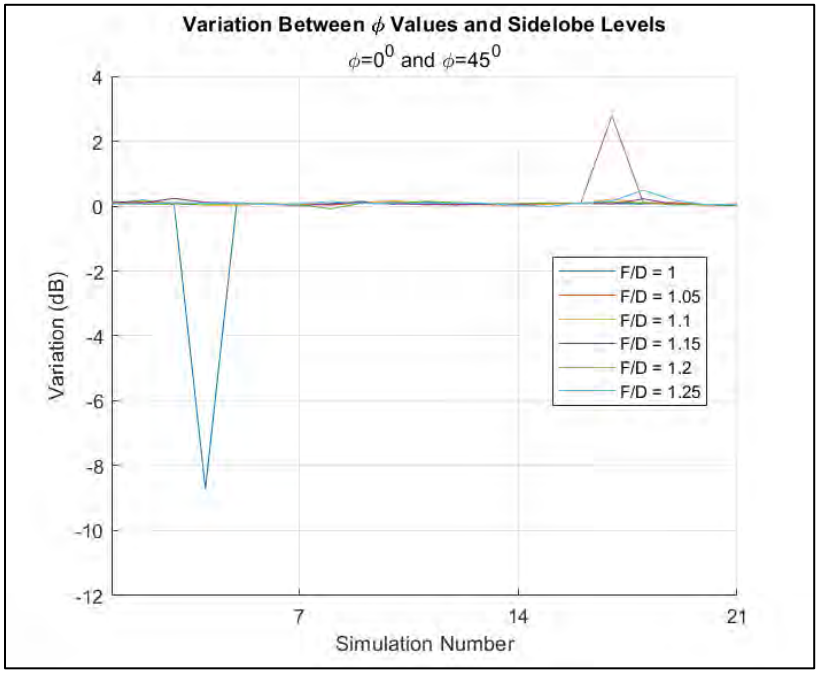

Figure 62. Difference in first side lobe levels between $\boldsymbol{\phi = 0^0}$ and $\boldsymbol{\phi = 45^0}$.

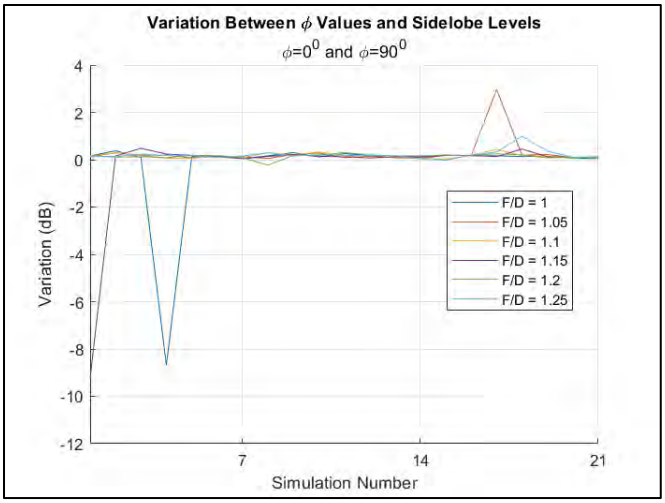

Figure 63. Difference in first side lobe levels between $\phi = 0^0$ and $\phi = 90^0$.

When analyzing the first sidelobe location of the second set of parameters, there were negligible differences between $\phi = 0^0, 45^0$ and 90^0, therefore only $\phi = 0^0$ is shown in Figure 64. The values range from 0.47^0 to 1.15^0 and do not seem to have specific correlation with the prescribed parameters. However, there are some individual cases that can be seen in Figure 64 where the location is closer or farther away from the main lobe.

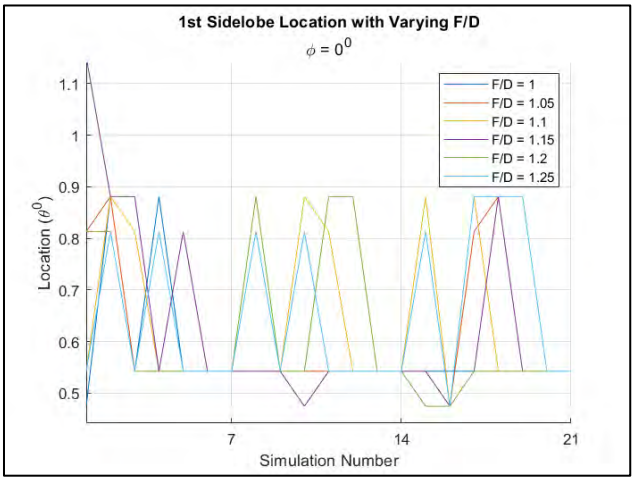

Figure 64. First sidelobe location in degrees over the search area for $\phi = 0^0$.

The final analysis for this section is the fratricide ratio analysis. The same y-axis limits were used in this section as in the previous sections to show visual similarities and differences. See Figure 65 through 67 for the fratricide ratio results. Notice the peak values in the $\phi = 0^0$ and 90^0 are dramatically reduced.

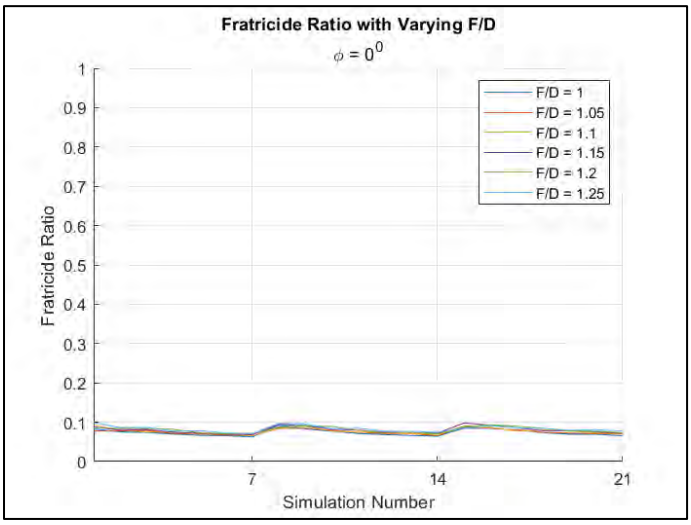

Figure 65. Fratricide ratio for the center fed Cassegrain antenna using the second set of parameters for $\phi = 0^0$.

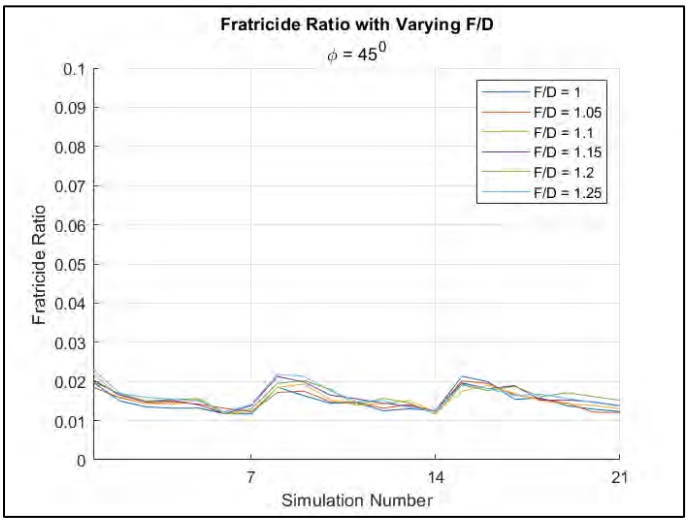

Figure 66. Fratricide ratio for the center fed Cassegrain antenna using the second set of parameters for $\phi = 45^0$.

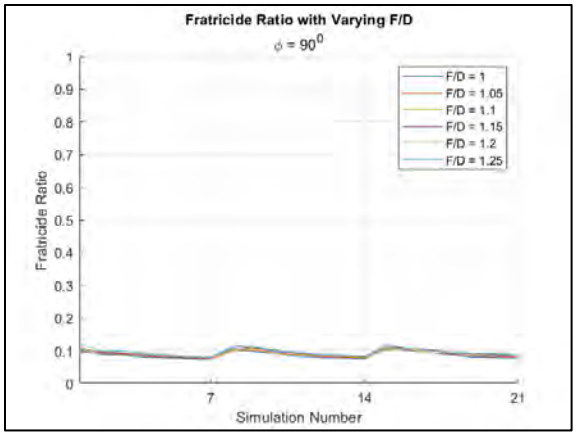

Figure 67. Fratricide ratio for the center fed Cassegrain antenna using the second set of parameters for $\phi = 90^0$.

Eccentricity had a similar effect on the fratricide ratio as in the first set of parameters. As eccentricity increased, the back lobe energy decreased. Varying the distance from the feed to the main reflector vertex did not provide a clear effect on the fratricide ratio, nor did the F/D ratio. See Figure 68 for the observations noted in this paragraph. Only $\phi = 45^0$ is shown to highlight the trend apparent in all three ϕ values.

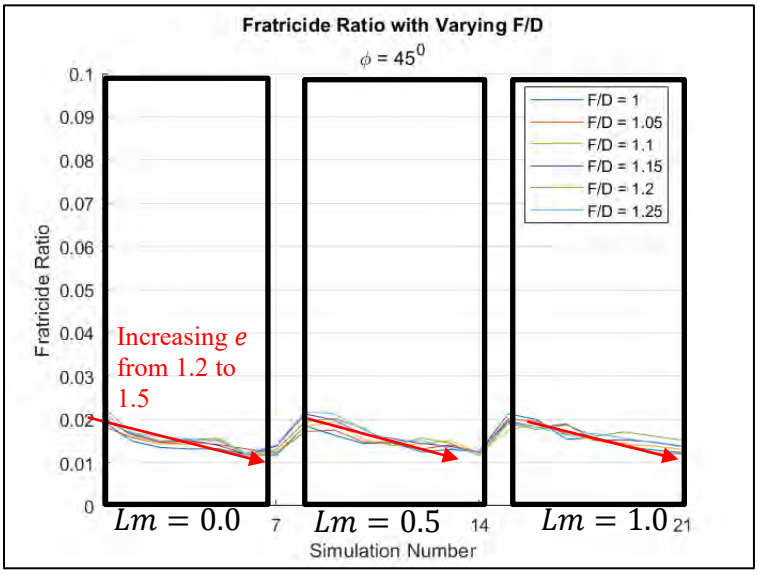

Figure 68. Effects of eccentricity and Lm on the fratricide ratio for varying F/D ratios.

4.3.2 Offset Fed Cassegrain Results

This section will present the data collected utilizing the second set of parameters. See Figure 69 for the peak gain values with varying F/D ratios. Only $\phi = 0^0$ is shown due to the negligible difference between $\phi = 45^0$ and 90^0. Again, as eccentricity increases over each seven simulations, the gain also increases. It is more difficult to see the effect of Lm on these results, however, all Lm increases, the lowest gain peaks appear to be lower. This does not seem to affect the high peaks, however. See Figure 70 for the graphical representation of how eccentricity and Lm affect the peak gain values.

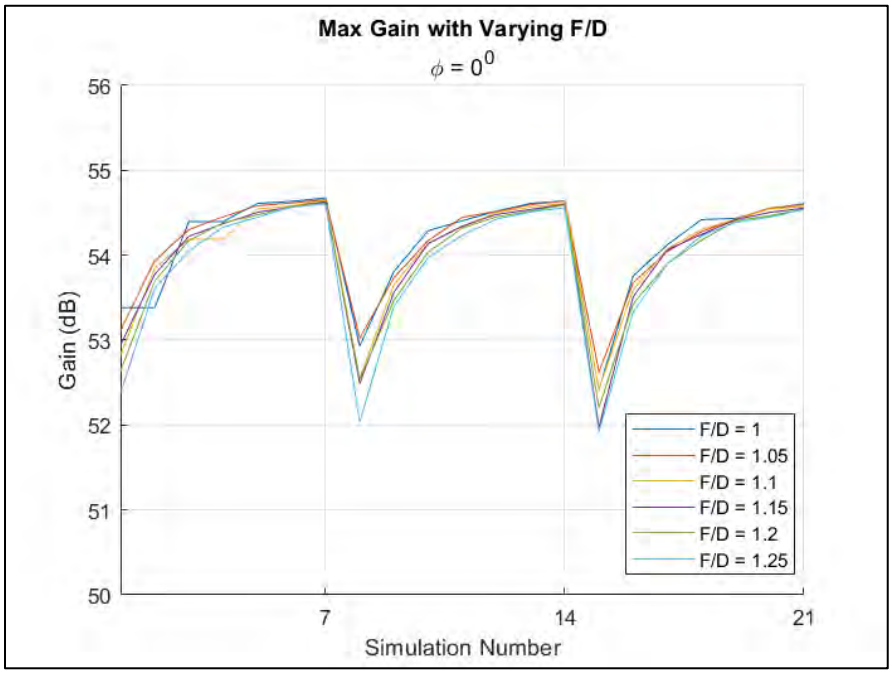

Figure 69. Peak gain values over the search area for the offset Cassegrain.

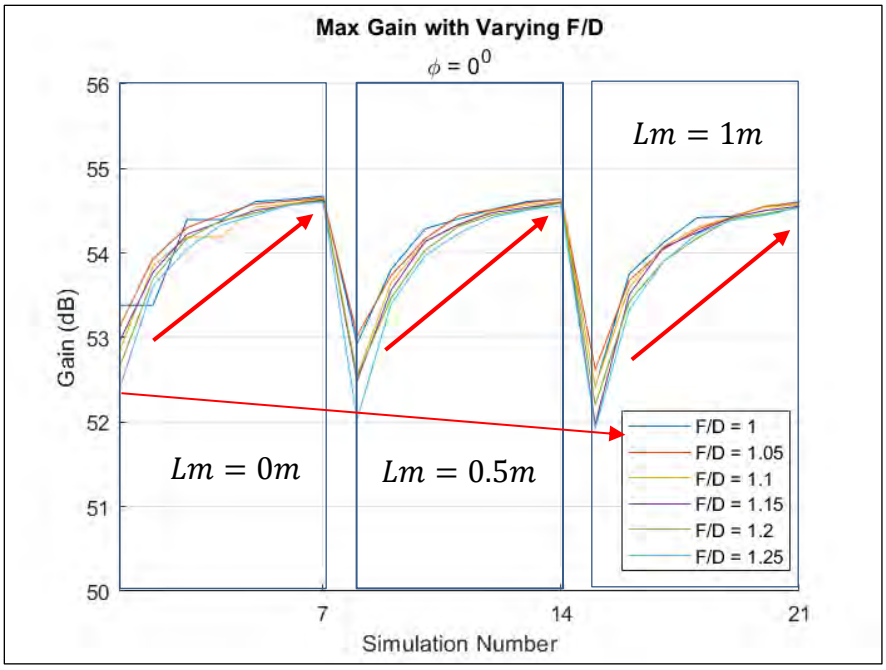

Figure 70. Effects of eccentricity and *Lm* on the peak gain values for the offset Cassegrain.

See Figure 71 for the half power beamwidth (HPBW) results. Only $\phi = 0^0$ is shown due to negligible differences between the other ϕ values. There is no clear correlation in the data between the F/D ratio and any other parameter that was varied. The range between all ϕ values stayed between 0.3^0 and 0.37^0 for the beamwidth.

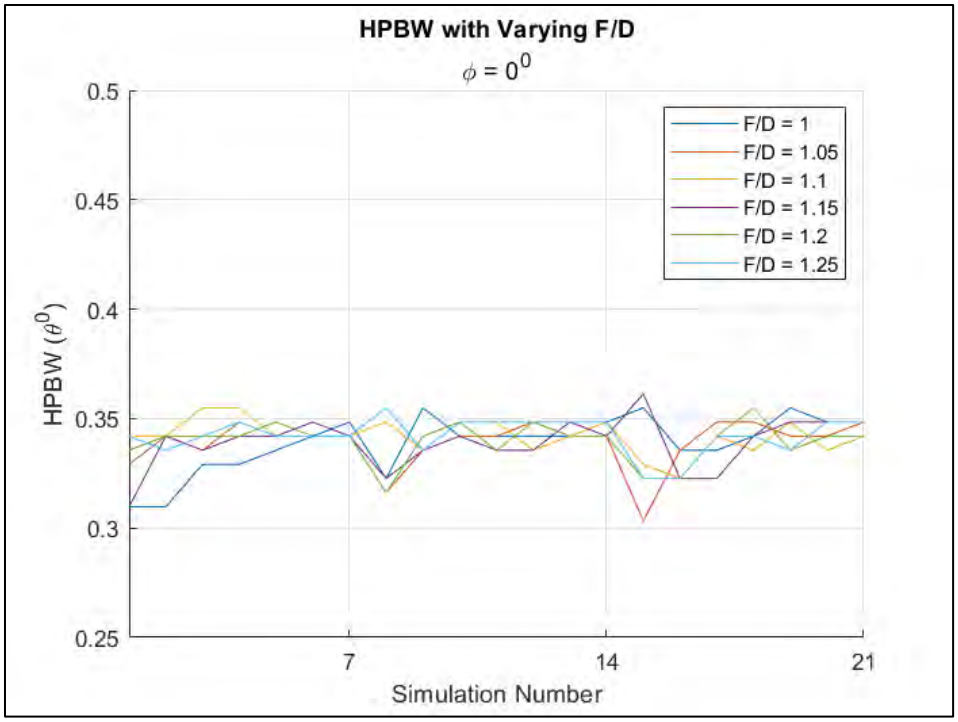

Figure 71. Half power beamwidth over the search area for the offset Cassegrain.

Next, the first side lobe level data will be presented in Figure 72. The first side lobe data was not as sporadic as the center fed Cassegrain data. There are strings of simulations where the different F/D values begin to converge, however, there is no clear correlation between the data and other parameters and their effect on the first side lobe level. It is for that reason that $\phi = 45^0$ is shown and not the other ϕ values.

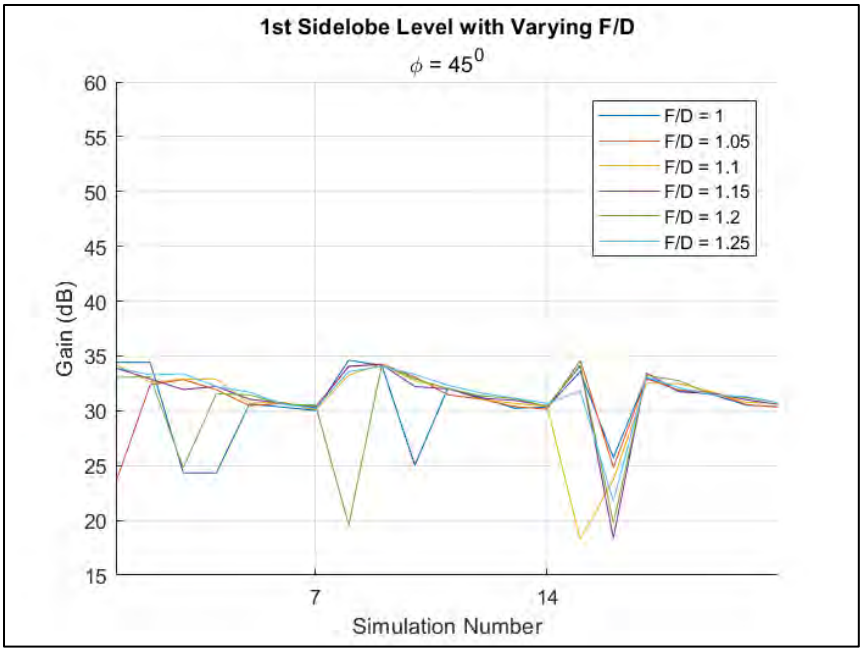

Figure 72. First side lobe level in dB for the offset Cassegrain.

The first side lobe location data was analyzed, and no clear observations could be made with the data and relating it to any of the varied parameters. See Figure 73 for the first side lobe location data over the search area. Notice the y-axis only spans 1^0 and the data acquired from all three ϕ values only differed as much as 0.4^0. Only $\phi = 90^0$ is shown as this was the most varied data out of all three ϕ values. Also note that overlapping data for the F/D values may not be visible.

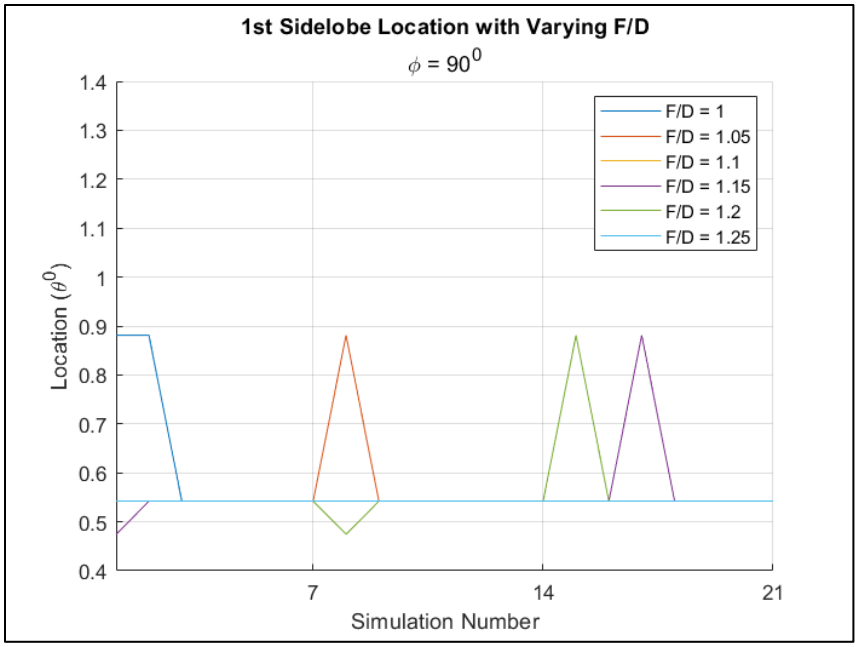

Figure 73. First sidelobe location for the offset Cassegrain over the search area.

Finally, the fratricide ratio data was analyzed. See Figure 74 through 76 for $\phi = 0^0, 45^0$ and 90^0 respectively. Recall that the first set of parameters in Table 4 gave very high back lobe levels, which drove the need to investigate and potentially adjust the designs to yield lower back lobes. Furthermore, similar observations as the previous sections can also be made with the fratricide ratio data presented in this section. See Figure 75 for the effect of eccentricity on the back lobe energy; as the eccentricity is increased, the energy apparent in the back lobes decreases.

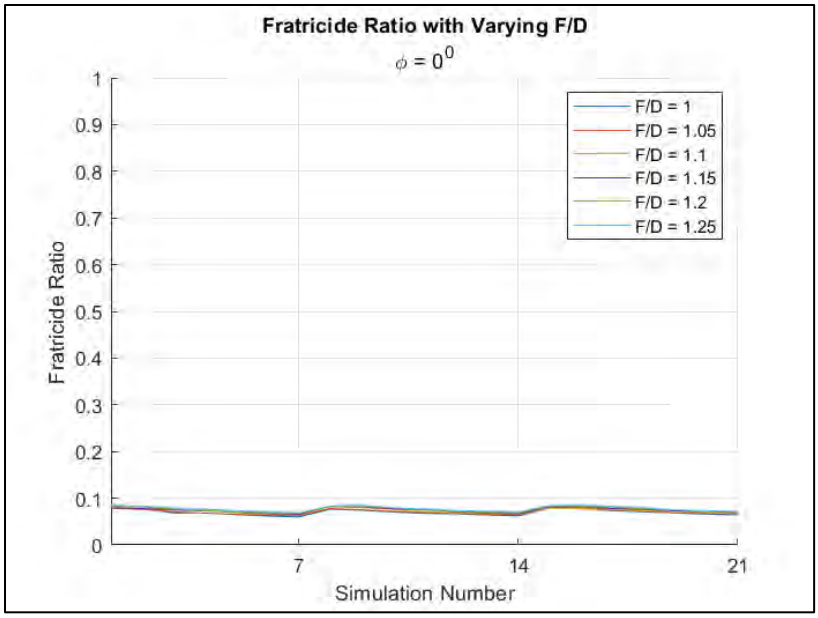

Figure 74. Fratricide ratio with varying F/D ratios for the offset Cassegrain; $\phi = 0^0$.

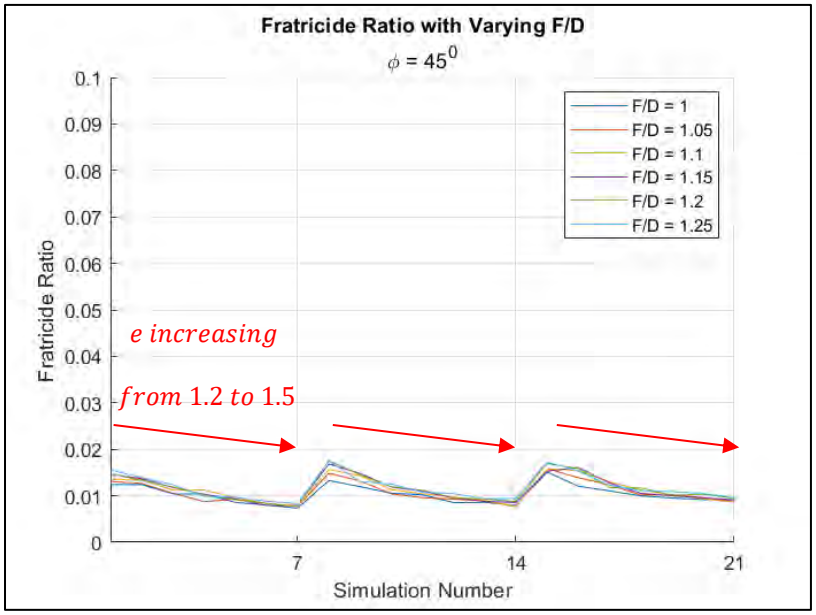

Figure 75. Fratricide ratio with varying F/D ratios for the offset Cassegrain; $\phi = 45^0$. Red lines label the effect of eccentricity on the fratricide ratio.

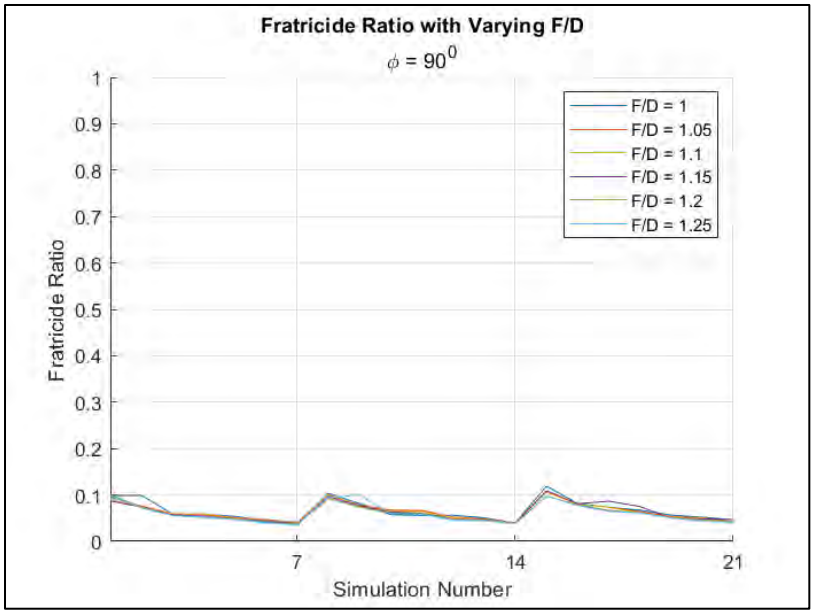

Figure 76. Fratricide ratio with varying F/D ratios for the offset Cassegrain; $\phi = 90^0$.

4.3.3 Output Comparison for Second Parameter Set

The output comparison between the center fed and offset Cassegrain antennas will be presented in this section. First, the maximum values of each output of interest will be shown in Table 9, followed by the minimum values in Table 10. In both tables, the specific F/D ratio will be noted that corresponds to the maximum/minimum value.

The maximum values and changes in Table 9 present very little differences. The first side lobe level has the largest change from center fed to offset fed of -4.26 dB. Other parameters appear to be change by negligible amounts.

Maximum Values and Change				Corresponding F/D	
	Center Fed	Offset	Change	Center Fed	Offset
Gain (dB)	54.81	54.68	-0.13	1.1	1
HPBW (^{0})	0.35	0.36	0.01	1.1, 1.2, 1.25	1.15
First SL (dB)	39.86	35.6	-4.26	1.2	1
First SL Loc (^{0})	1.15	1.49	0.34	1.15	1.15
Frat Ratio	0.12	0.12	0	1.25	1

Table 9. Maximum values for the offset and center fed Cassegrain with corresponding F/D ratio.

The data in Table 10 represents the minimum overall values extracted from the data and the corresponding F/D value(s). Negligible change occurred when comparing the two Cassegrain variants except for the first side lobe level. The offset Cassegrain was unable to attenuate the first side lobe more than the center fed; the minimum value was 0.99 dB higher than the center fed.

Minimum Values and Change				Corresponding F/D	
	Center Fed	Offset	Change	Center Fed	Offset
Gain (dB)	51.31	51.92	0.61	1.25	1.25
HPBW (^{0})	0.3	0.3	0.0	1.25	1.05, 1.2
First SL (dB)	17.27	18.26	0.99	1.25	1.1
First SL Loc (^{0})	0.47	0.47	0	All	All
Frat Ratio	0.01	0.01	0	1.2	1

Table 10. Minimum values for the offset and center fed Cassegrain with corresponding F/D ratios.

4.3 Optimized Beam Patterns

The optimized beam patterns acquired across all the data, including both sets of parameters will be presented in this section. The design parameters used will be noted along with each optimized result. The radiation patterns that achieved the highest gain

from each antenna variant (all three ϕ values) will be presented first, along with the parameters used. See Figure 77 for the center fed design that achieved that highest gain and Table 11 for the parameters used.

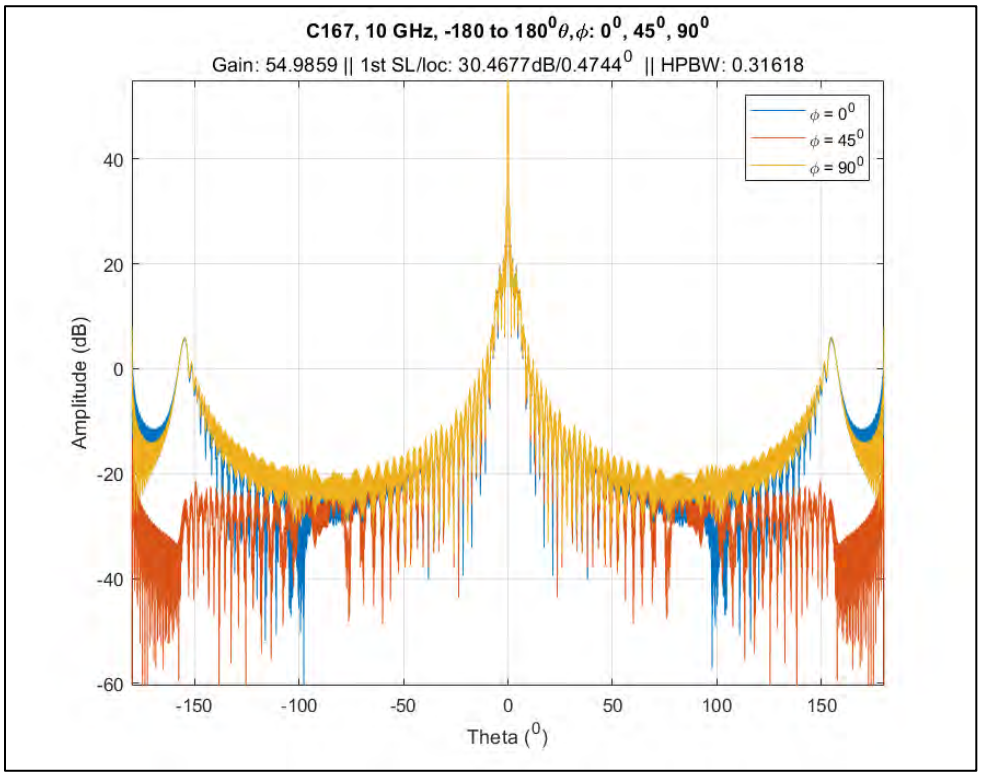

Figure 77. Center fed optimized gain pattern with $\theta - 180^0$ to 180^0, $\phi = 0^0, 45^0, 90^0$ collected from the first set of parameters.

F/d	Ds/Dm	Ecc	Feed Taper (dB)	Lm (m)
1.25	0.14	1.3	-12	0

Table 11. Parameters used for the center fed optimized gain pattern.

For the optimized gain center fed pattern in Figure 77, the design achieved a maximum gain of 54.99 dB. Although this design achieved the highest gain value, it was not the most efficient in terms of back lobe analysis. Furthermore, the optimized gain pattern for the offset Cassegrain in Figure 78 was also not the most efficient. Notice in

Figure 78 the asymmetrical properties of the graph. The peak just to the right of the main lobe suggests the diameter of the subreflector was too small, therefore feed energy was allowed to spillover and create a rather high side lobe. The back lobe energy in Figure 78 is also asymmetrical for $\phi = 0^0$. This "extra" back lobe energy at ϕ 100^0 to 180^0 and $\phi = 0^0$ suggests main reflector spillover from the subreflector. Both facts combined suggest the subreflector should either be moved, oversized, or both.

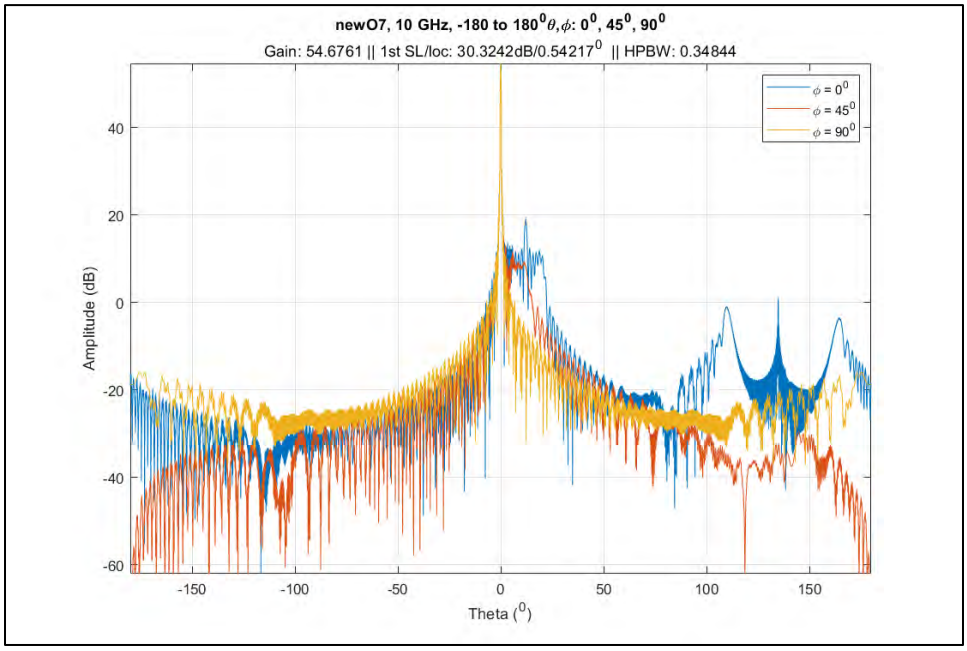

Figure 78. Offset fed optimized gain pattern with $\theta - 180^0$ to 180^0, $\phi = 0^0, 45^0, 90^0$ collected from the second set of parameters.

F/d	Ds/Dm	Ecc	Feed Taper (dB)	Lm (m)
1	0.1858	1.5	-12	0

Table 12. Parameters used for the offset fed optimized gain pattern.

A more efficient radiation pattern than previously presented should include maximum gain with the most attenuated side lobe. See Figure 79 for the radiation pattern

of the center fed design that achieved the highest attenuation of the first side lobe level, and Table 13 for the parameters used. See Figure 80 for the offset fed design that performed the best with the first side lobe level and Table 14 for the parameters used. The design in Figure 80 achieved a -20 dB attenuation. Finally, the fratricide ratio optimized results are presented. See Figure 81 for the radiation pattern of the optimized center fed fratricide ratio results and Table 15 for the parameters used. See Figure 82 for the optimized offset fed fratricide ratio results and Table 16 for the parameters used.

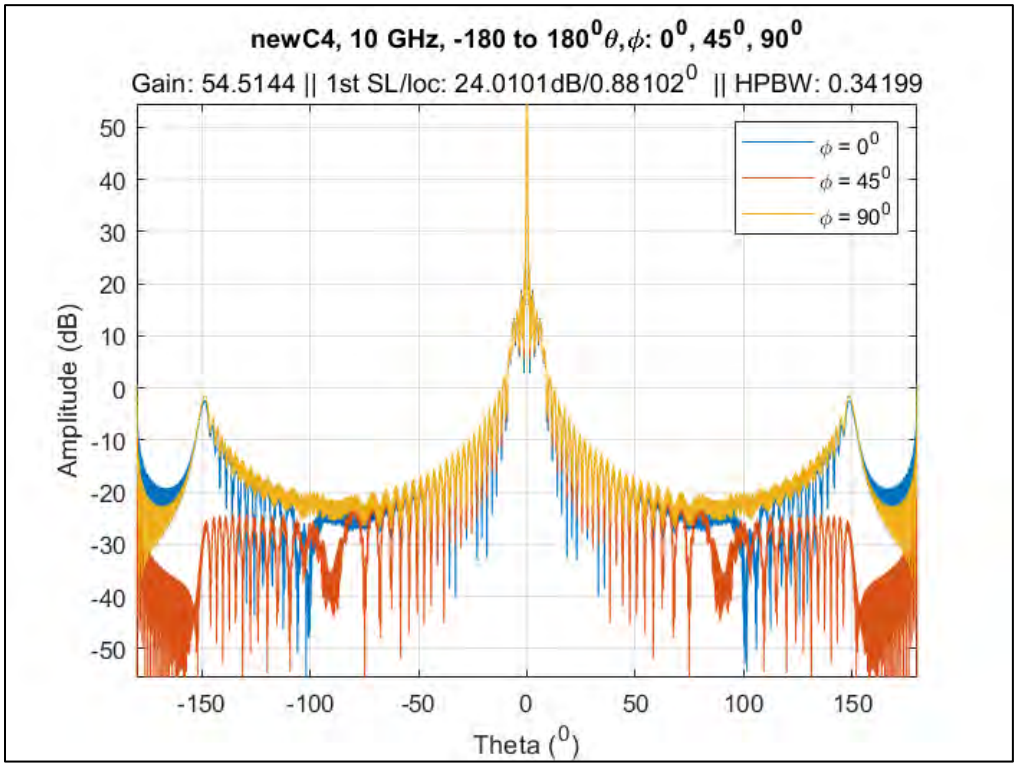

Figure 79. Center fed Cassegrain design with the greatest side lobe attenuation; $\boldsymbol{\phi = 0^0, 45^0, 90^0}$.

F/d	Ds/Dm	Ecc	Feed Taper (dB)	Lm (m)
1	0.13085	1.35	-12	0

Table 13. Parameters used for the optimized sidelobe attenuation.

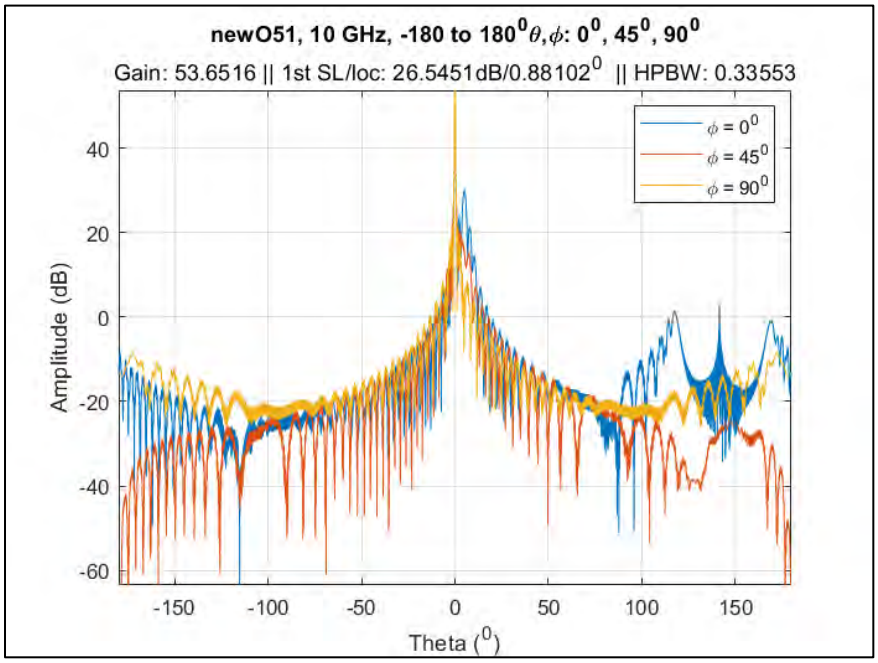

Figure 80. Offset set fed design that achieved the highest attenuation of the first side lobe level; $\boldsymbol{\phi = 45^0}$.

F/d	Ds/Dm	Ecc	Feed Taper	Lm
1.1	0	1.25	-12	0.5

Table 14. Parameters used for the Offset fed optimized side lobe attenuation.

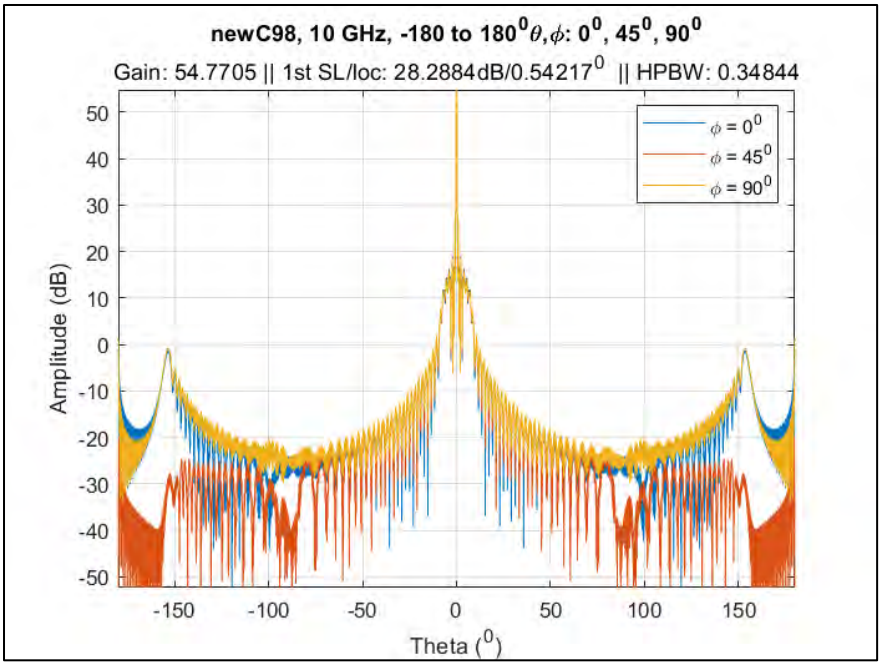

Figure 81. Radiation pattern for the center fed design with optimized fratricide ratio.

F/d	Ds/Dm	Ecc	Feed Taper (dB)	Lm (m)
1.2	0.15645	1.5	-12	0.5

Table 15. Center fed parameters used for the optimized fratricide ratio design.

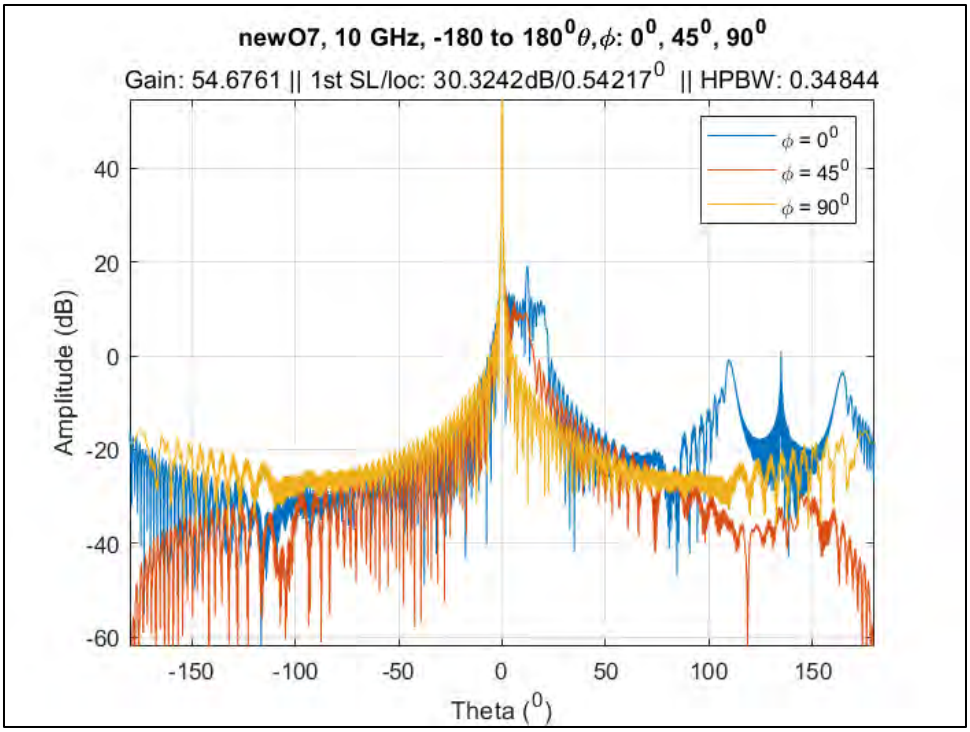

Figure 82. Offset fed design with optimized fratricide ratio results.

F/d	Ds/Dm	Ecc	Feed Taper (dB)	Lm (m)
1	0.1858	1.5	-12	0

Table 16. Offset parameters used for optimized fratricide ratio.

4.4 Center Fed Analysis of Variance Study

This section will present the results of multiple 3-factor analysis of variance (ANOVA) studies. Refer to Chapter 3 for a brief description of how to interpret the results. The tables presented in the section will attempt to make probable connections between the parameters of interest and the outputs of interest. The center fed parameter

set one will be presented first, followed by parameter set two. See Table 17 for the results of the 3-factor ANOVA with peak gain as the output of interest.

R^2	0.991		Gain		
Source	DF	Sum of squares	Mean squares	F	Pr > F
F/d	5.000	7.985	1.597	**23.685**	**0.000**
Ds/Dm	4.000	111.717	27.929	**414.219**	**0.000**
Ecc	2.000	3515.551	1757.775	**26069.560**	**0.000**
F/d*Ds/Dm	20.000	6.499	0.325	**4.819**	**0.000**
F/d*Ecc	10.000	17.112	1.711	**25.379**	**0.000**
Ds/Dm*Ecc	8.000	62.090	7.761	**115.107**	**0.000**

Table 17. Three-factor ANOVA results for the center fed Cassegrain peak gain using first parameter set.

According to Table 17, all parameters did influence gain, with eccentricity having, by far, the most, followed by Ds/Dm, and finally the interaction of eccentricity and Ds/Dm. See Table 18 for the results of the three-factor ANOVA test on the half power beamwidth (HPBW).

R^2	0.925		HPBW		
Source	DF	Sum of squares	Mean squares	F	Pr > F
F/d	5.000	0.005	0.001	**80.247**	**0.000**
Ds/Dm	4.000	0.010	0.002	**216.471**	**0.000**
Ecc	2.000	0.038	0.019	**1679.230**	**0.000**
F/d*Ds/Dm	20.000	0.003	0.000	**12.878**	**0.000**
F/d*Ecc	10.000	0.006	0.001	**57.107**	**0.000**
Ds/Dm*Ecc	8.000	0.007	0.001	**76.449**	**0.000**

Table 18. Three-factor ANOVA results for the center fed Cassegrain HPBW using first parameter set.

Notice in Table 18 that the p-values are all zero, thus all parameters listed influenced the variability of the HPBW. Also notice that eccentricity and Ds/Dm had the largest impact on variability, followed by F/D. See Table 19 for the three-factor ANOVA results for the fratricide ratio.

R^2	0.362		Fratricide Ratio		
Source	DF	Sum of squares	Mean squares	F	Pr > F
F/d	5.000	0.001	0.000	**0.003**	**1.000**
Ds/Dm	4.000	0.672	0.168	**4.477**	**0.001**
Ecc	2.000	9.715	4.857	**129.394**	**0.000**
F/d*Ds/Dm	20.000	0.004	0.000	**0.005**	**1.000**
F/d*Ecc	10.000	0.008	0.001	**0.022**	**1.000**
Ds/Dm*Ecc	8.000	0.027	0.003	**0.090**	**0.999**

Table 19. Three-factor ANOVA results for the center fed Cassegrain fratricide ratio using first parameter set.

In Table 19, notice that for all parameters except eccentricity and Ds/Dm the p-value was practically 1.0. The parameters with very low F-statistic (F) values and high p-values can be assumed to have no effect on the variability of the fratricide ratio. Also notice the R^2 value in the top of Table 19 equal to 0.362. This means that only 36.2% of the variability can be attributed to the parameters under investigation, in this case, eccentricity and Ds/Dm. Next, the data collected from the center fed Cassegrain using parameter set two will be used to perform three-factor ANOVA tests. Recall that for parameter set two, Ds/Dm was not considered an independent variable. Instead, Lm was chosen as an independent variable while GRASP was allowed to vary Ds/Dm automatically. See Table 20 for the ANOVA gain results using the center fed Cassegrain parameter set two.

R^2	0.883		Gain		
Source	DF	Sum of squares	Mean squares	F	Pr > F
F/d	5.000	2.637	0.527	**6.123**	**0.000**
Ecc	6.000	170.812	28.469	**330.504**	**0.000**
Lm	2.000	7.595	3.798	**44.087**	**0.000**
F/d*Ecc	30.000	9.137	0.305	**3.536**	**0.000**
F/d*Lm	10.000	3.541	0.354	**4.111**	**0.000**
Ecc*Lm	12.000	8.443	0.704	**8.168**	**0.000**

Table 20. Three-factor ANOVA results for the center fed Cassegrain gain using second parameter set.

In Table 20, notice that eccentricity had the most effect on the variability of max gain, followed by Lm, then F/D. The interaction of parameters had a small effect on the variability. Also notice the R^2 value of 0.883, which may allude to a parameter not on the list that is also contributing to the variability of gain. See Table 21 for the results from the three-factor ANOVA with HPBW under investigation.

R^2	0.578		HPBW		
Source	DF	Sum of squares	Mean squares	F	Pr > F
F/d	5.000	0.001	0.000	**2.813**	**0.017**
Ecc	6.000	0.006	0.001	**22.546**	**0.000**
Lm	2.000	0.001	0.000	**8.111**	**0.000**
F/d*Ecc	30.000	0.005	0.000	**4.382**	**0.000**
F/d*Lm	10.000	0.002	0.000	**4.385**	**0.000**
Ecc*Lm	12.000	0.004	0.000	**7.202**	**0.000**

Table 21. Three-factor ANOVA results for the center fed Cassegrain HPBW using second parameter set.

In Table 21, eccentricity had the highest influence on the variability of the HPBW, followed by Lm, then the interaction of the two parameters. It is important to note that all parameters had high probability of influence on HPBW when examining the

p-values. The R^2 number is indicating that 57% of the variability of HPBW can be explained by the listed parameters. See Table 22 for the results from the three-factor ANOVA with the fratricide ratio under investigation.

R^2	0.044		Fratricide Ratio		
Source	DF	Sum of squares	Mean squares	F	Pr > F
F/d	5.000	0.002	0.000	0.342	0.887
Ecc	6.000	0.015	0.003	1.876	0.084
Lm	2.000	0.001	0.000	0.334	0.716
F/d*Ecc	30.000	0.000	0.000	0.010	1.000
F/d*Lm	10.000	0.000	0.000	0.010	1.000
Ecc*Lm	12.000	0.000	0.000	0.025	1.000

Table 22. Three-factor ANOVA results for the center fed Cassegrain fratricide ratio using second parameter set.

Notice in Table 22, the low R^2 value, meaning that only 4.4% of the variability can be explained by the listed parameters. Also notice that all parameters failed to show any impact on the variability of the fratricide ratio. One can conclude from Table 22 that the listed parameters had no effect on the fratricide ratio.

4.4 Offset Fed Analysis of Variance Study

This section will present the results of the three-factor analysis of variance (ANOVA) study performed on the data collected from the offset Cassegrain. The results from the first parameter set will be presented, followed by the second parameter set. See Table 23 for the three-factor ANOVA gain results using the offset Cassegrain first parameter set.

R^2	0.988		Gain		
Source	DF	Sum of squares	Mean squares	F	Pr > F
F/d	5.000	91.862	18.372	**490.890**	**0.000**
Ds/Dm	4.000	1.769	0.442	**11.818**	**0.000**
Ecc	2.000	1191.848	595.924	**15922.330**	**0.000**
F/d*Ds/Dm	20.000	7.018	0.351	**9.375**	**0.000**
F/d*Ecc	10.000	53.994	5.399	**144.265**	**0.000**
Ds/Dm*Ecc	8.000	164.110	20.514	**548.102**	**0.000**

Table 23. Three-factor ANOVA results for the offset fed Cassegrain gain using first parameter set.

In Table 23, all parameters and interactions have a significant impact on the variability of the gain output. Specifically, eccentricity had the most impact, followed by the F/D, then the interaction between eccentricity and Ds/Dm. Also, 98.8% of the variability can be explained by the parameters listed. See Table 24 for the results from the three-factor ANOVA results with the half power beamwidth (HPBW) as the output of interest.

R^2	0.663		HPBW		
Source	DF	Sum of squares	Mean squares	F	Pr > F
F/d	5.000	0.023	0.005	**1.802**	**0.111**
Ds/Dm	4.000	0.120	0.030	**11.596**	**0.000**
Ecc	2.000	2.222	1.111	**429.769**	**0.000**
F/d*Ds/Dm	20.000	0.013	0.001	**0.251**	**1.000**
F/d*Ecc	10.000	0.041	0.004	**1.580**	**0.109**
Ds/Dm*Ecc	8.000	0.072	0.009	**3.475**	**0.001**

Table 24. Three-factor ANOVA results for the offset fed Cassegrain HPBW using first parameter set.

Notice in Table 24 that the F/D, and the interactions that include F/D have a low probability of influence on the HPBW. Eccentricity does, however, have an impact on the

variability of the HPBW, followed by the Ds/Dm, and the interaction of the two. The R^2 value indicates that there is a parameter not included that is affecting the variability of the HPBW. See Table 25 for the three-factor ANOVA results with the fratricide ratio as the output of interest.

R^2	**0.029**		**Fratricide Ratio**		
Source	DF	Sum of squares	Mean squares	**F**	**Pr > F**
F/d	5.000	0.013	0.003	**0.026**	**1.000**
Ds/Dm	4.000	0.469	0.117	**1.192**	**0.313**
Ecc	2.000	0.866	0.433	**4.401**	**0.013**
F/d*Ds/Dm	20.000	0.004	0.000	**0.002**	**1.000**
F/d*Ecc	10.000	0.028	0.003	**0.029**	**1.000**
Ds/Dm*Ecc	8.000	0.047	0.006	**0.059**	**1.000**

Table 25. Three-factor ANOVA results for the offset fed Cassegrain fratricide ratio using first parameter set.

In Table 25, the only parameter that had a probable impact on the fratricide ratio variability was eccentricity. Also notice that only 2.9% of the variability can be explained by the listed parameters, denoted by the R^2 value at the top of Table 25. Recall that these parameters may still have an impact on the variability of the fratricide ratio, however, not within the data set and parameter ranges provided. Finally, the three-factor ANOVA results using the second parameter set will be presented. See Table 26 for the ANOVA gain analysis using the second parameter set.

R^2	0.992		Gain		
Source	DF	Sum of squares	Mean squares	F	Pr > F
F/d	5.000	2.820	0.564	**124.935**	**0.000**
Ecc	6.000	171.299	28.550	**6325.254**	**0.000**
Lm	2.000	2.255	1.127	**249.748**	**0.000**
F/d*Ecc	30.000	2.886	0.096	**21.311**	**0.000**
F/d*Lm	10.000	0.142	0.014	**3.151**	**0.001**
Ecc*Lm	12.000	2.107	0.176	**38.906**	**0.000**

Table 26. Three-factor ANOVA results for the offset fed Cassegrain gain using second parameter set.

In Table 26, 99.2% of the gain variation can be explained by the listed parameters. Eccentricity had the largest impact, followed by Lm, then the F/D ratio. All parameters and interactions listed in Table 26 had impact on the variability of the gain with high probability. See Table 27 for the three-factor ANOVA results using the HPBW offset Cassegrain data.

R^2	0.519		HPBW		
Source	DF	Sum of squares	Mean squares	F	Pr > F
F/d	5.000	0.000	0.000	**1.210**	**0.304**
Ecc	6.000	0.010	0.002	**40.640**	**0.000**
Lm	2.000	0.000	0.000	**1.306**	**0.272**
F/d*Ecc	30.000	0.001	0.000	**1.129**	**0.298**
F/d*Lm	10.000	0.002	0.000	**3.951**	**0.000**
Ecc*Lm	12.000	0.000	0.000	**0.928**	**0.519**

Table 27. Three-factor ANOVA results for the offset fed Cassegrain gain using second parameter set.

In Table 27, eccentricity, and the interaction between F/D and Lm were the main contributors to the variability of the HPBW. An observation can be made in Table 27 where F/D and Lm on their own did not have a probable effect on the HPBW, however,

the interaction of the two parameters did. Also note that the R^2 value indicate that there may be hidden parameters that affect the HPBW. See Table 28 for the three-factor ANOVA study on the fratricide ratio.

R^2	0.092		Fratricide Ratio		
Source	DF	Sum of squares	Mean squares	F	Pr > F
F/d	5.000	0.000	0.000	0.021	1.000
Ecc	6.000	0.030	0.005	**5.032**	**0.000**
Lm	2.000	0.001	0.000	0.422	0.656
F/d*Ecc	30.000	0.000	0.000	0.008	1.000
F/d*Lm	10.000	0.000	0.000	0.013	1.000
Ecc*Lm	12.000	0.000	0.000	0.016	1.000

Table 28. Three-factor ANOVA results for the offset fed Cassegrain gain using second parameter set.

The eccentricity in Table 28 has the only probable impact on the fratricide ratio variability. All other parameters and interactions in Table 28 have no probable impact on the fratricide ratio variability. Furthermore, the R^2 value indicates that only 9.2% of the variability can be explained by the listed parameters.

4.5 Data Verification

This section will take one design from GRASP SE and compare the results with the same design in SATCOM. A design was chosen at random; the parameters can be seen in Table 29. Note: the parameters are from the first set where Ds/Dm is an independent variable. See Figure 83 for the GRASP and SATCOM gain outputs together. Only $\theta 0^0$ to 180^0 is shown due to symmetry. See Figure 84 for the decibel difference

plot of the two sets of data collected. The peak gain value from the GRASP data was 54.4 dB while the SATCOM peak was 54.9 dB, a 0.5 dB difference. At the maximum levels of difference, the data differs by 28.7 dB at $\theta 86.6^0$ and -27.5 dB at $\theta 22.3^0$. The first side lobe from GRASP was 34.2 dB while SATCOM reported 33.1 dB, a 1.1 dB difference. Both side lobe locations were identical at 0.5^0. Finally, the half power beamwidth was the same between both data sets at 0.3^0.

F/d	Ds/Dm	Ecc	Feed Taper	Lm
1	0.15	1.3	-12	0

Table 29. Parameter used for data verification.

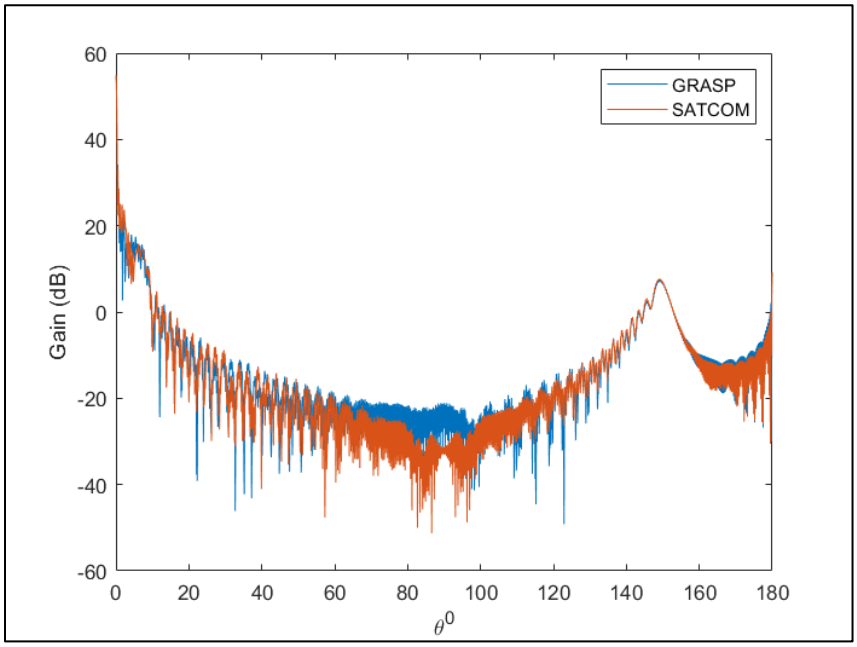

Figure 83. Data verification plots with GRASP (blue) and SATCOM (orange) outputs from $\theta 0^0$ to 180^0.

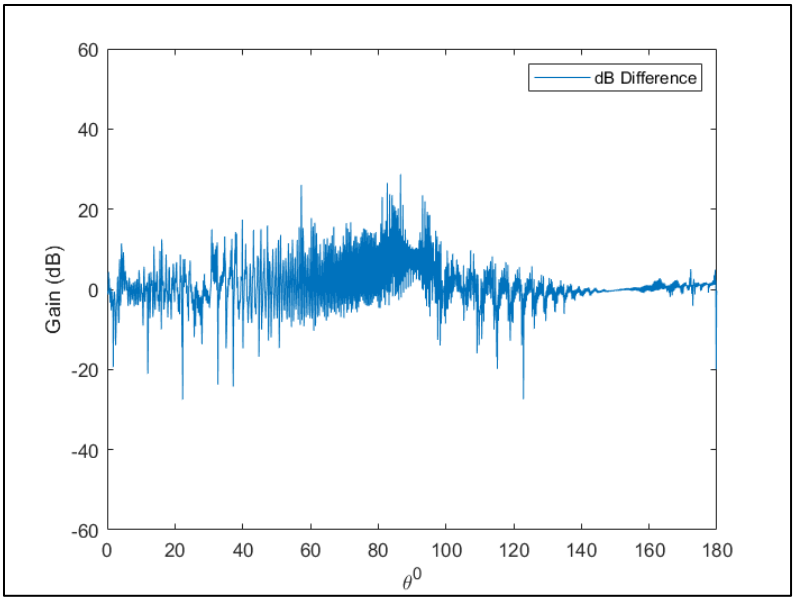

Figure 84. Data verification decibel difference plot between GRASP and SATCOM gain outputs from $\theta 0^0$ to 180^0.

V. Conclusions and Future Work

5.1 Preamble

The research and results presented in this work focused on the center fed and offset fed Cassegrain antennas with two varying sets of parameters. Large focal length to main reflector diameter (F/D) ratios greater than 1.0 were investigated along with eccentricity, subreflector diameter to main reflector diameter (Ds/Dm), distance from main reflector vertex to feed (Lm), and feed edge taper. A factorial design of experiments (DEO) approach was used along with a thorough analysis of variance (ANOVA) study to determine, if any, influence on the variability of the outputs of interest. Recall that the ANOVA tests were performed on each of the four data sets collected, one for each antenna variant, and one for each parameter set. Optimized beam patterns with maximum gain, most efficient side lobe attenuation, and lowest fratricide ratio were also presented. This Chapter aims to summarize the observations made and combine them with the ANOVA study based on the parameters of interest. See Chapter 4 for the ANOVA results for all four data sets.

5.2 F/D Change Effects

Based on the observations given in Chapter 4, the F/D value influenced certain outputs on an individual basis. The F/D value of 1.25 did, however, provide the highest gain pattern for the center fed design. The F/D value of 1.1 was observed to provide less

variation of data for the center fed design when using the first parameter set. The F/D was confirmed by ANOVA to provide influence on gain for both parameter sets and Cassegrain variants, but only HPBW influence on the center fed Cassegrain. The ANOVA tests on the fratricide ratio were inconclusive with respect to the F/D ratio, meaning the parameter had no effect on the back lobe energy variations.

5.3 Eccentricity Change Effects

Eccentricity was, by far, the strongest influencer on all data sets among the parameters of interest. The eccentricity was observed to increase peak gain values with both parameter sets for the center fed variant as well as the offset using the second parameter set. When observing the offset fed variant using the first parameter set, the eccentricity of 1.2 attained the highest gain values. The HPBW was observed to increase when the eccentricity was increased for the first parameter set on both variants. The first side lobe levels and locations were observed to decrease as eccentricity increased for the offset fed first parameter set. The fratricide ratio was observed to be the lowest when eccentricity was 1.2 for the offset fed first parameter set, but decreased on all other data sets when eccentricity increased.

The ANOVA results confirmed that eccentricity had to most influence on the variability of the data sets. Eccentricity ranked the highest on gain and HPBW for all four data sets in the ANOVA results. The influence on the fratricide ratio was the strongest on

all data sets except for the center fed Cassegrain second parameter set, where none of the parameter of interest had an influence on variability.

5.4 Ds/Dm Change Effects

Recall that the Ds/Dm parameter was only an independent variable for the first parameter set for both variants, therefore, observations and ANOVA results only pertain to the first set of parameters. The peak gain was observed to be the lowest when Ds/Dm was the highest for the center fed Cassegrain, while there was a slight convergence to 48 dB observed with the offset Cassegrain. The HPBW was observed to decrease as Ds/Dm increased on both the offset and center fed variants. For the first side lobe levels, the only observation made was the center fed, where the level seemed to converge to 30 dB as Ds/Dm increased. No intuitive observations could be made with the side lobe location. The fratricide ratio increased as Ds/Dm increased for both the center fed and offset fed data sets.

When reviewing the ANOVA results for the Ds/Dm ratio, the parameter had the second most influence on gain, HPBW, and fratricide ratio, behind eccentricity for the center fed design. For the offset design, the Ds/Dm had the fifth most influence on gain, the second most influence on HPBW, and no influence on fratricide ratio for the offset variant.

5.5 Lm Change Effects

The distance from the main reflector vertex to the feed Lm was an independent variable strictly for the second set of parameters. Recall that GRASP was allowed to vary the subreflector diameter automatically based on the second set of parameter inputs. Therefore, Lm only applies to two sets of data, one for each antenna variant. Gain was observed to only influence the offset antenna where the parameter seemed to lower the gain as it was increased. No other visual observations could be made that connected Lm to any of the other outputs of interest.

The ANOVA tests did shed more light on the influence of Lm. The parameter was the second most influential parameter on gain for both variants behind eccentricity. Lm ranked second on HPBW influence but only for the center fed design. All other outputs were uninfluenced by the Lm parameter.

5.6 Edge Taper Change Effects

Edge taper was only varied on the first parameter set. The decision to hold the edge taper constant for the second parameter set was due to -12 dB feed taper being more efficient across both variants. The gain was observed to increase with using the lower feed taper and fratricide ratio decreased. Holding edge taper constant for the second set of parameters allowed for more values of eccentricity and the addition of the Lm parameter. Edge taper was not included in the ANOVA tests.

5.7 Parameter Interactions

This section will summarize the results from the ANOVA parameter interactions. The ANOVA test allowed for three interactions: the F/D and Ds/Dm, the F/D and eccentricity, and the Ds/Dm and eccentricity. Among the interactions, a ranking of one to three was given to the interaction based on the results, one being the most influential. For the center fed Cassegrain first parameter set gain and HPBW results, Ds/Dm and eccentricity ranked first, F/D and eccentricity ranked second, and F/D and Ds/Dm placed third. No interaction played a role in the variability of the fratricide ratio for the center fed first parameter set.

For the offset fed Cassegrain using the first parameter set gain results, Ds/Dm and eccentricity ranked first, F/D and eccentricity ranked second, and F/D and Ds/Dm ranked third. The HPBW ANOVA results only confirmed that the interaction between Ds/Dm and eccentricity provided influence on the data, while the other two interactions failed the p-value test. Furthermore, all three interactions failed the p-value test for the fratricide ratio.

The three interactions measured for the second set of parameters are F/D and eccentricity, F/D and Lm, and eccentricity and Lm. For the center fed Cassegrain using the second set of parameters, eccentricity and Lm ranked first, followed by F/D and Lm, and F/D and eccentricity for gain and HPBW influence. ANOVA reported no parameter interaction influence on the fratricide ratio with respect to the center fed Cassegrain second parameter set.

Finally, the offset fed second parameter set interactions will be summarized. For gain influence, eccentricity and Lm ranked first, while F/D and eccentricity ranked second, and F/D and Lm ranked third. ANOVA only reported that F/D and Lm had an influence on HPBW, while no interaction played a role in varying the fratricide ratio.

5.8 Future Work

After a thorough analysis of the 6m center fed and offset fed Cassegrain antennas using prescribed parameters, there are many suggestions for future work. Taking the results from the ANOVA tests may provide a beneficial insight into the most influential parameters and interactions among the data sets. Different variants can be incorporated along with the use of other CEM software. This section will conclude with a bulleted list of possible areas in which future work could be investigated.

- Investigate different antenna variants such as Gregorian center fed and offset fed, single reflector, or array-type antennas.
- Compare different models to atmospheric propagation efficiency and determine the optimized design. Use high power, shortwave, continuous pulse emitters.
- Incorporate realistic feed models to attain optimized beam patterns. Recall that GRASP SE only allowed for the Gaussian beam feed pattern.
- Use the fratricide ratio analysis with a realistic power profile and determine exposure limits for equipment and personnel in the back lobes. Integrate over all ϕ and θ values for a 3D model to determine potential problem areas.

- Continue varying the parameters used in this work and acquire more data to process. Find the optimization limits for each output and perform extensive ANOVA tests that produce more than two interactions.
- Determine the benefits of using smaller or larger F/D values with respect to main reflector illumination. This could extend to finding the air breakdown thresholds in standard temperature and pressure (STP) and sulfur hexafluoride (SF6) gas.
- Considering the large amount of data acquired through this work, efforts can be made to preserve the raw data for future research purposes.

Bibliography

[1] Peter W. Hannan. Microwave Antennas Derived from the Cassegrain Telescope. *IRE Transactions on Antennas and Propagation*. 1960.

[2] Y. Mizugutch, M. Akagawa and H. Yokoi. Offset dual reflector antenna. *1976 Antennas and Propagation Society International Symposium*. pp. 2-5, 1976.

[3] Christopher Granet. Designing Axially Symmetric Cassegrain or Gregorian Dual-Reflector Antennas From Combinations of Prescribed Geometric Parameters. *IEEE Antennas and Propagation Magazine*. 4(2):76-82, 1998.

[4] Divya Gupta. A Review On Designing Of The Dual Reflector Axially Symmetric Cassegrain Antenna. *IOSR Journal of Electronics and Communication Engineering*, 4(1):48-51, 2012.

[5] W. V. T. Rusch, The current state of the reflector antenna are-entering the 1990s. *Proceedings of the IEEE*. 80(1):113-126, 1992.

[6] James Harris. Characterization and Sensitivity Analysis of 6 Meter Cassegrain Antenna. Master's Thesis, Air Force Institute of Technology, 2020.

[7] Teh-Hong Lee, Roger C. Rudduck, and Kevin M. Lambert. Pattern Measurements of Reflector Antennas in the Compact Range and Validation with Computer Code Simulation. *IEEE Transactions on Antennas and Propagations,* 38(6), 1990.

[8] Osipov, Andrey V. and Tretyakov, Sergei A. *Modern Electromagnetic Scattering Theory with Applications*. John Wiley & Sons, Ltd., first edition.

[9] E. F. Knott and T. B. A. Senior. Comparison of three high-frequency diffraction techniques. *Proceedings of the IEEE.* 62(11):1468-1474, 1974.

[10] Joseph B. Keller. Geometrical Theory of Diffraction. *Journal of the Optical Society of America.* 52(1):116-130, 1962.

[11] Akira Ishimaru.. *Electromagnetic Wave Propagation, Radiation, and Scattering From Fundamentals to Applications*. John Wiley & Sons, Ltd, second edition.

[12] Christopher Granet. Designing classical offset Cassegrain or Gregorian dual-reflector antennas from combinations of prescribed geometric parameters. *IEEE Antennas and Propagation Magazine*. 44(3):114-123, 2002.

[13] Genichi Taguchi, Subir Chowdhury, Yuin Wu. Introduction to Design of Experiments. *Taguchi's Quality Engineering Handbook*. 501-505, 2005.

[14] J. W. M. Baars. A Comparison Between Prime Focus and Cassegrain Antennas. *National Radio Astronomy Observatory*. 1964.

[15] Hongge Wei and Zhengjun Li. Analysis of the Reflector Antenna's Feed Taper Level. *2019 IEEE 2nd International Conference on Computer and Communication Engineering Technology (CCET)*. 213-217, 2019.

[16] Paul Wade. Multiple Reflector Dish Antennas. *Focus*, 2004.

[17] Constantine A. Balanis. *Antenna Theory: Analysis and Design*. John Wiley & Sons, Inc., fourth edition, 2016.

[18] Andrew S. Podgorski, "High Power Microwave Weapon System," U.S. Patent, Mar. 1, 2018.

[19] John Tatum. High-Power Microwave Directed Energy Weapons: A Model and Simulation Toolbox. *Journal*. 2014.

[20] Radiofrequency radiation exposure limits. *Govinfo.gov*. 2022. [Online]. Available: https://www.govinfo.gov/content/pkg/CFR-2011-title47-vol1/xml/CFR-2011-title47-vol1-sec1-1310.xml.

Acronyms

ANOVA analysis of variance.

CEM computational electromagnetic software.

DOE design of experiments.

EM electromagnetic.

GO geometrical optics.

GRASP SE general reflector software package student edition.

GTD geometrical theory of diffraction.

HPBW half power beamwidth.

HPM high power microwave.

MR main reflector.

OSU Ohio State University.

PEC perfect electrical conductor.

PO physical optics.

PTD physical theory of diffraction.

RF radiofrequency.

SATCOM satellite communication.

SR subreflector.

UTD uniform theory of diffraction.

REPORT DOCUMENTATION PAGE

Form Approved
OMB No. 074-0188

1. REPORT DATE *(DD-MM-YYYY)*	2. REPORT TYPE	3. DATES COVERED *(From – To)*
22-03-2012	Master's Thesis	March 2010 – March 2012

TITLE AND SUBTITLE

Title of Thesis in Title Case

5a. CONTRACT NUMBER

5b. GRANT NUMBER

5c. PROGRAM ELEMENT NUMBER

6. AUTHOR(S)

Public, Joseph Q., Captain, USAF

5d. PROJECT NUMBER

5e. TASK NUMBER

5f. WORK UNIT NUMBER

7. PERFORMING ORGANIZATION NAMES(S) AND ADDRESS(S)

Air Force Institute of Technology
Graduate School of Engineering and Management (AFIT/EN)
2950 Hobson Way, Building 640
WPAFB OH 45433-7765

8. PERFORMING ORGANIZATION REPORT NUMBER

AFIT-ENG-MS-22-J-013

9. SPONSORING/MONITORING AGENCY NAME(S) AND ADDRESS(ES)

AGENCY (spelled out)
ADDRESS
PHONE and EMAIL
ATTN: POC
(no sponsor enter: Intentionally left blank)

10. SPONSOR/MONITOR'S ACRONYM(S)

AFRL/RHIQ (example)

11. SPONSOR/MONITOR'S REPORT NUMBER(S)

12. DISTRIBUTION/AVAILABILITY STATEMENT

DISTRUBTION STATEMENT A. APPROVED FOR PUBLIC RELEASE; DISTRIBUTION UNLIMITED.

13. SUPPLEMENTARY NOTES

14. ABSTRACT

High power microwaves (HPM) have been a topic of research since the Cold War era. This paper presents a comparison between two Cassegrain-type antennas: the axially, or center fed, and the offset fed. Specifically, the 10 GHz operating frequency is investigated with large focal length to diameter (F/D) ratios. Beam patterns which encompass the entire radiation pattern are included for data validation and optimization. The simulations follow a factorial model of design to ensure all possible combinations of prescribed parameters are included. This includes an analysis of variance (ANOVA) study to find parameter influence on the outputs of interest. Outputs such as maximum gain, beamwidth, and sidelobe levels and locations are of interest. Research in this area will greatly enhance the reader's understanding of the benefits and disadvantages of the two antennas mentioned.

15. SUBJECT TERMS

(Fill in with pertinent terminology related to the topic of your thesis.)

16. SECURITY CLASSIFICATION OF:			17. LIMITATION OF ABSTRACT	18. NUMBER OF PAGES	19a. NAME OF RESPONSIBLE PERSON
a. REPORT	b. ABSTRACT	c. THIS PAGE			Dr. Andrew J. Terzuoli, AFIT/ENG
U	U	U	UU	129	19b. TELEPHONE NUMBER *(Include area code)* (513) 307-3233 terzuoli@afit.edu

Standard Form 298 (Rev. 8-98)
Prescribed by ANSI Std. Z39-18